

THERMODYNAMICS OF MICROALLOYED AUSTENITES  
AND  
NONSTOICHIOMETRIC CARBIDES AND NITRIDES

By

KRISHNAMURTY BALASUBRAMANIAN B.Tech.

A Thesis

Submitted to the School of Graduate Studies  
in Partial Fulfillment of the Requirements  
for the Degree

Doctor of Philosophy

McMaster University

January 1988

(c) Copyright by Krishnamurty Balasubramanian 1988.

THERMODYNAMICS OF MICROALLOYED STEELS

DOCTOR OF PHILOSOPHY (1988)  
(Metallurgy)

McMASTER UNIVERSITY  
Hamilton, Ontario

TITLE: Thermodynamics of Microalloyed Austenites and  
Nonstoichiometric Carbides and Nitrides

AUTHOR: Krishnamurty Balasubramanian B.Tech., (Indian Institute of  
Technology, Kanpur)

SUPERVISOR: Professor J.S. Kirkaldy

NUMBER OF PAGES: xvii, 196

## ABSTRACT

The thermodynamics of Fe-Nb-C, Fe-Ti-C, Fe-Nb-N austenites and that of binary carbides and nitrides of Ti and Nb essential in the understanding of the precipitation behaviour in microalloyed steels has been investigated in this study. A dynamic gas equilibration technique has been used in the experimental investigation of the thermodynamics of ternary austenites and binary carbides of Ti and Nb. The results obtained in this study have been analyzed using the modified Wagner formalism for dilute ternary austenites and the sublattice - subregular model suggested by Hillert and Staffansson for the interstitial carbides and nitrides. The solubilities of NbC, TiC and NbN in austenite have been determined from the isoactivity measurements done in this study. The solubility minimum and the variation of solubility limits of carbides of Ti and Nb and the increase in carbon content at constant carbon activity have been quantitatively related to the ternary interaction parameter. The C-Nb, C-Ti and N-Nb interaction parameters have been determined. The dissolution free energies of Nb and Ti in fcc Fe have been obtained from the analysis of the solubilities of NbC, NbN and TiC in their respective austenites.

Expressions describing the variation of the partial molar free energies of the components in the binary carbides and nitrides of transition metals have been obtained via statistical mechanical considerations. The pair interaction free energies involved in the statistical mechanical description of interstitial solutions have been related to the interaction parameters in the sublattice model. The

carbon activity measurements in the  $NbC_y$  and  $TiC_y$  phases and the nitrogen activity measurements in the  $NbN_y$  phase obtained in this study together with the data available in the literature have been analyzed to obtain the interaction parameters in the sublattice model. The limitations in applying the classical Wagner-Schottky model to highly nonstoichiometric compounds have been discussed. The necessary modifications to this classical model have been made by referring to the expressions obtained via the statistical mechanical approach.

The microalloyed ternary austenite - nonstoichiometric carbide equilibrium has been evaluated for the Fe-Nb-C and Fe-Ti-C systems. The effects due to solute interactions and the nonstoichiometry of the precipitate have been clarified. The solubility of TiN in Fe-Ti-N austenite has been calculated using the dissolution free energy of Ti evaluated in this study. Rational correlations between the ternary interaction parameters and the free energies of formation of carbides and nitrides have been established. Using this correlation an approximate value of the nitrogen-titanium interaction parameter has been evaluated.

### ACKNOWLEDGEMENTS

The author is indebted to his supervisor Dr. J.S. Kirkaldy, for his inspiring guidance and assistance throughout the course of this study. Dr. Kirkaldy's bold and innovative approach to research, his passion for the science of thermodynamics, philosophy and logic have instilled in this author a scientific temper that will serve as a guiding force in his future career in science and engineering. The author also wishes to express his gratitude to Dr. T.R. Ramachandran of Indian Institute of Technology, Kanpur, India for his continued guidance and friendship. Sincere thanks are due to Drs. G.R. Purdy, and W.W. Smeltzer, for their advice and assistance. Special thanks are due to Dr. Purdy for motivating the author to join McMaster graduate school.

The advice and assistance rendered by Mr. Horst Neumayer in the construction and safe operation of the experimental equipment is deeply appreciated. The author also wishes to extend his thanks to Mr. Martin Van Oosten for his assistance in chemical analysis.

Sincere and heartfelt thanks are due to Dr. S.V. Subramanian for providing help, advice and support throughout the course of this study. His moral support during countless experimental setbacks and financial help in times of need are immensely appreciated. Special thanks are due to Ms. Domenica S. Misale for her support during many difficult periods. The quality phase diagrams prepared by Ms. Misale are greatly appreciated.

The timely help rendered by Mr. Devendra Jalihal in the word processing of the equations and other difficult parts of this thesis is appreciated. The assistance rendered by Mr. Milind Bhise and Mr. Jalihal in the preparation of the manuscript is gratefully acknowledged. The author ~~also~~ expresses his gratitude to Mr. Leo DeMeo for proofreading the thesis in a short period of time.

The author also wishes to express his heartfelt thanks to all the friends and well wishers in the department of Materials Science and Engineering for their continued support and friendship.

Financial support in the form of scholarships awarded by the McMaster University is gratefully acknowledged.

## TABLE OF CONTENTS

CHAPTER I	INTRODUCTION	1
CHAPTER II	LITERATURE REVIEW	4
2.1	Introduction	4
2.2	The Constitution of Fe-Ti and Fe-Nb Systems	4
2.2.1	Fe-Ti System	5
2.2.2	Fe-Nb System	5
2.3	Solution Behaviour of Ti and Nb in Iron Austenite	9
2.4	Solution Behaviour of Carbon and Nitrogen in Iron Austenite	10
2.5	Ternary Interactions In Fe-M-X Austenites (M=Ti,Nb and X=C,N)	11
2.6	Interstitial Compounds	12
2.6.1	Constitution Diagrams of Ti-C, Nb-C, Ti-N, and Nb-N Systems	12
2.6.1.1	Ti-C and Nb-C Systems	13
2.6.1.2	Ti-N and Nb-N Systems	13
2.7	Thermodynamics of $TiC_y$ , $NbC_y$ , $TiN_y$ , and $NbN_y$ Phases	18
2.7.1	Calorimetric Studies	18
2.7.2	Vapour Pressure, EMF, and Gas Equilibration Studies	20
2.8	Thermodynamic Models	22
2.8.1	Regular Solution Models	22
2.8.2	Schottky-Wagner Model	23
2.8.3	Sublattice-Subregular (Hillert-Staffansson) Model	23
2.8.4	Statistical Mechanical Approaches	25
2.9	Solubility of Carbides and Nitrides in Iron Austenite	25

CHAPTER III	EXPERIMENTAL PROCEDURE	33
3.1	Introduction-	33
3.2	Experimental Technique	33
3.2.1	Static Equilibration Methods	34
3.2.2	Dynamic Equilibration Methods	35
3.2.3	Chemical Analysis	35
3.3	Experimental Apparatus	36
3.3.1	Gas Metering and Blending System	36
3.3.2	Gas Cleaning System	39
3.3.3	Equilibration Furnace Assembly	40
3.3.4	Electrobalance Assembly	42
3.3.5	Vacuum System	43
3.4	Materials and Sample Preparation	44
3.4.1	Materials	44
3.4.2	Fe-Ti, Fe-Nb Alloy Preparation	44
3.4.3	Specimen Preparation	45
3.4.4	Titanium and Niobium Specimen Preparation	46
3.5	Experimental conditions	47
3.5.1	Temperature and Pressure	47
3.5.2	Flow Rate	48
3.5.3	Preliminary Experimental Procedures	48
3.6	Summary of Experiments	50
CHAPTER IV	EXPERIMENTAL RESULTS	55
4.1	Introduction	55
4.2	Results for the Fe-Nb-C and Fe-Ti-C Systems	55
4.3	Results for the Fe-Nb-N System	66

4.4	Results for the NbC <sub>y</sub> and TiC <sub>y</sub> Phases	72
4.5	Results for the NbN <sub>y</sub> Phase	75
CHAPTER V	THERMODYNAMIC MODELS	93
5.1	Introduction	93
5.2	Modified Wagner Formalism for Dilute Fe-M-X Austenites	93
5.3	Interaction Parameters in Fe-M Systems	96
5.4	Thermodynamics of Nonstoichiometric Monocarbides and Nitrides	101
5.4.1	Introduction	101
5.4.2	Assumptions	101
5.4.3	Theory	101
5.4.4	Hillert-Staffansson Model	105
5.5	Limitations of the Schottky-Wagner Model for Defect Compounds	108
CHAPTER VI	ANALYSIS AND DISCUSSION	116
6.1	Introduction	116
6.2	Analysis of Fe-Nb-C and Fe-Ti-C Austenites	117
6.2.1	Solubility Minimum and Ternary Interactions	118
6.2.2	Increase in Carbon Content and Ternary Interactions	122
6.2.3	The Niobium-Carbon Interaction Parameter	126
6.2.4	The Titanium-Carbon Interaction Parameter	130
6.2.5	The Carbide Solubility and the Ternary Interactions	134
6.2.6	Comparison with Results of Ohtani et.al.	137
6.2.6.1	Comparison of the Results in Fe-Nb-C System	137
6.2.6.2	Comparison of the Results in Fe-Ti-C System	140

6.2.7	Free Energy of Dissolution, (Henry's Law Coefficient) of Nb and Ti in Fcc Iron	142
6.3	Analysis of Fe-Nb-N Austenite	144
6.3.1	The Niobium-Nitrogen Interaction Parameter	145
6.3.2	Solubility of NbN in Fe-Nb-N Austenite	148
6.4	Analysis of NbC <sub>y</sub> Phase	149
6.5	Analysis of TiC <sub>y</sub> Phase	154
6.6	Analysis of NbN <sub>y</sub> Phase	157
6.7	Effect of Nonstoichiometry and Solute Interactions	163
6.8	Solubility of TiN in Fe-Ti-N Austenite	170
6.9	Periodic Table Trends in the Ternary Interaction Parameters	173
CHAPTER VII	CONCLUSIONS	185
REFERENCES		189

LIST OF TABLES \*\*

2.1	Heat of Formation of Niobium Carbides.	29
2.2	Free Energy of Formation of Stoichiometric Carbides and Nitrides of Titanium and Niobium	29
2.3	Experimental Investigations on the Partial Molar Free Energies of Binary carbides and Nitrides of Ti and Nb	30
2.4	Solubility of Ti/Nb Carbides in Iron Austenite	31
2.5	Solubility of Ti/Nb Nitrides in Iron Austenite	32
3.1	Impurity Contents in Fe-Nb and Fe-Ti Alloys	52
3.2	Composition of Fe-Nb Alloys	53
3.3	Composition of Fe-Ti Alloys	54
4.1	Carbon Contents of Fe-C and Fe-Nb-C Alloys at 1273K	78
4.2	Carbon Contents of Fe-C and Fe-Nb-C Alloys at 1373K	79
4.3	Carbon Contents of Fe-C and Fe-Nb-C Alloys at 1473K	80
4.4	Carbon Contents of Fe-C and Fe-Ti-C Alloys at 1273K	81
4.5	Carbon Contents of Fe-C and Fe-Ti-C Alloys at 1373K	82
4.6	Carbon Contents of Fe-C and Fe-Ti-C Alloys at 1473K	83
4.7	Solubility Limit of NbC in Fe-Nb-C Austenite	84
4.8	Solubility Limit of TiC in Fe-Ti-C Austenite	85
4.9	Nitrogen Contents of Fe-N and Fe-Nb-N Alloys at 1373K	86
4.10	Nitrogen Contents of Fe-N and Fe-Nb-N Alloys at 1473K	87
4.11	Nitrogen Contents of Fe-N and Fe-Nb-N Alloys at 1573K	88
4.12	Solubility Limit of NbN in Fe-Nb-N Austenite	89
4.13	Variation Composition with Carbon Potential in NbC	90
4.14	Variation Composition with Carbon Potential in TiC	91

4.15	Variation of Composition with Nitrogen Potential in NbN	92
5.1	Excess Free Energies of fcc Phases in Fe-Ti and Fe-Nb Systems	113
5.2	Excess Free Energies of fcc Phases in Fe-M Systems	114
5.3	Calculated Atomic Diameters (Coordination Number = 12)	115
6.1	Solubility Limit and Ternary Interactions in Fe-Ti-C and Fe-Nb-C Systems	179
6.2	Dissolution Free Energy of bcc Nb from Solubility Studies	180
6.3	Dissolution Free Energy of bcc Ti from Solubility Studies	181
6.4	Niobium Activity Data from Vapour Pressure and EMF Studies	182
6.5	Summary of Interaction Parameters in Fe-Nb-C, Fe-Ti-C and Fe-Nb-N and Fe-Ti-N Austenites.	183
6.6	Summary of Interaction Parameters for Ti and Nb Carbides and Nitrides	184

\*\* The tables have been placed at the end of Chapters II, III, IV, V and VI

## LIST OF FIGURES

- 2.1 The Fe-Ti Constitution Diagram
- 2.2 The Fe-Nb Constitution Diagram
- 2.3 Alpha-Gamma Phase Relationships in Fe-Ti and Fe-Nb Systems
- 2.4 The Ti-C Constitution Diagram
- 2.5 The Nb-C Constitution Diagram
- 2.6 The Ti-N Constitution Diagram
- 2.7 The Nb-N Constitution Diagram
- 3.1 A Schematic of the Experimental Apparatus
- 4.1 The Carbon Contents of Fe-C and Fe-Nb-C Alloys at 1273K
- 4.2 The Carbon Contents of Fe-C and Fe-Nb-C Alloys at 1373K
- 4.3 The Carbon Contents of Fe-C and Fe-Nb-C Alloys at 1473K
- 4.4 The Carbon Contents of Fe-C and Fe-Ti-C Alloys at 1273K
- 4.5 The Carbon Contents of Fe-C and Fe-Ti-C Alloys at 1373K
- 4.6 The Carbon Contents of Fe-C and Fe-Ti-C Alloys at 1473K
- 4.7 Variation of the Solubility Product of NbC with Carbon Content
- 4.8 Variation of the Solubility Product of TiC with Carbon Content
- 4.9 The Nitrogen Contents of Fe-N and Fe-Nb-N Alloys at 1373K
- 4.10 The Nitrogen Contents of Fe-N and Fe-Nb-N Alloys at 1473K
- 4.11 The Nitrogen Contents of Fe-N and Fe-Nb-N Alloys at 1573K
- 4.12 Variation of the Composition of Niobium Carbide with Gas Ratio
- 4.13 Variation of the Composition of Titanium Carbide with Gas Ratio
- 4.14 Variation of the Composition of Niobium Nitride with Partial Pressure of Nitrogen
- 5.1 Correlational Relationship : Free Energy of Dissolution of Solute in fcc Fe vs Atomic Size Difference

- 5.2 Correlational Relationship : Free Energy of Dissolution of Solute in fcc Fe vs Atomic Number of the Solute
- 6.1 Determination of Niobium-Carbon Interaction Parameter (T=1273K)
- 6.2 Determination of Niobium-Carbon Interaction Parameter (T=1373K)
- 6.3 Determination of Niobium-Carbon Interaction Parameter (T=1473K)
- 6.4 Determination of Titanium-Carbon Interaction Parameter (T=1273K)
- 6.5 Determination of Titanium-Carbon Interaction Parameter (T=1373K)
- 6.6 Determination of Titanium-Carbon Interaction Parameter (T=1473K)
- 6.7 Solubility Limit of NbC in Austenite (T=1373K)
- 6.8 Solubility Limit of NbC in Austenite (T=1473K)
- 6.9 Solubility Limit of TiC in Austenite (T=1373K)
- 6.10 Solubility Limit of TiC in Austenite (T=1473K)
- 6.11 Variation of Partial Molar Free Energy of Niobium in Niobium Carbide (T=1273K)
- 6.12 Variation of Partial Molar Free Energy of Niobium in Niobium Carbide (T=1600K).
- 6.13 Variation of Partial Molar Free Energy of Niobium in Niobium Carbide (T=2400K)
- 6.14 Variation of Partial Molar Free Energy of Carbon in Titanium Carbide (T=1473K)
- 6.15 Variation of Composition of Niobium Nitride with Nitrogen Partial Pressure of Nitrogen (Results of Shchurik et al.(94))
- 6.16 Determination of Parameters in NbN phase (a,b) (Results: This Study)
- 6.17 Variation of Partial Molar Free Energy of N in NbN Phase Comparison of Predictions: Shchurik and This Study.
- 6.18 Effect of Nonstoichiometry and Solute Interactions: Austenite - Niobium Carbide Equilibrium. (T=1273K and 1473K)
- 6.19 Effect of Nonstoichiometry and Solute Interactions: Austenite - Titanium Carbide Equilibrium. (T=1273K and 1473K)
- 6.20 Variation of Solubility of TiN in Fe-Ti-N Austenite with

Temperature.

- 6.21 Correlational Relationship: Carbon-Metal Interaction Parameter, in Austenite vs Free Energy of Formation of Carbide
- 6.22 Correlational Relationship: Nitrogen-Metal Interaction Parameter in Austenite vs Free Energy of Formation of Nitride

## LIST OF SYMBOLS

- $a_i$  = Activity of solute "i"
- A, B, g, h = Interaction parameters in Fe-M systems
- $A_i, B_i$  = Interaction parameters in  $MX_y$  compound phase
- $EG_m$  = Excess molar free energy
- $\overline{EG}_i$  = Partial molar excess free energy
- F = Helmholtz free energy of  $MX_y$  compound phase
- $F_i$  = Free energy to transfer a mole of element "i" from pure substance state to NaCl structure
- $F_{ij}$  = Pair interaction free energies in the  $MX_y$  compound phase
- $G_m$  = Molar free energy
- ${}^0G_m^{fcc}$  = Free energy of metal M in fcc state.
- ${}^0G_m^{bcc}$  = Free energy of metal M in bcc state.
- $\overline{G}_i$  = Partial molar free energy of solute "i"
- K = Solubility Product  $[X_i][X_j]$
- K' = Solubility Product  $_{[Wt\%i]}[Wt\%j]$
- $L_0, L_1$  = Interaction parameters in Hillert-Staffansson model
- Q = Partition function
- R = Universal gas constant
- T = Temperature

- Wt% i = Concentration of solute "i" in weight percent units
- $X_i$  = Concentration of solute "i" in mole fraction units
- $X_C^E, X_N^E$  = Carbon and nitrogen contents in binary Fe-C and Fe-N alloys
- $X_C^T, X_N^T$  = Carbon and nitrogen contents in ternary alloys
- $(X_C)_{opt}$  = Carbon content at the solubility minimum  $(\frac{dX_N}{dX_C}) = 0$
- $(X_N)_{opt}$  = Metal content at the solubility minimum  $(\frac{dX_C}{dX_N}) = 0$
- v = nonmetal/metal atom ratio in the compound phase  $MX_y$
- $\gamma_i$  = Activity coefficient of solute "i"
- $\gamma_i^0$  = Henry's law coefficient
- $\Delta F_{va}$  = Free energy change due to addition of a mole of vacancies in the interstitial sublattice
- $\Delta G_{-}^0$  = Free energy of formation of stoichiometric compound MX (The reference state given in the context)
- $\Delta_e \text{Wt\% } i$  = Absolute error in the determination of concentration of solute "i" in weight percent units
- $\Delta_e X_i$  = Absolute error in the determination of concentration of solute "i" in mole fraction units
- $\Delta X_C, \Delta X_N$  = Increase in carbon and nitrogen contents
- $\epsilon_i^i$  = self interaction parameter for solute "i"
- $\epsilon_i^j$  = Cross interaction parameter

## CHAPTER I

### INTRODUCTION

The development of high strength low alloy steels for line pipe and other sheet metal applications has been one of the important endeavours in the design of steels. One of the main reasons for the success in the design of these steels is the effective utilization of the microalloying additions such as niobium, titanium, and vanadium. These transition metals form fine carbide, nitride and carbonitride precipitates during hot deformation of austenite, thereby influencing its recrystallization and growth kinetics. The thermodynamics of microalloyed austenite and the precipitate phases is one of the many important factors that are involved in the complex interplay of deformation and precipitation in these steels.

The solubility of carbides, nitrides, and carbonitrides of Ti, Nb, V etc. in alloyed austenite has been the focus of many investigations in the past two decades. The mutual stability is generally understood in terms of solubility limits of the binary stoichiometric compounds of these elements in austenite devoid of solute interactions. The carbides and nitrides of Ti and Nb are nonstoichiometric and hence their composition can vary when precipitated in steels. As the Group IV and V transition metals are very strong carbide and nitride formers, their interaction with carbon and nitrogen in austenite is very pronounced. The effects of nonstoichiometry and the solute interactions on the solubility of these precipitates have not

been addressed in the past investigations. All of these investigations were performed at low carbon levels (below 0.2 Wt%) and hence are not capable of predicting the solubility at higher levels where the effects of solute interactions become significant. The present work was undertaken to gain insight into the nature and the magnitude of these interactions in microalloyed austenite.

In this study, the thermodynamics of the Fe-Ti-C and Fe-Nb-C austenites and the solubility of the carbides in these austenites in the temperature range 1273K-1473K and at carbon levels greater than 0.1 Wt% have been experimentally investigated using gas equilibration methods. The experimental results are then analyzed in terms of solution models to obtain the parameters defining the interaction between the solutes in the austenites as well as in the carbides. The thermodynamics of Fe-Nb-N austenite and the solubility of NbN have also been investigated using nitrogen atmospheres and the Nb-N interaction is determined to a reasonable degree of accuracy. The effects of solute interactions and the nonstoichiometry on the solubility of the precipitates have been clarified. Rational correlations between the dissolution free energies of transition metal solutes in fcc iron and the atomic number of the solute and the size factor are shown to exist. Correlational relationships between the ternary interaction parameters and the free energy of formation of carbides and nitrides from austenite have also been established. These relationships are utilised in the assessment as well as systematization of thermodynamic data.

The predominant interactions in steels arise from the substitutional-interstitial solute combinations. The results on solute

interactions obtained in this study pave the way for completing the much needed information on the thermochemistry and the phase diagram of the commercially important iron rich Fe-Ti-Nb-C-N pentenary austenites and the quaternary (Ti,Nb)(C,N) carbonitride precipitates.

## CHAPTER II

### LITERATURE REVIEW

#### 2.1 Introduction

In this chapter we briefly review the experimental and theoretical investigations, on thermochemistry and phase diagrams pertaining to (a) iron austenite alloyed with titanium and niobium; (b) carbides, nitrides of titanium and niobium; and (c) solubility of the aforementioned compounds in iron austenite.

#### 2.2 The Constitution of Fe-Ti and Fe-Nb Alloys

The NBS Alloy Phase Diagram Data Programme has compiled all the information regarding the crystallographic, constitutional and some thermodynamic aspects of many binary systems in recent years. Kubaschewski(1) has compiled the equilibrium diagrams of iron binary systems. Hence attention is drawn mainly to the investigations relating to the alpha-gamma phase relationships in Fe-Ti and Fe-Nb systems. Transition metals like Ti, Nb, and V are ferrite stabilizers and so the constitution diagrams of Fe-Ti and Fe-Nb show a closed gamma loop. The constitution diagrams of these systems recently proposed by Murray(2) and Paul and Swartzendruber(3) are shown in Figures 2.1-2.3. In both the systems the gamma phase (fcc) does not extend beyond 1.5 atom percent.

### 2.2.1 Fe-Ti System

The equilibrium phases in Fe-Ti include (a) the liquid, (b) the close packed hexagonal ( $\alpha$ Ti), (c) the body centered cubic solutions ( $\beta$ Ti), ( $\alpha$ Fe), (d) face centered cubic solution ( $\gamma$ Fe), (e) the equiatomic compound FeTi with CsCl structure, and (f) C14 phase which is the stoichiometric compound  $TiFe_2$  with  $MgZn_2$  Laves phase structure. The ( $\alpha$ Fe) and ( $\gamma$ Fe) phase boundaries form a closed loop. The intermetallic phases exist over considerable solution ranges.

Fischer et al.(4) investigated the gamma loop by employing thermo-magnetic measurements and microscopy and they reported the maximum solubility of Ti in fcc Fe to be 0.8 at%. Previous investigations(5-7) on solubility of Ti in fcc Fe agree well with that of Fischer. Murray(2) recently reviewed the available constitutional and thermodynamic information in order to revise the phase diagram as proposed by Shunk(8) and Hultgren et al.(9). Kaufman(10) and Murray(2) analysed the most accurate of the available data to evaluate parameters defining the free energy of the  $\gamma$ Fe phase using the subregular solution model. Their results have been absorbed into this study for further analysis.

### 2.2.2 Fe-Nb System

The Fe-Nb system consists of (a) the liquid, (b) two intermetallic phases with considerable homogeneity range, namely,  $Fe_3Nb_6$  and the Laves phase  $Fe_2Nb_3$ , (c) bcc solid solutions ( $\alpha$ Nb), low temperature ( $\alpha$ Fe) and high temperature ( $\delta$ Fe) and (d) face centered cubic ( $\gamma$ Fe) phase. There is some uncertainty regarding the reporting of three more intermetallic phases in Nb-rich alloys. An  $\eta$  carbide type phase

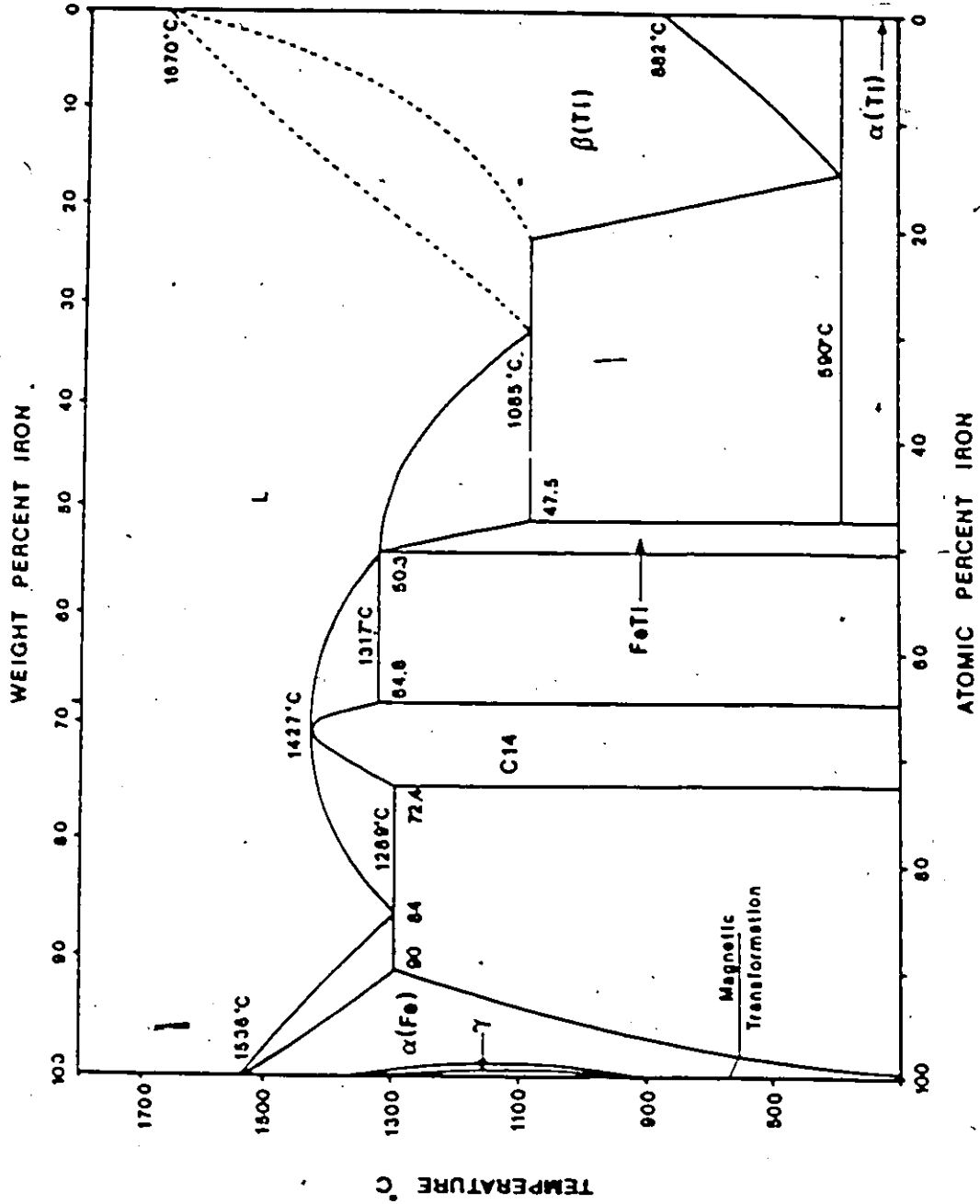


FIG. 2.1 THE Fe-Ti CONSTITUTION DIAGRAM

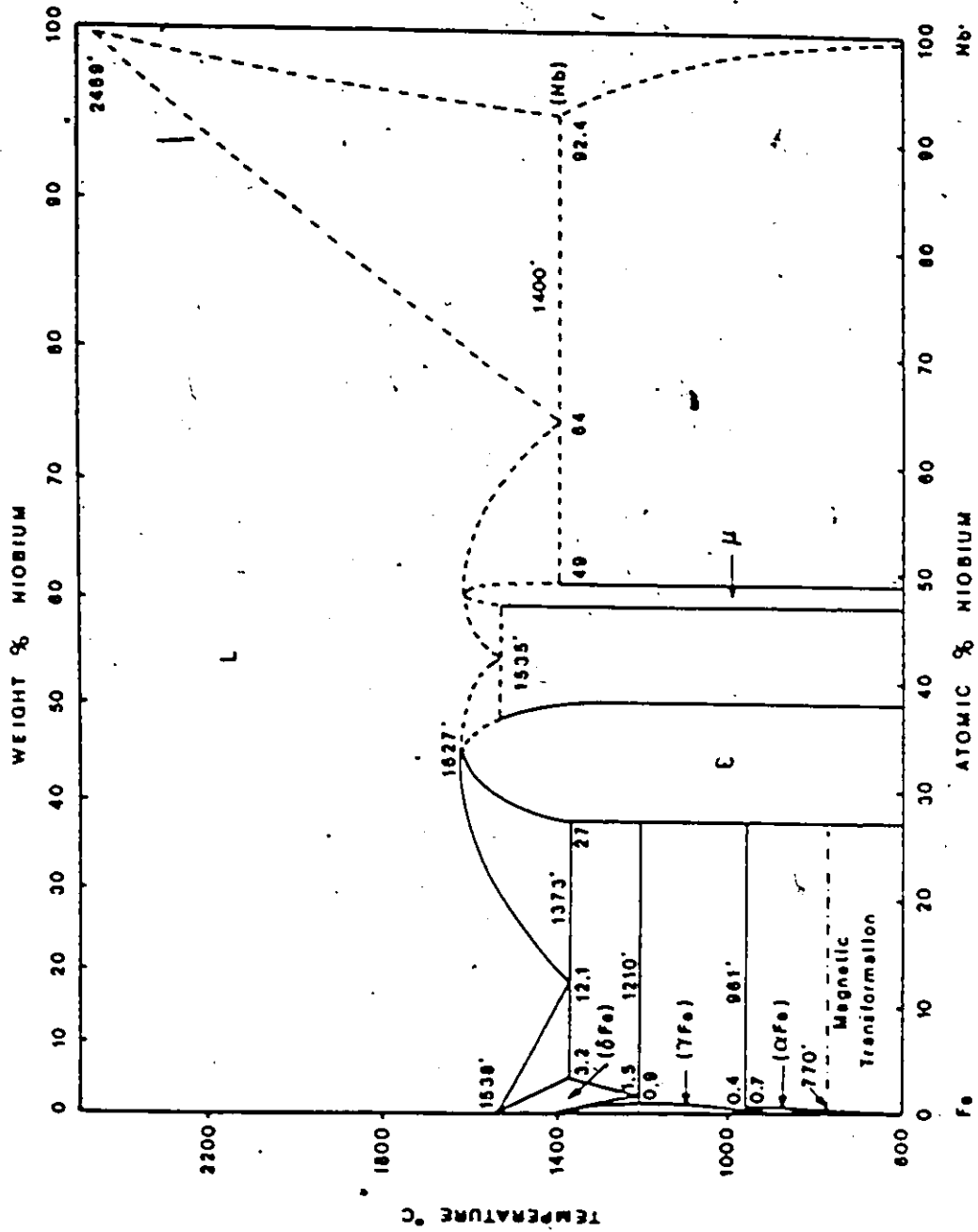


FIG. 2.2 THE Fe-Nb CONSTITUTION DIAGRAM

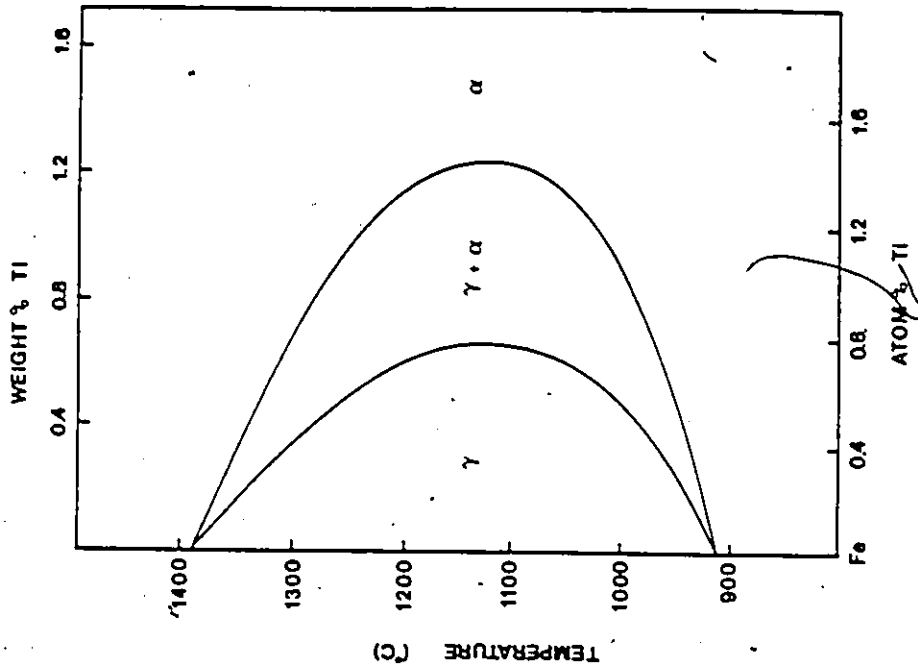
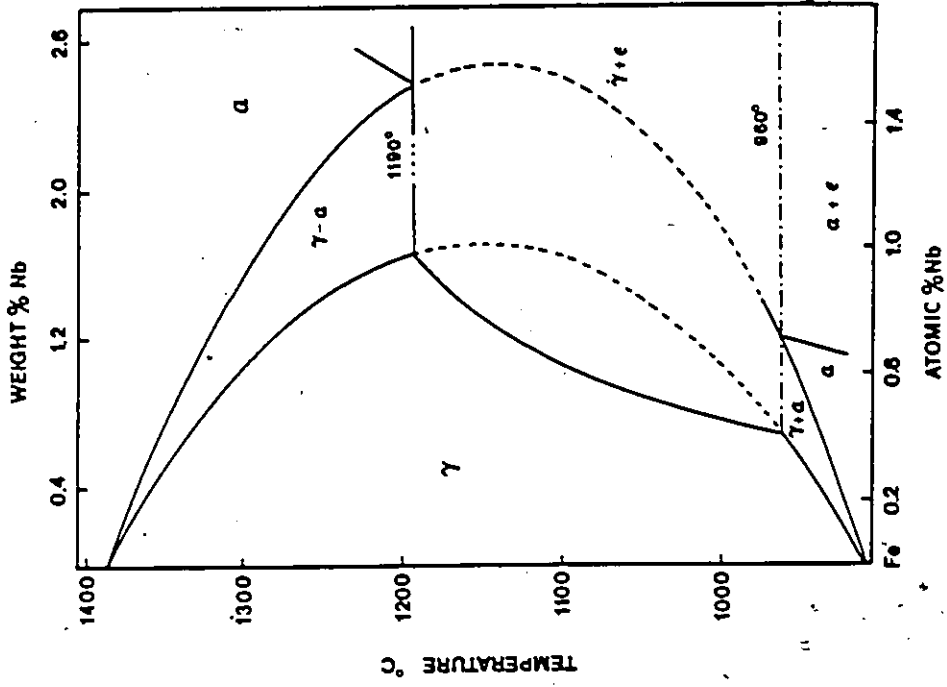


FIG. 2.3 ALPHA-GAMMA PHASE RELATIONSHIPS IN Fe-Ti AND Fe-Nb SYSTEMS

associated with  $\text{Fe}_2\text{Nb}_3$  compound, an equiatomic compound  $\text{FeNb}$  (zeta phase, stable between 600 C and 1500 C), and a high temperature phase (stable between 1200 C and 1600 C) based on a possible Nb-rich compound near 90 at% Nb have been suggested but have not been confirmed. The recently proposed phase diagram(3) under the NBS Data Programme does not include these three phases.

The Fe-rich portion of the diagram was also investigated by Eggers and Peter(11), Peter(12), Vogel and Ergang(13), Genders and Harrison(14), Gibson and Hume-Rothery(15,16), Ferrier et al.(17), and Fischer et al.(4). Fischer et al. were the principal investigators of the ( $\alpha+\gamma$ ) equilibrium. They report a maximum solubility of 1.0 at% Nb in fcc Fe. Paul and Swartzendruber(3) have recently reviewed all the available information on Fe-Nb system for the NBS alloy data programme. Kaufman and Nesor(10) calculated the Fe-Nb phase diagram using the subregular solution model for analytical descriptions of various phases.

### 2.3 Solution Behaviour of Ti and Nb in Iron Austenite

The solution behaviour of Ti and Nb in iron austenite has not been well investigated. Most of the available information in the literature has been determined by computer calculations using experimental phase diagrams and thermodynamic data on liquid and bcc phases. Recent calculations by Murray(2) and Kaufman(10) necessitated a sub-regular description for the  $\gamma\text{Fe}$  phase in order to reproduce the experimental ( $\alpha+\gamma$ ) phase boundaries in the above systems. Hence at least two parameters are required for satisfactory description of the iron austenite phase. The present investigation on the solubility of

carbides of Ti and Nb in iron austenite also indicates the nonideal solution behaviour of the transition metal solutes. The modified Wagner formalism (18-21) for dilute solutions has been used to describe the thermodynamics of the fcc phase in the above three systems in the present study. The Henry's law coefficient (infinitely dilute standard state) and self interaction parameter ( $\epsilon_M^M$ , M=Ti, Nb, V) have been extracted from the expressions for partial molar excess free energies in the subregular model given by the aforementioned investigators. The methodology involved in the calculation is dealt with in the subsequent chapters.

#### 2.4 Solution Behaviour of Carbon and Nitrogen in Iron Austenite

The thermodynamics and phase diagram of the Fe-C system have been extensively studied. Darken and Gurry(22) and Benz and Elliott(23) were some of the first investigators to analyze the experimental data in thermodynamic terms and to combine the phase equilibrium information with thermochemical data. More recently Harvig(24) made a detailed evaluation of the solid equilibria, while a comprehensive thermodynamic analysis of all the equilibria in the Fe-C system was considered by Chipman(25). Agren(26) presented an analysis of the Fe-C system based on the description of the magnetic contribution to the Gibbs energy of bcc-iron due to Hillert and Jarl(27) and on the experimental width of the  $(\alpha+\gamma)$  two-phase region. The most recent and comprehensive analysis of the Fe-C system has been provided by Gustafson(28). The thermodynamic analyses of Harvig, Agren, and Gustafson were based on the sublattice model suggested by Hillert and Staffansson(29). Chipman used

essentially the Wagner formalism(18) for dilute solutions to describe the thermodynamics of the various phases in the Fe-C system. The austenite phase has been investigated thoroughly in the last two decades more than a dozen expressions (22-28,30-39) have been proposed for the activity of carbon as a function of composition and temperature.

There are a very large number of reports on the solution behaviour of nitrogen in austenite. Hillert and Jarl(40) have presented an excellent review of all available information and have rationalized them after a rigorous thermodynamic analysis. Agren(26) revised the parameters given by Hillert and Jarl in the light of magnetic contributions to the Gibbs energy.

### 2.5 Ternary Interactions in Fe-M-X Austenites (M=Ti,Nb and X=C,N)

The ternary interactions between substitutional solutes like Mn, Si, Cr, Mo, and Ni and interstitial solutes like C and N have been experimentally studied in the last two decades. However, interactions between solutes Ti and Nb with C and N have not been determined. One of the main objectives of this study has been to experimentally determine the thermodynamic interaction of strong carbide and nitride formers like Ti and Nb with carbon and nitrogen in austenite. Because of this compound forming tendency, these solutes can be expected to interact strongly with carbon and nitrogen. The experimental investigation undertaken in this study confirms such an interaction. Nishizawa et al.(41,42) investigated the solubility of TiC, NbC and VC and reported in CALPHAD XIV(1985) increased solubility at high carbon concentrations. Based on theoretical work and preliminary experiments on Fe-Nb-C system

from this study, increased solubilities of the carbides were also reported in the same meeting by this author. However, further experimentation and theoretical analysis undertaken in this study gave larger values for the interaction between Ti and Nb with carbon compared to those of Nishizawa. Detailed analysis and comparison between the two sets of data will be presented in the subsequent chapters.

## 2.6 Interstitial Compounds

The transition, actinide, and rare earth elements form a number of compounds which have high hardness, high melting points, and metallic properties which make them attractive for use at high temperatures. These compounds are sometimes called "refractory hard metals" because of their metallic properties, "interstitial compounds" because the small non-metal atom occupies the interstitial voids between metal atoms, and "defect compounds" because both metal and non-metal lattices can tolerate atom vacancies in rather large concentrations. The compounds which comprise this group include carbides, nitrides, phosphides, borides, sulphides, and silicides. Of these, mainly carbides and nitrides of transition metals existing in the NaCl(B1) structure will be considered in this study.

### 2.6.1 Constitution Diagrams of Ti-C, Nb-C, Ti-N and Nb-N Systems

The transition metal-carbon diagrams are primarily characterized by the features (a) solid solubility of carbon in metal, (b) solid solubility (almost nil) of metal in carbon, and (c) non-stoichiometric compounds  $M_2C$  and  $MC$  with solid solution ranges. Group IV nitrogen

systems also follow a similar trend but other groups exhibit many nitrides apart from  $M_2N$  and the MN type of compounds.

#### 2.6.1.1 Ti-C and Nb-C systems

The phase diagrams of Ti-C and Nb-C systems as given by Rudy(43) are presented in Figures 2.4 and 2.5. The composition range of interest in this study is 35-50 atom % in Nb-C and 30-50 atom % in Ti-C, which is the range of nonstoichiometry of the carbide phase  $MC_y$ . The structural type of these carbides is cubic B1 (NaCl). There have been many investigations(44-46) of the relationship between lattice parameter and nonstoichiometry and this has been widely used for identifying these compounds. A hexagonal semi-carbide  $Nb_2C$  exists in the Nb-C system whereas the Ti-C system does not exhibit this phase.

#### 2.6.1.2 Ti-N and Nb-N system

The Ti-N phase diagram as given by Hultgren et al.(9) is shown in Figure 2.6. This diagram was taken from the study by McClaine and Coppel(48) with the insertion of the N-rich phase boundary for  $TiN_y$  at  $X_N=0.503$ . Some studies based on the X-ray analysis of alloys prepared by sintering mixtures of magnesium reduced Ti and TiN showed the existence of an fcc  $TiN_y$  phase up to  $X_N=0.512$ . Using thermodynamic analysis and McClaine and Coppel's vapour pressure measurements over  $TiN_y$ , the N-rich phase boundary has been fixed at  $X_N=0.503$  by Hultgren et al.

The Nb-N constitutional diagram proposed by Guard et al.(49) is shown in Figure 2.7. Due to lack of experimental data on the many

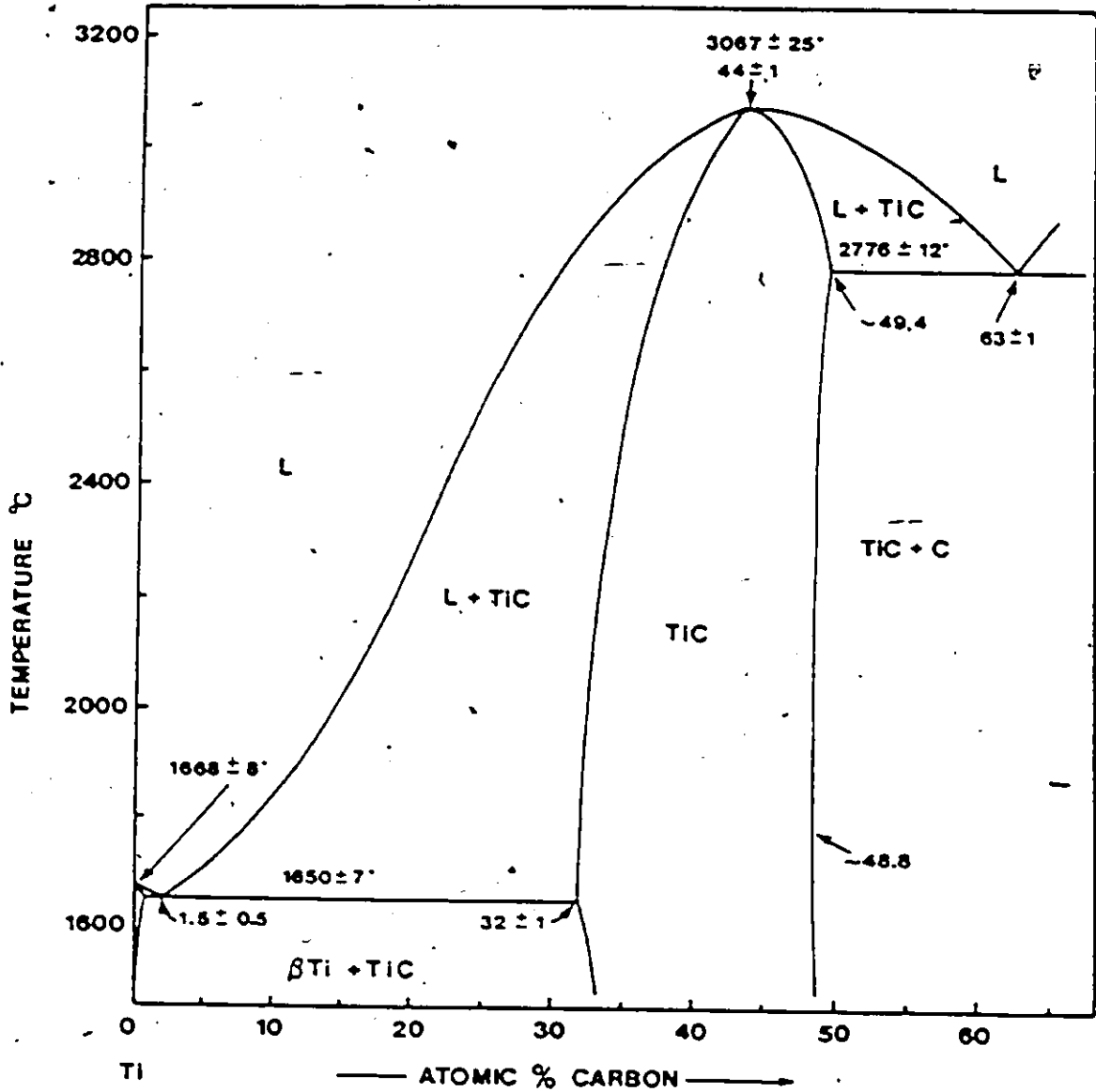


FIG. 2.4 THE Ti-C CONSTITUTION DIAGRAM

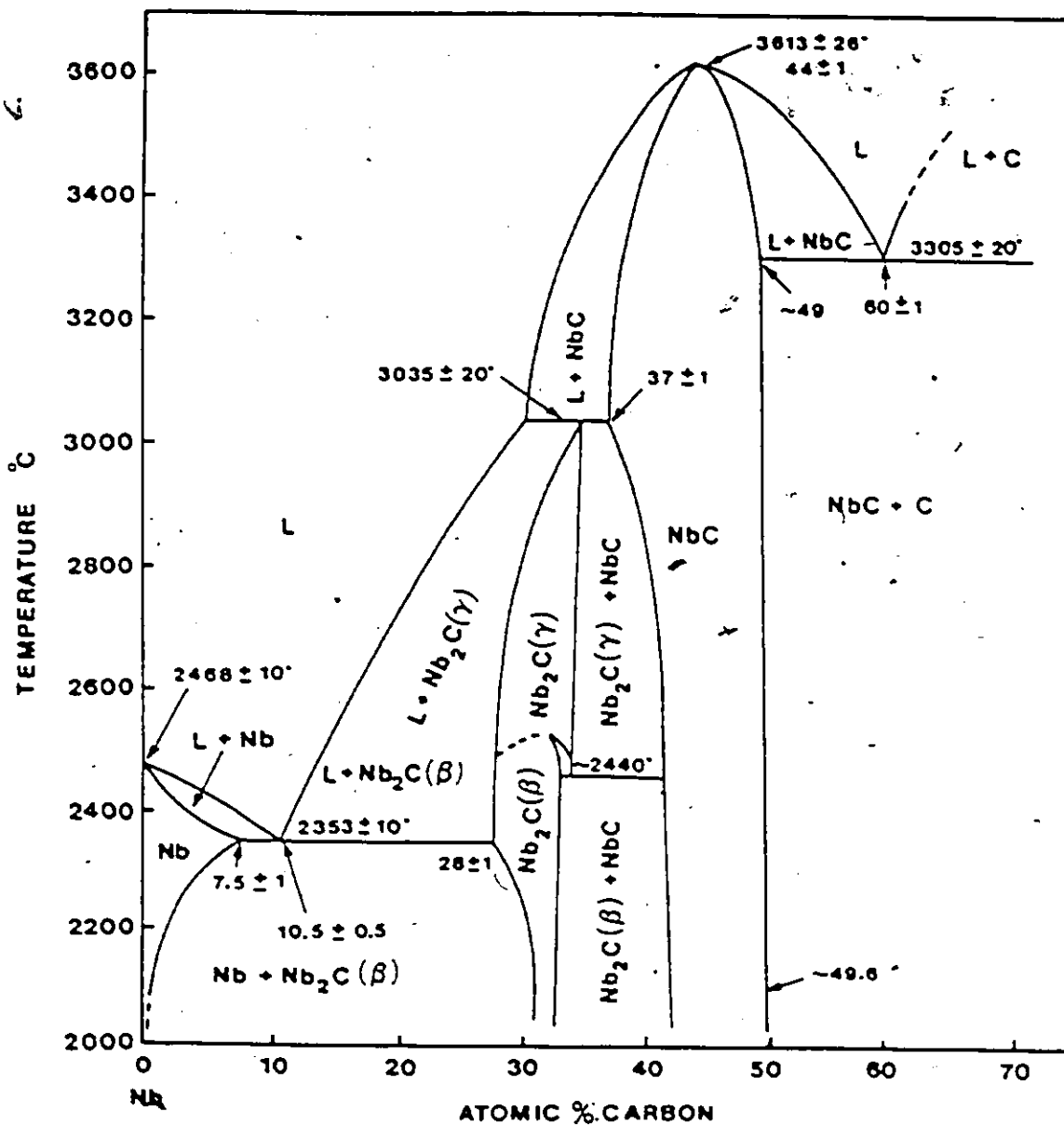


FIG. 2.5 THE Nb-C CONSTITUTION DIAGRAM

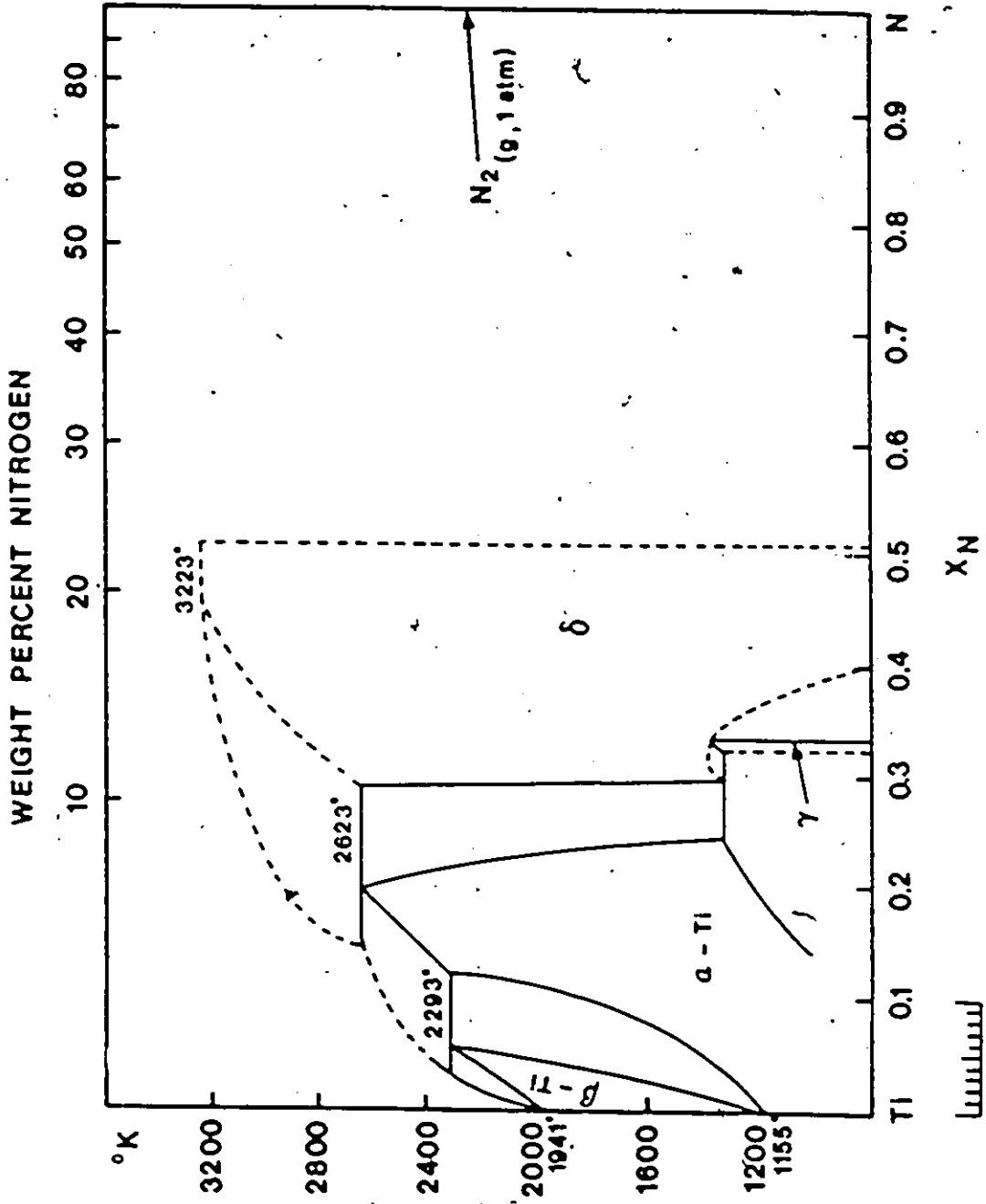


FIG. 2.6 THE Ti-N CONSTITUTION DIAGRAM

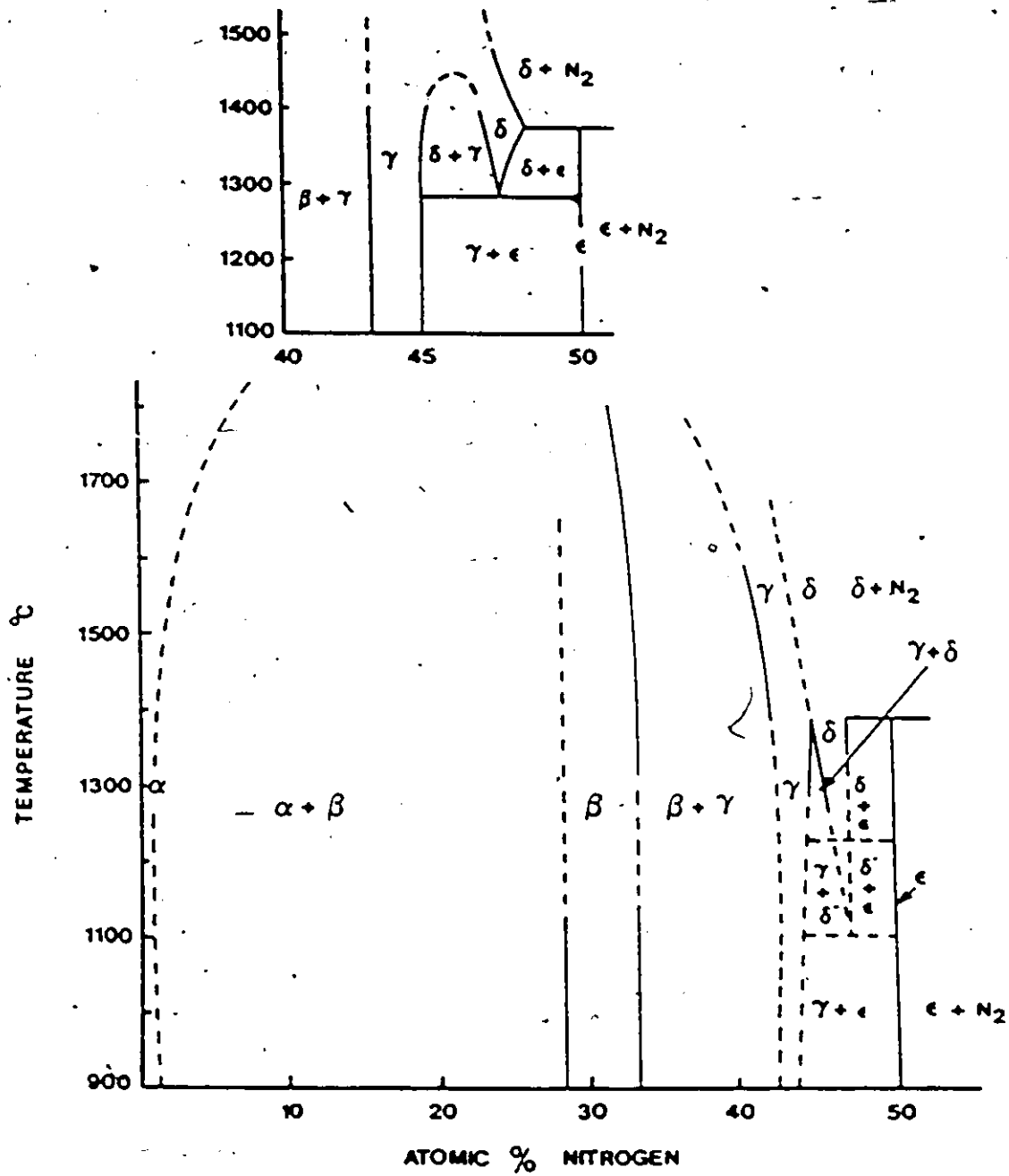


FIG. 2.7 THE Nb-N CONSTITUTION DIAGRAM

nitrides that occur in this system, thermodynamic analysis is not possible. The wide variety of crystal structures exhibited in the composition range 40-50 atom % nitrogen suggests a possible complexity of phases when precipitated in steels. However, only cubic niobium nitrides have been observed in the precipitation studies of HSLA steels. Hence only cubic niobium nitride phase ( $\text{NbN}_{0.8-1.0}$ ) will be investigated in this study.

## 2.7 Thermodynamics of $\text{TiC}_y$ , $\text{NbC}_y$ , $\text{TiN}_y$ , $\text{NbN}_y$ Phases

Phase diagrams are the primary source of thermodynamic information on these systems. Experimental information on the thermodynamics of individual phases is lacking in most of these systems. Some information on the partial molar properties of cubic phases ( $\text{MX}_y$ ) is available from a limited number of vapour pressure, emf, and gas equilibration studies. Most of the experimental information is limited to calorimetric studies of integral properties and heat capacities of essentially stoichiometric carbides and nitrides.

### 2.7.1 Calorimetric Studies

One of the thermodynamic quantities needed to describe the stability of a substance is the entropy. The standard entropy of solids at 298.15 K may be obtained from low temperature heat capacity measurements using the following relation.

$${}^{\circ}S_{298\text{K}} = {}^{\circ}S_{0\text{K}} + \int_0^{298} \frac{C_p}{T} dT \quad (2.1)$$

where  $^{\circ}S$  stands for standard entropy in energy/mole deg $^{\circ}$  units.  $^{\circ}S_{OK}$  is zero for pure crystals.

Very low temperature (1.5-18K) heat capacities of five compositions in the  $NbC_y$  phase field have been measured by Toth et al.(50,51). Other measurements by Geballe et al.(52), Pessall et al.(53), and Caudron et al.(54) are also available. Three more sets of heat capacity measurements are available for the  $NbC_y$  phase and they are very useful in extending the very low temperature data to the vicinity of room temperature. Pankratz et al.(55) determined the heat capacity of  $NbC_{0.996}$  from 51K to 298K. Storms and Sandenaw(56) investigated three compositions in the  $NbC_y$  phase field in the temperature range 7.5 to 320 K. A third investigation by Rempel et al.(57) measured the heat capacities of six compounds in the solution range of  $NbC_y$  and in the temperature range 80-300 K.

There are many investigations(58-64) on the high temperature heat content of stoichiometric  $NbC$  and some hypostoichiometric compositions. Huber et al.(60), Mah and Boyle(62), and Kornilov et al.(64) investigated the standard heat of formation of niobium carbide as a function of composition using combustion calorimetric methods. Storms(47) reviewed all the available information till 1967. Recently Smith, Carlson and de Avillez(65,66) made a comprehensive review of the available information on crystallographic, thermodynamic and constitutional aspects of Nb-C system. Table 2.1 taken from that study lists the standard heat of formation of niobium carbides.

In contrast to the wealth of calorimetric studies on  $NbC_y$  phase,  $TiC_y$  has hardly been investigated. Kelly et al.(67) were the only

investigators of low temperature heat capacities of  $TiC_y$  phase. Their investigation was restricted to the stoichiometric carbide. Naylor(68) measured the heat content of TiC over the temperature range 360-1735 K. Heat content measurements were also made by Pears et al.(69) between 590 K and 2894 K. Their results scatter widely, probably due to the nitrogen impurity levels in their samples.

Calorimetric studies on nitrides are few in number. Pessel et al.(70) determined the heat capacity of TiN in the range 3-25 K while Shomate(71) made measurements from 52K to 297K. Only estimated low temperature heat capacities are available for NbN. Naylor(68), McDonald et al.(72), Neel et al.(73) were the principal investigators of high temperature heat content and heat capacity of stoichiometric TiN. The oxygen bomb calorimetric measurements of Humphrey(74) and Neumann et al.(75) have been considered for tabulation of standard heat of formation values of TiN by Hultgren et al.(9). Morozova and Khernberg(76) were the only investigators to study the heat of formation of the  $TiN_y$  phase as a function of composition.

Most of the calorimetric data on stoichiometric titanium and niobium carbides and titanium nitride have been reviewed by Hultgren et al.(9). Their data for these compounds have been summarized in Table 2.2.

#### 2.7.2 Vapour Pressure, EMF, and Gas Equilibration Studies

There have been a limited number of investigations on the variation of partial molar free energy of components as a function of composition and temperature in the cubic carbides and nitrides of

titanium and niobium. Since these compounds are stable up to very high temperatures (above 3000 K), measurement of vapour pressures has been successfully used to determine the partial molar quantities of the evaporating species of interest. Transition metal carbides and nitrides preferentially evaporate metal atoms at high temperatures (above 2000 K), and hence measurement of vapour pressures allows the direct determination of the metal activity in the nonstoichiometric compound. Principal techniques that are employed for vapour pressure measurements are Knudsen effusion, free evaporation (Langmuir), torsion effusion and mass spectrometry.

As the vapour pressure of metal atoms above the compound is very low at low temperatures (below 2000 K) and for compositions high in carbon content, the abovementioned techniques are not very useful. Gas equilibration (nitrogen gas in the case of nitrides and  $H_2-CH_4$  mixtures in the case of carbides) and EMF techniques lend themselves as alternatives. Gas equilibration has been used in this study to measure the carbon and nitrogen activities as a function of composition and temperature in  $TiC_y$ ,  $NbC_y$  and  $NbN_y$  phases. As the partial pressure of nitrogen over  $TiN_y$  is very low even for compositions close to stoichiometry, that system could not be studied experimentally. However available information in the literature has been reviewed in order to complete the data set. Table 2.3 outlines a summary of experimental investigations of partial molar free energies pertaining to the systems that are of interest in this study.

## 2.8 Thermodynamic Models

Thermodynamic modelling of the aforementioned interstitial compounds is necessary in order (i) to assess the experimental data obtained by different techniques, (ii) to obtain analytical expressions describing the variation of partial molar free energies, (iii) to facilitate extrapolation into uninvestigated and metastable regimes, (iv) to construct self consistent phase diagrams, and (v) to predict ternary and higher order systems. Energy interaction parameters derived from sound solution models also give insight into the nature of bonding between the constituent atoms. Many investigators have analyzed the thermodynamics of these compounds using essentially four main approaches which shall be briefly reviewed in the following sections.

### 2.8.1 Regular Solution Models

The quick and simplest way to analyze any phase is to use a regular solution model. The interaction parameter which describes the excess free energy, if necessary, can be expanded as a power series in composition (subregular formalism) for satisfactory fitting of the data. There are a variety of expressions available for the expansion but the preferred ones should be symmetric with respect to both components. Recently Teyssendier et al., (77) used the Redlich-Kister polynomial with the following expansion for the excess free energy to describe the thermodynamics of the  $TiC_y$  phase.

$$EG_m = X_M X_C \cdot L \quad (2.2)$$

$$L = L_0 + L_1(X_M - X_C) + L_2(X_M - X_C)^2 + L_3(X_M - X_C)^3 \quad (2.3)$$

### 2.8.2 Schottky-Wagner Model

The second approach as followed by Kaufman(78) and Chang(79) has been to treat these binary transition metal carbides and nitrides as defect compounds and to use the Schottky-Wagner(80) model to describe the variation of partial molar free energies. However these compounds are highly nonstoichiometric (eg.  $TiC_y$ ,  $0.6 < y < 1.0$ ) and hence violate the assumption of small deviations from stoichiometry required in the above model. At large deviations from stoichiometry, as in the present case, the free energy to create structural vacancies in the lattice is not constant. Indeed one can obtain the composition dependence of the free energy change due to formation of interstitial vacancies by comparing the expressions from Schottky-Wagner with those from other models that take into account such variations. This comparison has been undertaken in this study and an additional term for Schottky-Wagner expressions has been obtained for treating cases with large variations from stoichiometry.

### 2.8.3 Sublattice-Subregular (Hillert-Staffansson) Model

One of the main features of the transition metal-carbon and metal-nitrogen systems, is that the variation of the partial molar free energies of both components with composition is quite strong, while the integral free energy of mixing does not vary significantly. Moreover the variation of activity of components near the carbon rich phase boundary is quite pronounced. This kind of variation near the stoichiometric composition requires a high power series for satisfactory description, if one adopts a substitutional regular solution model as

outlined in the first approach. This then would result in too many parameters to be determined from limited experimental data. In addition, these carbides and nitrides exist in the B1 (NaCl) crystal structure, with metal atoms forming the fcc lattice and the nonmetal atoms occupying octahedral sites. Since the component atoms occupy different sublattices and hence do not mix, the substitutional solution model is strictly not applicable.

The sublattice-subregular solution model suggested by Hillert and Staffansson(29) is well suited for these phases as it adequately takes care of the above-mentioned characteristics. There are many other advantages inherent in this model. For one thing, this model generally requires fewer parameters to adequately describe the data. The partial molar excess free energy expressions come out as Legendre polynomials and hence are ideally suited for curve fitting. The model uses the free energy of formation of the stoichiometric phase as a reference for the nonmetal which is readily available for the transition metal carbides and nitrides from calorimetric studies. A variety of crystal structure characteristics can be incorporated into the model by appropriate definition of sublattices and hence can be used to treat defect complexes with ease. This particular feature has been of immense use in treating nonstoichiometric oxides like  $Fe_{1-x}O$ ,  $CeO_{2-x}$ , etc., that exhibit complicated and interesting defect clusters(81). Finally this model is easy to extend to multicomponent systems. It has been successfully applied by Kaufman and Agren(82), and Uhrenius(83) to describe the thermodynamics of the  $TiC_y$  phase.

#### 2.8.4 Statistical Mechanical Approaches

There have been a few other attempts to describe the thermodynamics of these interstitial compounds by treating them as a united ensemble of metal and nonmetal atoms. DePoorter(84) and Hoch(85) obtained equations relating activities with composition and temperature by considering nearest neighbour interactions in terms of bond energies. Their models do not take into account the non-ideal entropy contributions and the variation of pair interaction energies with composition. It is interesting to note that the expressions obtained via statistical mechanical considerations are similar to those obtained in Hillert and Staffansson's model. Hence the two approaches can be integrated to gain insight into the nature of bonding in these compounds. In this investigation, equations describing the variation of partial molar free energies have been obtained based on the statistical mechanical treatment of interstitial solutions including the vibrational component of entropy and the variation of pair interaction energies (bond energies) with composition. These pair interaction energies can be related to the interaction parameters in the Hillert-Staffansson model.

#### 2.9 Solubility of Carbides and Nitrides in Iron Austenite

Mutual stability of austenite and transition metal carbides/nitrides has been the subject of many investigations on microalloyed steels. The important features that emerged from these studies are (a) very low solute contents (especially the transition elements Ti, V, and Nb), (b) the precipitates are very fine (50 nm) and

their extraction is difficult and inefficient, and (c) the precipitate phase is generally nonstoichiometric. These features are to be contrasted with the carbide precipitates in other systems like Fe-Cr-C, Fe-Mn-C, Fe-Mo-C etc., which are characterised by relatively high solubilities of stoichiometric carbides.

There have been many experimental determinations(95-117) of the solubility products  $K_{MC} = [M][C]$ ,  $K_{MN} = [M][N]$  etc where  $[M]$ ,  $[C]$ , and  $[N]$  refer to concentrations of transition metal M, carbon, and nitrogen in austenite. One of the earliest determinations and thermodynamic analyses on solubility of carbides and nitrides is that of Narita(95). Narita analyzed his results on solubility in austenite assuming the carbide or nitride to be stoichiometric and the austenite to be devoid of any solute interactions. Many other investigators have also analyzed the solubility on similar lines. The methodology has always been to consider the austenite - precipitate equilibrium in terms of the mass action law viz:



$$RT \ln [a_M a_X] = {}^0G_{MX} \quad (2.5)$$

Assuming ideal/henrian behaviour for the solutes in austenite, the following solubility products have been obtained.

$$RT \ln [X_M][X_X] = \Delta^0 G_{MX} \quad (2.6)$$

$$\log [X_M][X_X] = A + B/T \quad (2.7)$$

where  $[M]$  and  $[X]$  are the weight percents of solutes M and X respectively,  $\Delta G_{MX}^{\circ}$  is the free energy of formation of stoichiometric carbide from 1 wt% standard austenite solution, B and A are approximate constants corresponding to the enthalpy and the entropy of formation of the carbide. A summary of various investigations on the solubilities of niobium and titanium carbides and nitrides is given in terms of the A and B values in Tables 2.4 and 2.5. Some investigators(102,104,105) have showed an improved prediction of solubility of carbides if the carbide is assumed to be  $NbC_{0.87}$ .

There are two main drawbacks in this methodology, namely (a) titanium and niobium are very strong carbide and nitride formers and they interact very strongly in austenite. This results in increased solubility at higher carbon levels, as observed by this author and Ohtani and Nishizawa(41,42); (b) the nonstoichiometry of the carbide together with strong solute interactions rules out the above mass action law analysis.

The overall aim of this study is to gain a complete understanding of the thermodynamics controlling precipitation of carbides, nitrides, and carbonitrides of titanium and niobium in microalloyed steels. Effects due to solute interactions and nonstoichiometry of the precipitating compounds on (a) solubility of the compound, (b) equilibrium austenite composition and (c) mole fraction of the precipitate have been the primary focus of this investigation. Detailed equilibration experiments have been used to determine titanium-carbon, niobium-carbon and niobium-nitrogen interactions in austenite as well as the activity-composition relationships in binary

$TiC_y$ ,  $NbC_y$  and  $NbN_y$  phases. This data together with others in the literature has been analysed using the sublattice-subregular model suggested by Hillert and Staffansson. The experimental procedure and the theoretical analysis undertaken in this study will be outlined in the subsequent chapters.

TABLE 2.1.

Heat of Formation of Niobium Carbides\*\*

y in NbC <sub>y</sub>	-ΔH <sup>o</sup> <sub>298K</sub> *	y in NbC <sub>y</sub>	-ΔH <sup>o</sup> <sub>298K</sub> *
0.489	90.2 ± 3.6	0.861	134.5 ± 2.5
0.500	97.5 ± 2.5	0.889	133.3 ± 1.7
0.500	98.0	0.900	133.1 ± 3.8
0.686	115.9 ± 1.7	0.900	136.8
0.699	116.5 ± 1.7	0.913	133.3 ± 2.5
0.700	112.8	0.935	143.7 ± 5.4
0.739	123.6 ± 2.1	0.945	132.8 ± 3.4
0.783	124.5 ± 2.9	0.979	141.2 ± 1.7
0.786	125.9 ± 5.9	0.980	142.0
0.800	126.7	0.984	138.7 ± 1.5
0.838	125.5 ± 2.1	1.0	141.9

\*\* Compilation by Smith, Carlson and de Avillez(65)  
 \* All values in KJ/Mole of Metal

TABLE 2.2

Free Energy of Formation of Stoichiometric Carbides and Nitrides of Titanium and Niobium

Compound	ΔG <sup>o</sup> = $\overset{o}{G}_{MX} - \overset{o}{G}_M - \overset{o}{G}_X$ (KJ/Mole of Metal)
NbC	- 137.65 + 1.78E-03 T
TiC	- 188.33 + 14.34E-03 T
NbN	- 228.03 + 80.63E-03 T
TiN	- 337.67 + 93.39E-03 T

TABLE 2.3

Experimental Investigations on Partial Molar Free Energies of  
Binary Monocarbides and Nitrides of Titanium and Niobium

Phase	Property Measured	Composition Range	Temperature Range	Expt. Technique	Ref.
TiC	(1) $p_{Ti}$	$0.30 < X_C < 0.50$	1900 K	Vap. Pr	Storms (47)
	(2) $a_C$	$0.41 < X_C < 0.47$	1173-1373 K	Gas Eqn.	Alekseev (86)
	(3) $a_C$	$0.40 < X_C < 0.50$	1273, 1473 K	Gas Eqn.	Grievesson (87)
	(4) $a_{Ti}$	$0.47 < X_{Ti} < 0.60$	1045-1135 K	EMF	Malkin (88)
	(5) $a_{Ti}$	$0.42 < X_C < 0.50$	853 K	EMF	Koyama (89)
NbC	(1) $p_{Nb}$	$0.40 < X < 0.50$	2300-2500 K	Vap. Pr	Storms (90)
	(2) $a_{Nb}$	$0.42 < X < 0.495$	1100-1300 K	EMF	Hong (91)
TiN	(1) $p_{N_2}, p_{Ti}$	$0.45 < X_N < 0.495$	1473-1953 K	Gas Eqn.	McClaine (48)
	(2) $p_{N_2}$	$0.30 < X_N < 0.50$	1273, 1673 K	Gas Eqn.	Grievesson (87)
	(3) $p$	$X_N = 0.45$	2120 K	Vap. Pr.	Linevsky (92)
	(4) $p_{N_2}$	$X_N = 0.44$	2000-2275 K	vap. Pr	Hoch (93)
NbN	(1) $p_{N_2}$	$0.42 < X < 0.50$	1523-1853 K	Gas eqn.	Shchurik (94)

TABLE 2.4

Solubility of Ti/Nb Carbides in Iron Austenite

Compound	T Range	Solubility Product		Ref
		A + B/T = log[%M][%C]		
		A	B	
	1173 - 1473 K	2.90	-7500	de Kazinczy (96)
	1273 - 1573 K	3.18	-7700	Mori (97)
	1323 - 1573 K	3.42	-7900	Narita (98)
	1173 - 1573 K	3.04	-7290	Meyer (99)
	1273 - 1573 K	3.70	-9100	Smith (100)
NbC	1223 - 1323 K	4.37	-9290	Johansen (101)
	1173 - 1473 K	3.11	-7520 *	Nordberg (102)
	1323 - 1423 K	3.31	-7970	Koyama (103)
	1273 - 1523 K	3.40	-7920 *	Lakshmanan (104)
	1173 - 1473 K	2.81	-7020 *	Sharma (105)
	1173 - 1473 K	5.33	-10475	Narita (106)
TiC	1173 - 1473 K	2.75	-7000	Irvine (107)
	1273 - 1523 K	4.03	-8720	Sharaiwa (108)

\* The precipitate was assumed to be NbC<sub>0.87</sub> in the analysis.

TABLE 2.5

Solubility of Ti/Nb Nitrides in Iron Austenite

Compound	T Range	Solubility Product		Ref	
		A + B/T = log[%M][%N]			
		A	B		
	1473 - 1623 K	4.04	-10230	Smith	(109)
	1523 - 1623 K	2.80	-8500	Narita	(95)
NbN	1273 - 1573 K	3.79	-10150	Mori	(110)
	1273 - 1573 K	2.86	-7929 *	Sharma	(105)
	1473 - 1573 K	3.93	-15180	Narita	(111)
	1373 - 1643 K	4.72	-16190	Sawamura	(112)
	1473 - 1573 K	3.82	-15020	Chino	(113)
TiN	1423 - 1623 K	0.32	-8000	Matsuda	(114)
	1173 - 1623 K	5.00	-14400	Roberts	(115)
	1373 - 1623 K	5.19	-15490	Kunze	(116)
	1473 - 1673 K	4.94	-14400	Wada	(117)

\* The precipitate was assumed to be NbN<sub>0.87</sub> in the analysis.

## CHAPTER III

### EXPERIMENTAL PROCEDURE

#### 3.1 Introduction

In this chapter, details concerning the gas equilibration experimentation carried out in this study will be outlined. In the following sections, (i) the experimental technique, (ii) design and construction of the apparatus, (iii) materials and sample preparation, (iv) experimental conditions, and (v) a summary of experiments conducted will be discussed.

#### 3.2 Experimental Technique

One of the principal methods of investigation of thermodynamics of any phase is to obtain a total or a partial equilibration with another phase, thermodynamic properties of which are known and hence are controllable. Since the chemical potentials of carbon and nitrogen can be easily fixed using gas mixtures, steels have traditionally been investigated via gas equilibration methods. The gas equilibration technique has been chosen in this study for the investigation of the thermodynamics of austenite alloyed with niobium and titanium. This technique in both static and dynamic forms has been used by many investigators in the past to study the activity-composition relationships in binary Fe-C and Fe-N austenites as well as ternary austenites. Since the binary Fe-C system is well established, carbon analysis of both binary and ternary samples equilibrated under identical conditions with  $H_2-CH_4$  or  $CO-CO_2$  mixtures provide thermodynamic

information on the carbon activity as a function of composition and temperature in the ternary system. The technique is equally applicable for the investigation of the thermodynamic properties of nonstoichiometric transition metal carbides like  $TiC_y$  and  $NbC_y$ . Nitrogen and nitrogen-inert gas mixtures have been widely used to study the thermodynamic properties of binary nitrogen systems like Fe-N, Nb-N etc and also ternary nitrogen austenites.  $H_2-NH_3$  mixtures are useful at low temperatures (below 550 C) for providing a constant nitrogen potential. However at higher temperatures ammonia dissociates and therefore pure nitrogen or nitrogen diluted in inert gases have to be used for equilibration.

### 3.2.1 Static Equilibration Methods

The static equilibration technique involves equilibration of binary Fe-C samples together with ternary Fe-M-C (M= Mn, Cr, Si, Mo etc.) in quartz capsules sealed with small amounts of hydrogen (usually 100mm Hg). CO-CO<sub>2</sub> mixtures are also attainable in capsules either by intentional addition of CO or CO<sub>2</sub> or by taking advantage of residual oxygen present in evacuated capsules. Since Ti and Nb are strong oxide formers CO-CO<sub>2</sub> atmospheres are not useful in investigating Fe-Ti-C and Fe-Nb-C austenites. Leakage of hydrogen through quartz, reduction of SiO<sub>2</sub> to Si due to prolonged exposure in hydrogen, thermal segregation of hydrogen and methane, and lack of control over carbon potential are some of the drawbacks in static equilibration techniques using H<sub>2</sub>-CH<sub>4</sub> mixtures. Moreover, carbides of titanium and niobium could not be studied easily using the capsule technique as equilibration times are

very long and loss of hydrogen becomes significant. This results in incomplete equilibration.

### 3.2.2. Dynamic Equilibration Methods

In dynamic equilibration methods, the gases comprising the mixtures are metered and hence the carbon or nitrogen potential in the gas can be controlled. By proper choice of flow rates thermal segregation of component gases in the mixtures can be avoided. Since the gas is continuously replenished, problems due to leakage of small quantities of hydrogen through the ceramic working tube is minimised. On the other hand an elaborate leakproof high temperature apparatus together with gas metering and blending equipment and gas cleansing chambers are required.

### 3.2.3 Chemical Analysis

Accurate chemical analysis following equilibration is essential for obtaining the necessary thermodynamic quantities. Carbon contents in the equilibrated samples are usually determined via microcombustion methods, while the Kjeldahl method, spectroscopic methods, and combustion methods are used in nitrogen determination. An alternative technique is to use a microbalance to obtain the carbon or nitrogen content from weight gain measurements. This technique, better known as thermogravimetric analysis (TGA), is extensively used in oxidation and sulphidation studies. Dunwald and Wagner(118) used the microbalance in their classic study on the thermodynamics of ferrite in the Fe-C system. A sensitive microbalance is ideally suited for continuously monitoring

small weight changes and hence the attainment of equilibrium can be firmly established once the weight change with time becomes negligible. A modern CAHN 1000 microbalance with capabilities of lifting large sample weights (lifting capacity 100 gms) and very high sensitivity (1 microgram weight change) together with a dynamic gas equilibration system has been used in this study. Details regarding the design and construction of the experimental apparatus will be described in the succeeding section.

### 3.3 Experimental Apparatus

The experimental apparatus consists of five parts, namely, gas metering and blending system, gas cleaning furnaces and chambers, high temperature furnace assembly for equilibration, the electrobalance for weighing, and finally a vacuum system for evacuation. A schematic of the apparatus is given in Figure 3.1.

#### 3.3.1 Gas Metering and Blending System

The gas metering and blending system comprises four mass flow controllers which are electronically operated using transducers that control the opening of the solenoid valves. These controllers perform better than rotometers as the feedback mechanism maintains the flow at a preset value even in the event of pressure or temperature fluctuations. Each of the flow controllers was calibrated for a particular gas or gas mixture and the performance of the controllers was checked with another identical system which had been independently calibrated. The Matheson Dyna Blender was used for fixing ratios in gas mixtures. This blending

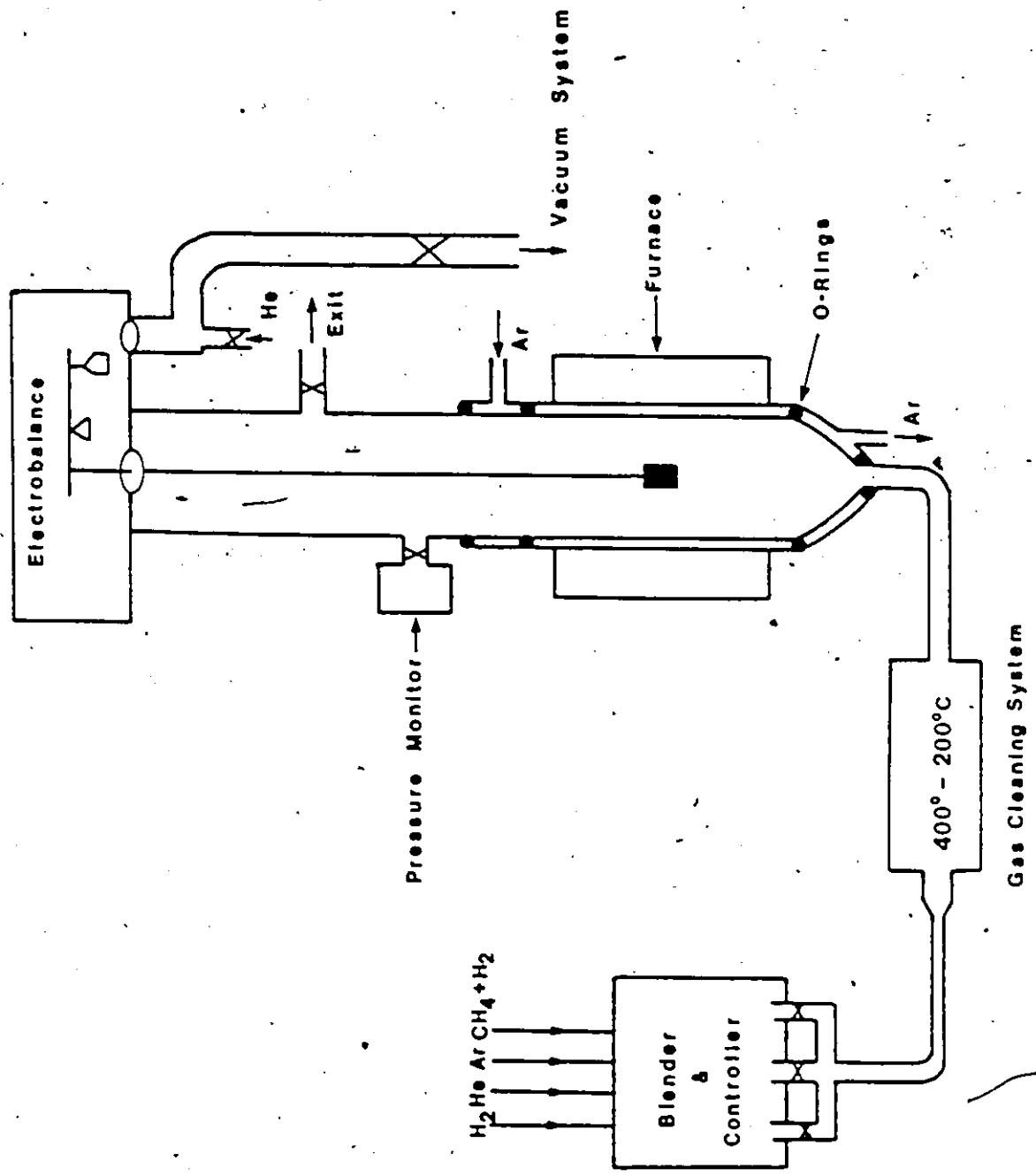


FIG. 3.1 A SCHEMATIC OF THE EXPERIMENTAL APPARATUS

system efficiently mixes two or more gases (up to a maximum of four per blending unit) at preset ratios by controlling the flow rates of individual gases. The ratio(s) of the component gases in the mixture that is delivered is held constant at all total flow rates and pressures and hence the carbon/nitrogen potential in the gas is held constant for days at a time. The blending system also allows one to obtain a wide range of ratios of two gases.

Investigation in the austenitic temperature range requires methane/hydrogen ratios ranging from  $1.0E-05$  to  $1.0E-02$ . Since methane levels corresponding to these ratios are very low, pure methane and hydrogen cannot be mixed to obtain these ratios and hence premixed methane-hydrogen mixtures are required. High purity (Matheson primary standard) gases/gas mixtures, namely hydrogen, helium, 1% methane in hydrogen, and 50ppm methane in hydrogen were used as primary gases for obtaining the required methane-hydrogen ratios for equilibration. Nitrogen and 1% nitrogen in helium and helium were used as primary gases for obtaining partial pressures of nitrogen ranging from  $1.0E-03$  to 1.0 atm. Helium was used as the inert gas diluent, for very high purity grades are readily available and the basic impurity in helium is hydrogen which is already in the system as a major component in the carburizing mixture. Argon, on the other hand, contains higher levels of moisture and oxygen as impurities compared to helium. The gases were delivered just above one atmosphere (1.05 atm.) in order to sustain the flow through the packed beds containing various gas cleaning reagents and these shall be discussed in the next section.

### 3.3.2 Gas Cleaning System

Titanium and niobium are strong oxide formers and hence the presence of small amounts of impurities like moisture, oxygen, and carbon dioxide in the equilibration gas can cause oxidation of the sample. Partial pressures of these impurities below  $1.0E-20$  are required for satisfactory carburization and nitridation of the sample. These impurities have been removed from the gas stream in three stages. The moisture in the gas is initially reduced by passing it over a packed desiccant bed containing silica gel, anhydrous calcium chloride and anhydrous phosphorous pentoxide. In the second stage copper turnings held at 400 C in a two zone furnace were used to remove oxygen down to  $1.0E-10$  or so. Further reduction of oxygen partial pressure has been achieved by passing the gas over very fine copper particles in a commercial getter called Ridox held at 180 C in the second zone of the furnace. Since hydrogen is present in large quantities most of the oxygen is converted to water vapour in the presence of the finely divided copper catalyst. This moisture is again absorbed from the stream using granulated phosphorous pentoxide. In the final stages the gas is made to pass over hot iron sponge held at 450-500 C near the bottom end of the equilibration furnace. Since the carbon potential of hydrogen-methane mixtures decrease exponentially with temperature, the carbon loss from the gas to the iron sponge is negligible. However, any residual oxygen or water vapour present in the system should be removed to fairly low levels. The oxygen partial pressure at the working temperature of 1273 K was measured using solid electrolyte sensors and it was found to be less than  $1.0E-20$ .

In order to minimize the number of joints and fittings which are potential leak spots, and to allow enough residence time for the gas stream in the two zone gettering furnace, the whole gas cleaning system was made from one long quartz tube of about 130 cms in length and 3.0 cm in diameter. The fairly large diameter reduces the linear velocity of the gas and the long length allows enough time for the gas to heat up and cool down to the required temperatures. Alumina balls were used as separators between various zones and dessicants. The desiccants were kept in appropriate cooler regions in the tube. Titanium or zirconium could not be used as getters as they remove unacceptable amounts of carbon from the gas and hence alter the input gas ratio. Palladium cells could not be used to clean hydrogen gas mixtures as methane is efficiently removed by the cells.

### 3.3.3 Equilibration Furnace Assembly

The equilibration experiment was carried out in a vertical high temperature furnace heated by molybdenum disilicide elements. Since dynamic weight change measurements are made, magnetic fields that could be produced by elements carrying high currents must be avoided. This has been achieved by using U-shaped elements and by mounting them vertically. No net magnetic field is produced by the elements in this configuration and no weight difference was found for trial samples weighed in the presence and absence of current in the heating elements.

A pair of concentric recrystallized alumina tubes was used to provide the working chambers. An alumina tube of about 36 inches long and 2.75 inches in internal diameter served as the outer tube, while

another alumina tube of 42 inches in length and 2.25 inches in internal diameter served as the working chamber for equilibration. Argon was circulated in between the two tubes for minimising any permeation of oxygen from the atmosphere through the tubes at high temperatures. The inner tube was connected on one end to the quartz tubes delivering the gas mixture from the gettering furnace, and on the other end to the pyrex flow-through tube attached to the electrobalance assembly using water cooled O-ring fittings. The temperature inside the furnace was controlled within 1 K by regulating the power supply using an automatic feedback control system. The actual temperature inside the working chamber was measured many times using standardized platinum-platinum rhodium (type B and R) thermocouples under actual flow conditions and the furnace setting temperatures were calibrated for obtaining the required equilibration temperature in the hot zone. A 10 cm. long hot zone (temperature variation within 1 K) could be obtained and this length was more than sufficient for equilibrating samples, the dimensions of which never exceeded 4.0cm.x3.0cmx0.02cm. A array of staggered alumina baffles was placed on a pedestal (a short alumina tube) at the bottom of the working tube for efficiently preheating as well as mixing the gas before it enters the hot zone area. These baffles also served as radiation shields. A circular alumina disc with a half inch hole in the center was used as a radiation shield for the upper end of the working tube. The hole was needed for allowing the platinum wire suspending the sample in the hot zone to pass through.

### 3.3.4 Electrobalance Assembly

The Cahn Electrobalance used in this study was mounted on a sturdy steel frame three feet above the equilibration furnace tube. The pyrex flow-through tube from the balance assembly, as mentioned in the previous section was connected to the alumina tube of the equilibration furnace using water cooled O-ring joints. In order to protect the balance from hot gases emanating from the furnace tube, helium was admitted into the weighing chamber through a port at the bottom of the chamber. The helium gas from the chamber and the equilibration gas mixture from the furnace tube were made to exit through a port in the pyrex flow through tube located midway between the furnace and the balance.

Vibrations are a serious problem when small weight change measurements are required. The Cahn 1000 balance was equipped with an electronic filter that could suppress the random background noise to a great extent. However, care was taken to avoid excessive build up of vibrations. The sturdy steel frame supporting the balance was placed on a vibration isolation system. This vibration isolation system is made up of blocks of different materials so that both the frequency and the amplitude of the vibrations in the laboratory environment could be attenuated. Concrete, styrofoam, and wood were placed one above the other to form a basement. Inflated paddings are well known for absorbing vibrations and an array of twenty four tennis balls arranged (glued) on the basement was found to be adequate for that purpose. A 1/8 inch steel sheet placed on these tennis balls acted as a flat bottom for the steel frame.

The performance of the balance was checked under three different

conditions (air, vacuum, and flow conditions at room temperature and high temperature) before actual experiments were conducted. Special calibration weights certified by NBS, Washington were used for checking the consistency and reliability of the readings obtained from the balance control unit. The weight of dummy samples (approximately 1 gram) in air could be measured up to an accuracy of 5 micrograms. Under conditions of vacuum, a higher accuracy of about 2.5 micrograms could be obtained. In the presence of gas flow the accuracy was again 5.0 microgram, but the sample weight decreased due to buoyancy effects. The decrease was less than one milligram in a one gram sample. Since only weight change and not the total weight has to be accurately measured in this study, the buoyancy effect is negligible. For example if a Fe-Ti sample weighing one gram before equilibration, gains a weight of two milligrams after a carburizing run, the carbon content would then be  $(2 \times 100) / (1000 + 2 + x)$  where  $x$  is the correction for buoyancy effects. Since the buoyancy effects result in a weight decrease of less than one milligram ( $x < 1$  mg), the error in carbon content due to neglecting the same would be in the fourth decimal place., i.e., in the above example, the carbon content would be  $0.1995 \pm 0.0001$  wt%.

### 3.3.5 Vacuum System

A diffusion pump backed by a mechanical pump has been used for evacuating the system before the experimental run. The system had to be evacuated for removing occluded gases and other gases adsorbed on desiccants, etc. A special large diameter port at the bottom of the balance chamber was connected to the pump assembly. Bellow valves in

the connecting tube isolated the system from the pump during experimentation. The vacuum levels achieved during evacuation were monitored using an ionization gauge mounted near the balance. Since the system has a large volume and also contains large quantities of dessicants and other gas cleaning reagents initial evacuation was done for an extended period of time(nearly 2 days).

### 3.4 Materials and Sample Preparation

#### 3.4.1 Materials

The starting materials for making the Fe-Ti, Fe-Nb alloys were high purity iron slugs (99.995%) and high purity titanium (99.95%) and niobium (99.95%) wires of about 0.25 mm in diameter. For making alloys of very low solute contents (less than 0.01wt%) special ultra high purity iron (99.999%) was used. Pure (99.95%) titanium and niobium foils(25 microns) were used for the investigation of Ti<sub>3</sub>Cy and Nb<sub>3</sub>Cy phases. These materials were supplied by Alfa Products, Danvers, Mass., USA.

#### 3.4.2 Fe-Ti and Fe-Nb Alloy Preparation

To begin with, Fe-Ti and Fe-Nb master alloys containing 1 wt% Ti and 1 wt% Nb were prepared by melting the requisite amount of component metals in an argon arc furnace. The master alloys were melted and solidified four times in order to achieve homogeneity. They were then rolled into discs of about an inch in diameter for chemical analysis using emission spectroscopic techniques. Three to four spots were made and there was no significant difference in the analysis. The impurities

present in a typical alloy are listed in Table 3.1. Fifteen alloys ranging from 0.005 wt% to 1.0 wt% solute (Ti or Nb) were made from pure iron and the master alloy. These alloys (approximately 20 grams each) were melted and solidified similar to the master alloys. In addition, these alloys were rolled, then broken into pieces and melted many times to ensure complete homogeneity. Emission spectroscopy gave the composition as well as confirmed homogeneity of the sample.

### 3.4.3 Specimen Preparation

The specimens for equilibration were prepared from alloys rolled down to a thickness of approximately 0.10-0.15 mm (100-150 microns). Rectangular specimens measuring approximately 4.0cmx3.0cmx0.01cm were cut from the rolled foil. A typical specimen close to these dimensions weighs about a gram which is a suitable weight for carburization. However nitrogen levels are lower by an order of magnitude in steels. Hence eight to ten foils measuring the same dimensions and greater balance sensitivity (100 microgram weight change range) were used to enhance the resolution. A very small thickness was necessary to reduce the equilibration times. However, below 150 micron thickness, solid state diffusion of carbon is no longer rate controlling in the case of carburization. The low partial pressure of methane in the gas mixture results in surface adsorption of carbon being the rate controlling step. Moreover, further reduction in thickness reduces the sample weight and the weight change due to carbon. This results in lowering the accuracy of carbon content determination. The same arguments apply in the case of nitridation below  $1.0E-02$  atmospheres of nitrogen.

The ten best specimens from fifteen alloys in each system were selected for equilibration. It was made sure that the samples covered the whole range 0.005 wt% to 1.0 wt%. The selected specimens were cleaned in acetone and methanol to remove grease and other contaminants. They were then cleaned in dilute hydrochloric acid to remove any trace of surface oxides. Prior to actual equilibration all the specimens were annealed in pure hydrogen at 1000 C for 10 hours to remove any residual carbon, nitrogen, and oxygen impurities. They were then checked under the SEM for any trace of surface oxides. A long platinum wire of approximately 0.04 cm. in diameter was used for suspending the sample in the hot zone from the balance hook.

#### 3.4.4 Titanium and Niobium Specimen Preparation

In the case of carburization and nitridation of pure titanium and niobium, high purity (99.95) foils (10 microns thick) were obtained from the manufacturers. There were analyzed for metallic impurities and none was found to be above 250 ppm. Rectangular specimens measuring 3.0cmx3.0cm were cut from these foils. A typical titanium specimen of these dimensions weighs about 40 milligrams while a niobium specimen weighs about 80 milligrams. Carbon and nitrogen contents go up to 10 milligrams (close to stoichiometry). A single specimen is sufficient to access many carbon or nitrogen potentials for a given temperature. Since the carbides and nitrides are ceramic, the specimen tends to disintegrate after about five equilibration runs. New samples were introduced whenever the sample disintegrated. Compacted powder pellet specimens of approximately 1 cm in diameter and 3mm in thickness were

also tried, but the inner core of the specimen took a very long time (15 days) for one equilibration run. This was due to sintering of the outer layers which effectively sealed the pores and prevented the gas from reaching the inner layers. Hence foil specimens were used even though they lasted for only a few equilibration runs.

### 3.5 Experimental Conditions

#### 3.5.1 Temperature and Pressure

The equilibration was performed under isothermal and isobaric conditions. Excellent temperature control ( $\pm 1$ K) was possible because of a thyristor based automatic feed back control system that regulated the power input to the furnace. The equilibration experiments in the Fe-Ti-C, Fe-Nb-C, Ti-C and Nb-C systems were conducted at 1273 K, 1373 K, and 1473 K and the Fe-Nb-N system was investigated at 1373K, 1473K and 1573 K. The NbN<sub>y</sub> phase was studied at 1573 K, 1623K and 1673 K. The total pressure in the system under flow conditions was just above 1 atmosphere. The actual pressure in the system was continuously measured using a pressure transducer. The transducer operates between 1.0-1.3 atmosphere, and this pressure range is measured as millivolts on a 0-100 scale. This gives a resolution of 0.0015 atmosphere per millivolt and hence the total pressure of the system can be accurately determined. All the equilibration experiments were conducted at a total pressure of 1.05 (0.01) atmospheres. The gas blending system was preset to deliver at this pressure at all temperatures and ratios of gas mixtures.

### 3.5.2 Flow Rate

The total flow rate of all gas mixtures was fixed at 500 cc per minute. Two factors were taken into consideration in arriving at this value, viz., thermal segregation and residence time. Thermal segregation (separation of heavier and lighter gas molecules in the presence of a temperature gradient) is a serious problem at low flow rates (linear velocity less than 0.6 cm/s). Low flow rates also increase the time for equilibration since the surface adsorption is the rate controlling step for very thin specimens as used in this study. At high flow rates two problems arise, viz., (i) turbulence sets in due to rapid expansion of large quantities of gas near the hot zone which results in reduced accuracy in weight change measurements and (ii) there is too short a residence time for the gases in the gas cleaning chambers and in the hot zone. This short residence time results in the gas not being well purified and the gas not heating up to the equilibration temperature. Hence an optimum flow rate of 500 cc per minute was arrived at after many trial runs.

### 3.5.3 Preliminary Experimental Procedures

Prior to each experimental run, evacuation of the whole system is carried out using a mechanical pump down to about  $1.0E-02$  torr. The system is then flushed with argon and evacuated again and this procedure is repeated three or four times. In order to remove the occluded gases in the furnace chambers and other areas, the system is heated to about 200 C in the presence of flowing helium and subsequently evacuated to less than  $1.0E-06$  torr using a diffusion pump. The system is checked

for leaks by observing the pressure increase with time over a 24 hour period. Since the experiments are conducted at a slight positive pressure (1.05 atm.), leakage into the system is negligible. This has been checked by filling the system with helium and observing the joints and the ceramic tube for leaks using a mass spectrometer. The only problem is during the replenishment of dessicants and other gas cleaning reagents which bring in some adsorbed oxygen and moisture due to their large surface area. Therefore after every replenishment, the system is put under vacuum at  $1.0E-06 - 1.0E-04$  torr for 2 days to remove most of these trace impurities.

The actual experimental run is begun with helium flowing steadily at 500 cc per minute and the zero weight of the sample is measured after allowing sufficient time for the balance control unit to attain a steady state. The gas cleaning furnaces are then switched on. The temperature of the equilibration furnace is slowly raised to the required level. This initial heating takes roughly four hours. Any change in weight of the sample is due to heating and also due to loss of any trace impurities. Pure hydrogen is passed into the chamber and the sample is allowed to attain a constant weight. This weight is taken as the dynamic zero point. The equilibration experiment is then started by introducing carburizing or nitriding mixtures. The change in weight is continuously recorded on a chart recorder.

An appropriate range is chosen for recording the weight change. In the case of carburizing, a 1 gram sample picks up 1mg to 10mg of carbon when carburized to attain 0.1 to 1wt% levels. The balance control unit set to the 1mg range (measured as 100 divisions) gives a

resolution of 0.01 mg per division on the chart recorder. If the weight change goes above 1 mg the automatic range expander facility in the balance control unit resets the weight to zero by taring(counterweighing). Hence a weight change of 10mg. could be determined to an accuracy of 0.01mg. In the case of nitriding experiments, the weight change for a one gram sample is from 0.02mg to 0.2 mg corresponding to 20 ppm to 200 ppm nitrogen levels. To improve the resolution, the balance was set in the 100 microgram range and three 1 gram samples were used. The 100 microgram range is measured on the chart recorder on a scale of 100 divisions. This gives a theoretical limit of 1 microgram but in practice a resolution of 5 microgram was achieved. The reduction in resolution stems from the background noise generated due to the gas flow, vibrations and electronics in the control unit.

### 3.6 Summary of Experiments

In order to test the performance of the system as a whole, a pure Fe sample was carburized at 1273 K. The data generated in this study shows excellent agreement with the classic studies on this system by Smith(120). The results on binary Fe-C austenite is given along with the ternary systems in the next chapter. Ten Fe-Ti and Fe-Nb alloys with solute composition ranging from 0.005 wt% to 1.0 wt% were equilibrated with methane - hydrogen mixtures at 1273 K, 1373 K, and 1473 K. The gas ratio's were chosen so as to give carbon levels ranging from 0.1 wt% to 2.0 wt%. Carbon levels below 0.1 wt% were not accessed as the minimum in the solubility curve occurs around 0.4-0.5 wt%, and one

aim of this study was to obtain more data points near the minimum.

The Fe-Nb-N austenite was investigated in the temperature range 1373K - 1573 K. This system, unlike the carbon ternaries does not show any minimum in the solubility of the nitride. This is anticipated, as the amount of dissolved nitrogen is an order of magnitude smaller compared to that of carbon. However using the sensitive balance, the increase in the nitrogen content due to the addition of Nb to Fe austenite has been measured and the ternary Nb-N interaction in austenite has been determined to a reasonable degree of accuracy. The Fe-Ti-N austenite was not investigated in this study as the solubility of TiN<sub>y</sub> in austenite is very low even at 1473 K. The existing solubility product determinations in the literature scatter widely as shown in Table 2.5. In fact a fairly accurate determination of the solubility product was obtained from theoretical predictions as will be shown in subsequent chapters.

The binary TiC<sub>y</sub> and NbC<sub>y</sub> phases have been investigated using the same gas mixtures. However the lowest composition that could be attained was around  $y = 0.85$ . This composition corresponds to the lowest carbon potential experimentally achievable using gas mixtures. The NbN<sub>y</sub> phase has also been investigated. This phase has a narrow stability range and the investigation was limited to three temperatures 1573K, 1623K and 1673K and  $0.8 < y < 0.95$ . The experimental results obtained in this study are given in the next chapter.

TABLE 3.1

Impurity Contents in Fe-Nb and Fe-Ti Alloys\*\*

C	< 0.5 ppm	
N		
O	< 0.5 ppm	
Cu	< 10 ppm	
Ni	< not detected *	
Co	< 5 ppm	
Mn	< 50 ppm	\$\$
Cr	not detected *	
V	not detected *	
Mo	not detected *	
W	not detected *	
Ti	< 5 ppm	
Sn	< 10 ppm	

Al, Pb, Zr, Sb, Ca, Mg, Ce, B, P, S Not detected \*

\* Not detected refers to levels less than 1 ppm

\*\* Total impurity contents not more than 75 ppm

\$\$ Principal impurity

TABLE 3.2

Composition of Fe-Nb Alloys

	Wt% Niobium **	
(1)	0.005 %	( $\pm 0.0007$ )
(2)	0.010 %	( $\pm 0.0005$ )
(3)	0.019 %	( $\pm 0.0005$ )
(4)	0.037 %	( $\pm 0.0007$ )
(5)	0.054 %	( $\pm 0.001$ )
(6)	0.070 %	( $\pm 0.002$ )
(7)	0.092 %	( $\pm 0.0005$ )
(8)	0.185 %	( $\pm 0.002$ )
(9)	0.230 %	( $\pm 0.002$ )
(10)	0.368 %	( $\pm 0.002$ )
(11)	0.560 %	( $\pm 0.005$ )
(12)	0.74 %	( $\pm 0.02$ )
(13)	0.93 %	( $\pm 0.01$ )

\*\* The numbers in the brackets refer to the spread of compositions around the mean when measured using emission spectroscopy at four different spots on the sample.

TABLE 3.3

Composition of Fe-Ti Alloys

	Wt% Titanium **	
(1)	0.004 %	( $\pm 0.0015$ )
(2)	0.0095%	( $\pm 0.0015$ )
(3)	0.017 %	( $\pm 0.0015$ )
(4)	0.030 %	( $\pm 0.002$ )
(5)	0.041 %	( $\pm 0.001$ )
(6)	0.049 %	( $\pm 0.001$ )
(7)	0.061 %	( $\pm 0.003$ )
(8)	0.084 %	( $\pm 0.002$ )
(9)	0.102 %	( $\pm 0.002$ )
(10)	0.20 %	( $\pm 0.01$ )
(11)	0.34 %	( $\pm 0.01$ )
(12)	0.53 %	( $\pm 0.01$ )
(13)	0.84 %	( $\pm 0.003$ )
(14)	0.95 %	( $\pm 0.05$ )

\*\* The numbers in the brackets refer to the spread of compositions around the mean when measured using emission spectroscopy at four different spots on the sample.

## CHAPTER IV

### EXPERIMENTAL RESULTS

#### 4.1 Introduction

In this chapter the salient features involved in the gas equilibration experiments in Fe-Nb-C, Fe-Ti-C and Fe-Nb-N systems will be briefly described. The results obtained from these experiments systems will be tabulated. The errors associated with these results will also be discussed.

#### 4.2 Results for the Fe-Nb-C and Fe-Ti-C Systems

As mentioned in the previous chapter ten alloys with compositions ranging from 0.005 wt% Nb or Ti have been equilibrated under hydrogen - methane mixtures. The equilibration experiments were carried out in two stages. Initially all the ten alloys along with a pure Fe sample were simultaneously equilibrated to various levels of carbon ranging from 0.1 Wt% C to 2.0 Wt%. The carbon contents were determined by weighing the samples before and after equilibration. These 'simultaneous' equilibrations runs were performed to determine the austenite - carbide phase boundary (solubility limit) as a discontinuity in the variation of the carbon content as a function of Nb or Ti content for a given carbon potential. Once the solubility limit is known, five compositions, four lying in the single phase austenitic region and the fifth lying in the two phase region but close to the solubility limit were then chosen for 'individual' equilibration. These equilibration experiments were performed for accurately determining the increase in

the carbon content due to the addition of Nb or Ti via dynamic weight change measurements. The carbon potentials used in the 'simultaneous' runs were repeated for these five compositions. The equilibration was accessed from both higher and lower potential sides.

The increase in carbon content is measured as the difference in the total carbon contents of the ternary and binary samples. The carbon content in the binary Fe-C alloy is obtained from the equilibrated Fe sample as well as an extrapolation of the carbon levels of the ternary alloys. If there is a discrepancy between the two measurements, the experiments on the four alloys lying in the austenite region together with the Fe sample were repeated until concurrence is obtained. This concurrence is necessary as it will be shown in the Chapter VI that the binary carbon level and the increase above this level due to ternary additions are the two most important quantities needed for the determination of the ternary interaction parameter. In the case of carbon austenites, the increase in carbon content over and above the binary level is significant (i.e., above 50ppm) at carbon levels greater than 0.8% and at higher temperatures (1373K and 1473K). In order to obtain more data points for the determination of the ternary C-Nb and C-Ti interaction parameters from these carbon content measurements, equilibration was performed at four or five potentials above 0.8 Wt%. The increase in carbon contents were substantial (as high as 0.01 - 0.1 Wt%) and they could be determined to a high degree of accuracy (errors less than 3-5% of the value). The carbon contents of equilibrated Fe-Nb-C and Fe-Ti-C alloys at various carbon potentials are listed in Tables 4.1 - 4.6 as well as illustrated in Figures 4.1 - 4.6.

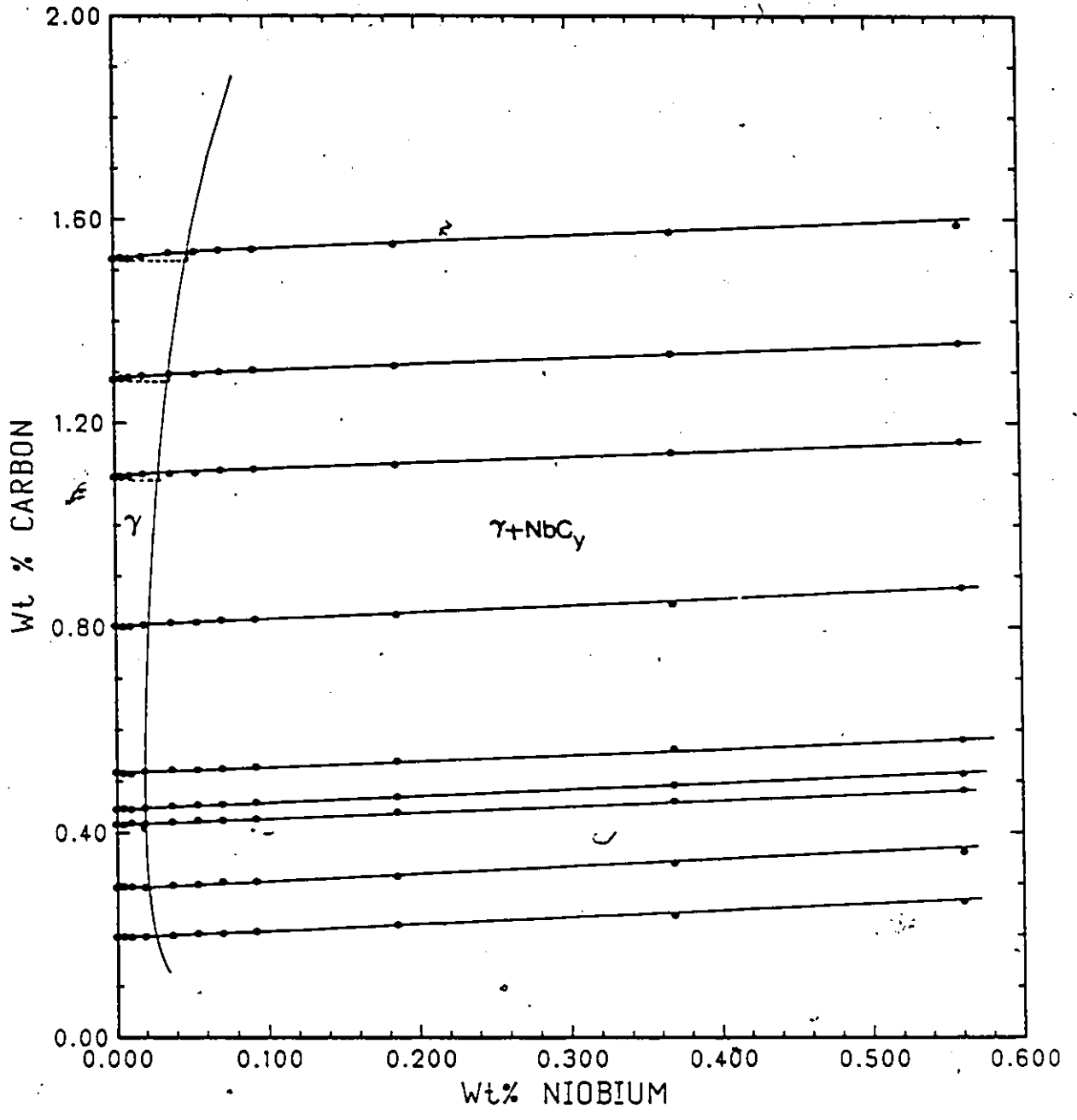


FIG. 4.1 CARBON CONTENTS OF EQUILIBRATED Fe-Nb-C ALLOYS (T=1273K)

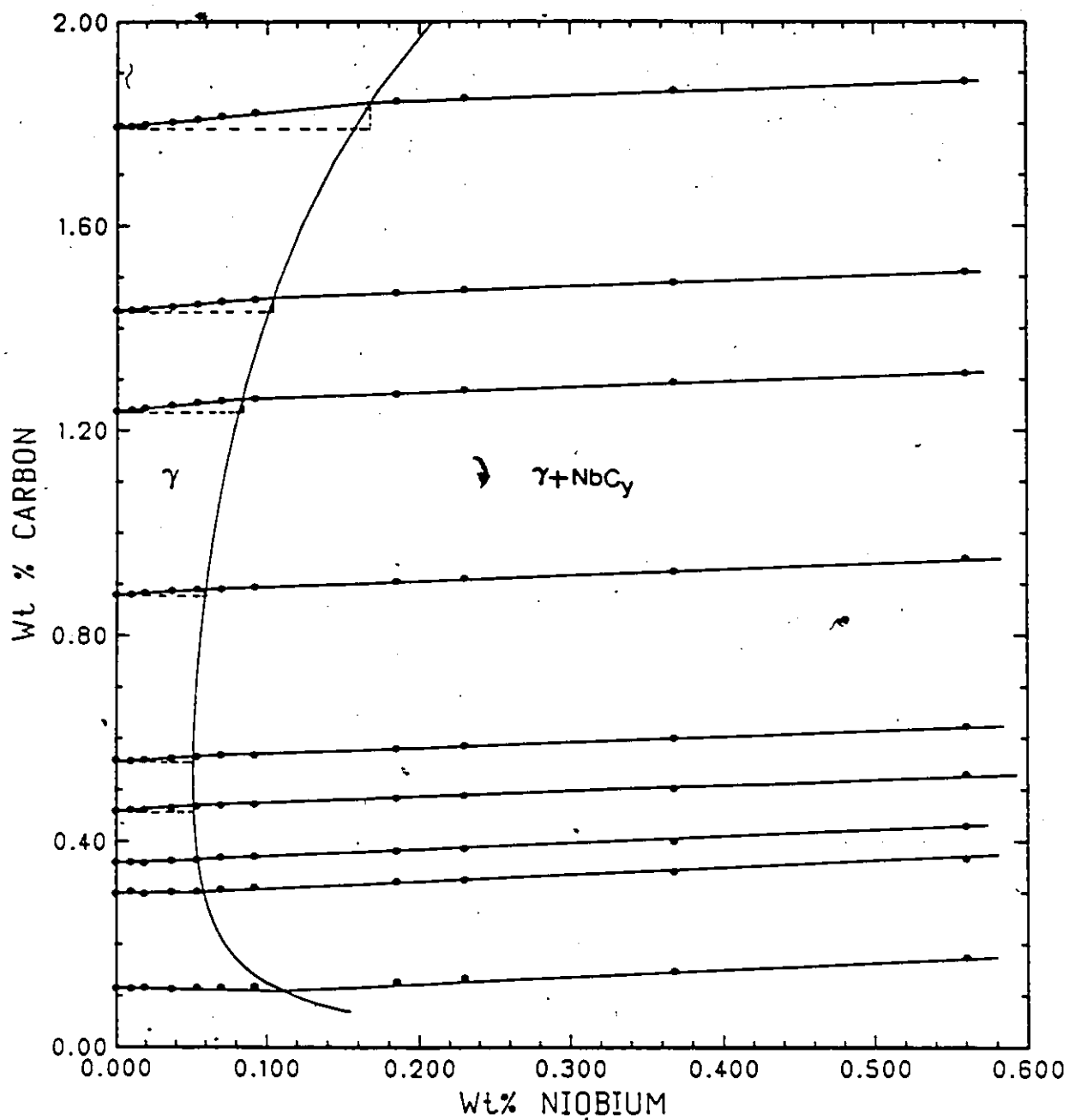


FIG. 4.2 CARBON CONTENTS OF EQUILIBRATED  
Fe-Nb-C ALLOYS (T=1373K)

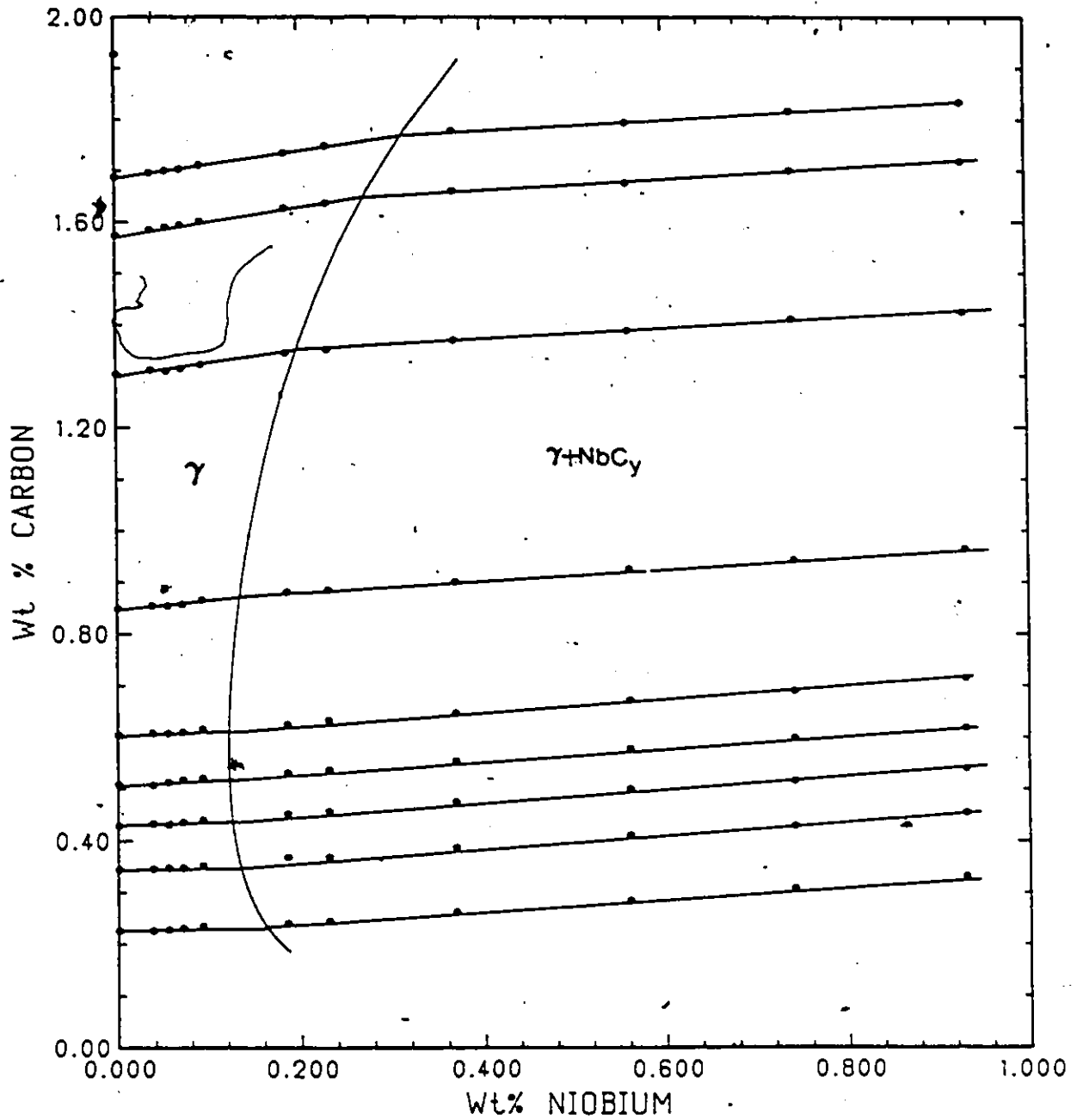


FIG. 4.3

CARBON CONTENTS OF EQUILIBRATED  
Fe-Nb-C ALLOYS (T=1473K)

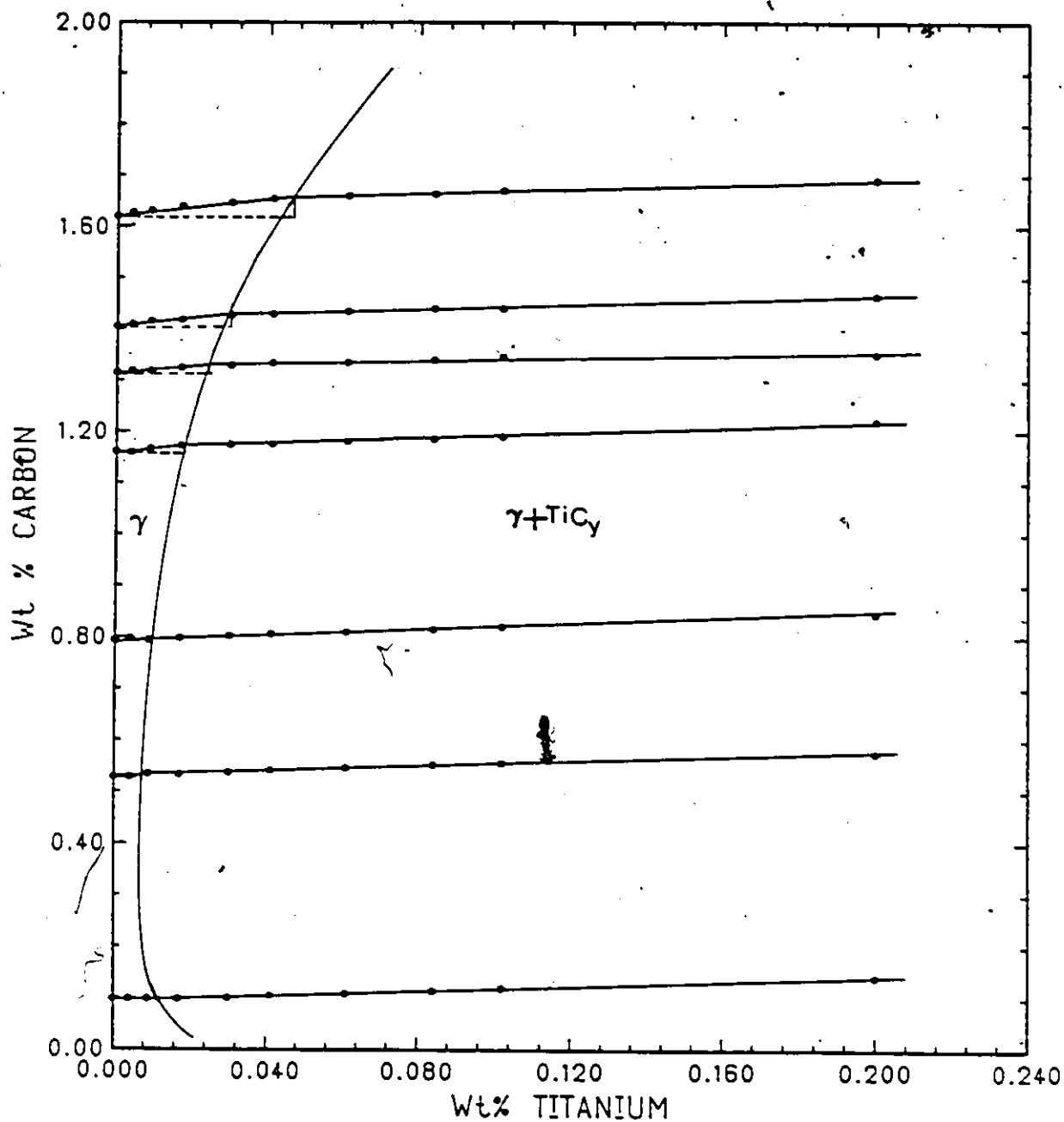


FIG. 4.4 CARBON CONTENTS OF EQUILIBRATED  
Fe-Ti-C ALLOYS (T=1273K)

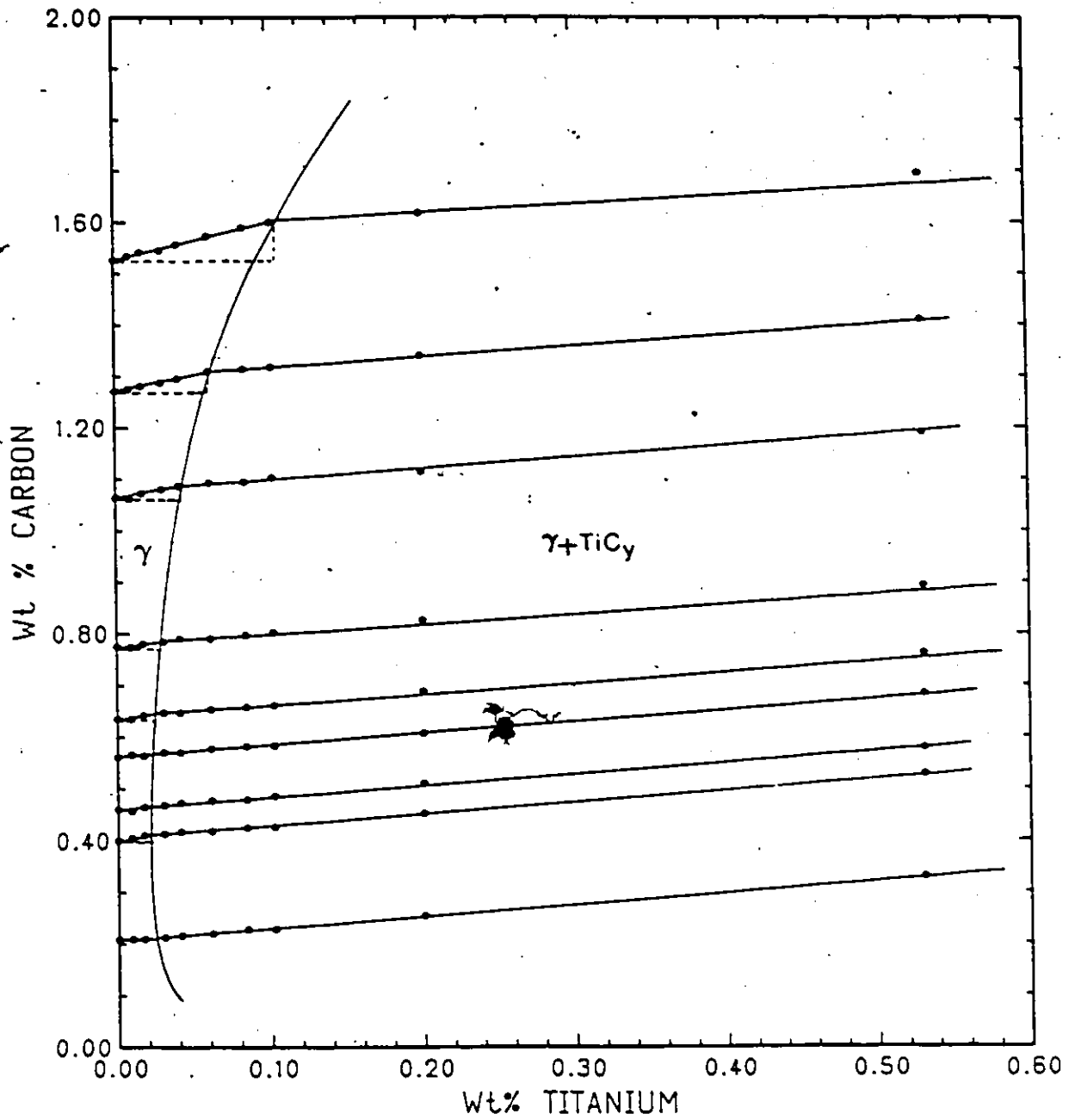


FIG. 4.5

CARBON CONTENTS OF EQUILIBRATED  
Fe-Ti-C ALLOYS (T=1373K)

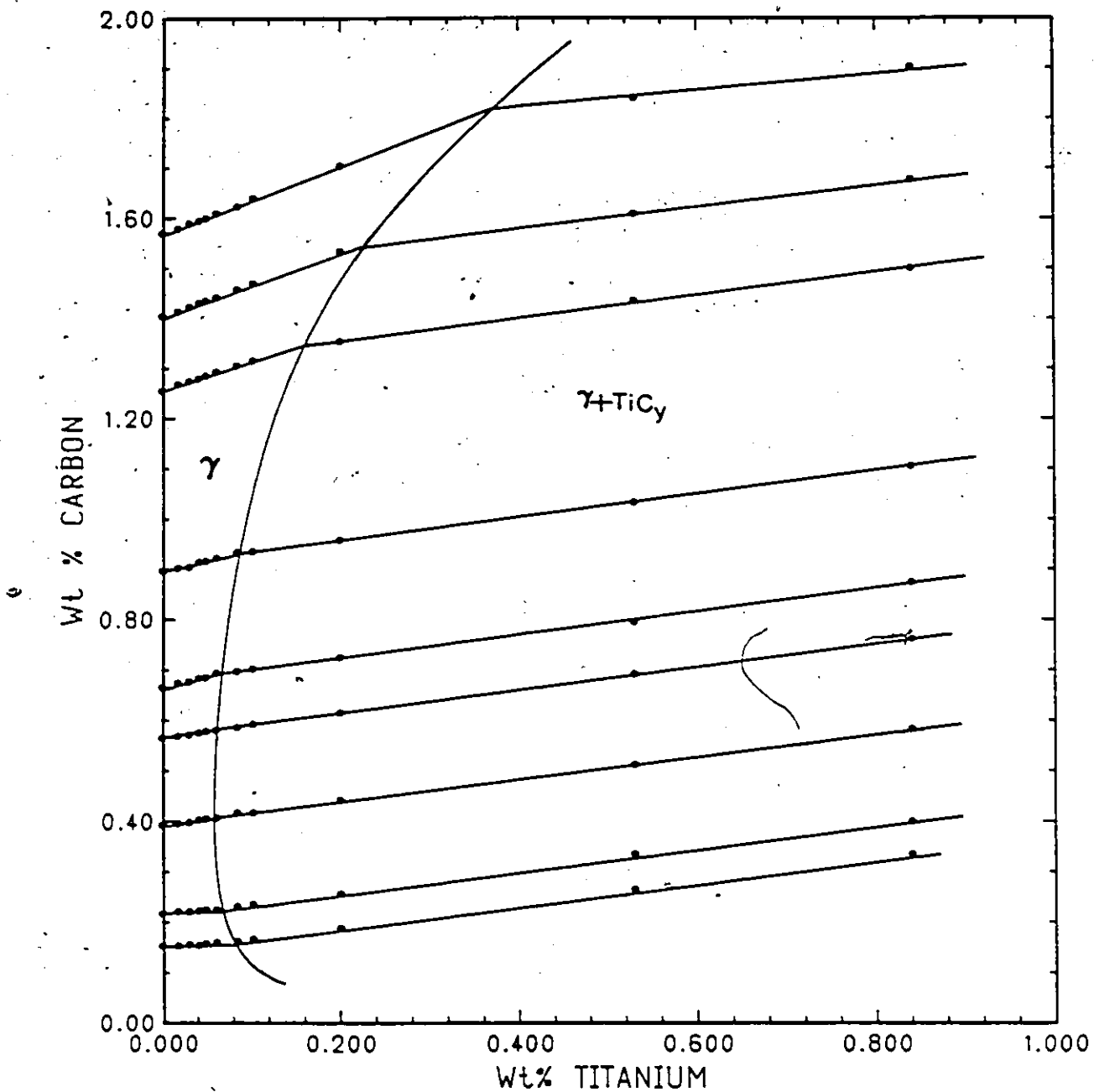


FIG. 4.6

CARBON CONTENTS OF EQUILIBRATED  
Fe-Ti-C ALLOYS (T=1473K)

Three important features are clearly borne out in Figures 4.1 - 4.6, viz., (i) the solubility limit obtained as the discontinuity in the isoactivity curves show a minimum between 0.4-0.50 wt% C in the Fe-Nb-C system and between 0.35-0.45 wt% C in the Fe-Ti-C system in the temperature range 1273K-1473K; (ii) the increase in carbon content over and above the binary level is very significant at higher carbon levels and higher temperatures as mentioned in the previous paragraph; and (iii) there is a substantial increase in the solubility limit at high carbon levels. These three features are manifestations of strong solute interactions in austenite and their analyses will be taken up in detail in Chapter VI.

The solubility limits and the solubility products  $\log K'$  and  $\ln K$  are listed in Tables 4.7 and 4.8 for the Fe-Nb-C and Fe-Ti-C systems, respectively. At high carbon levels the change of slope in the isoactivity curves is significant and hence the error in the determination of the composition (especially that of Ti or Nb) is small. However, near the minimum the error in the determination of the metal content is relatively higher due to a less pronounced change in slope. The effect of these errors on the solubility product will now be examined. Let  $\Delta W\%C$  and  $\Delta W\%M$  be the absolute errors in the measurement of the carbon and the metal content at the solubility limit. The absolute error in the solubility product is given by the Taylor expansion of the solubility product in terms of compositions.

$$\Delta \log[Wt\%M \cdot Wt\%C] = \frac{1}{2.303} \left[ \left( \frac{\Delta_e Wt\%C}{Wt\%C} + \frac{\Delta_e Wt\%M}{Wt\%M} \right) - \frac{1}{2} \left[ \left( \frac{\Delta_e Wt\%C}{Wt\%C} \right)^2 + \left( \frac{\Delta_e Wt\%M}{Wt\%M} \right)^2 \right] \right] \quad (4.1)$$

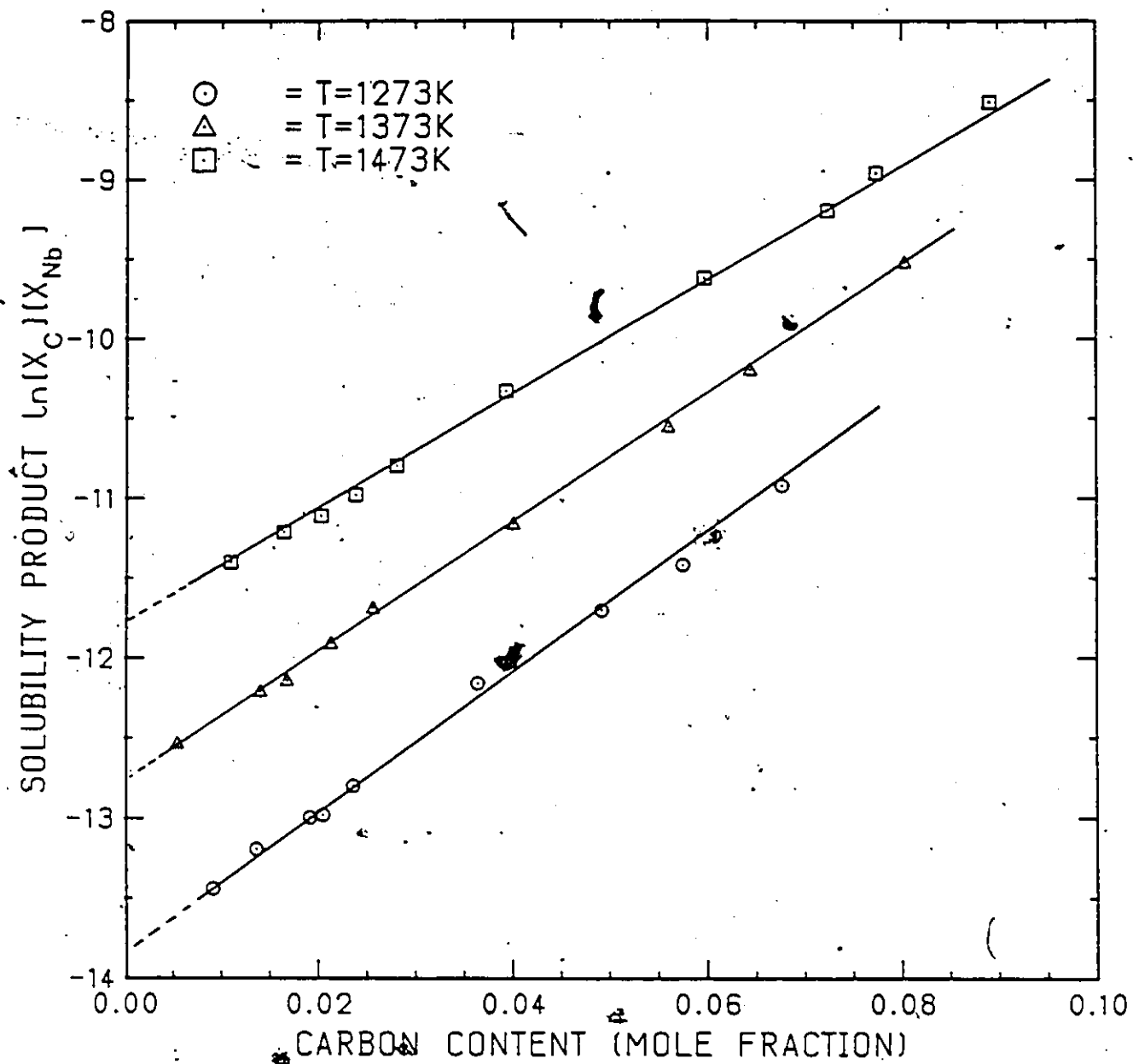


FIG. 4.7 VARIATION OF SOLUBILITY LIMIT OF NbC IN Fe-Nb-C AUSTENITE

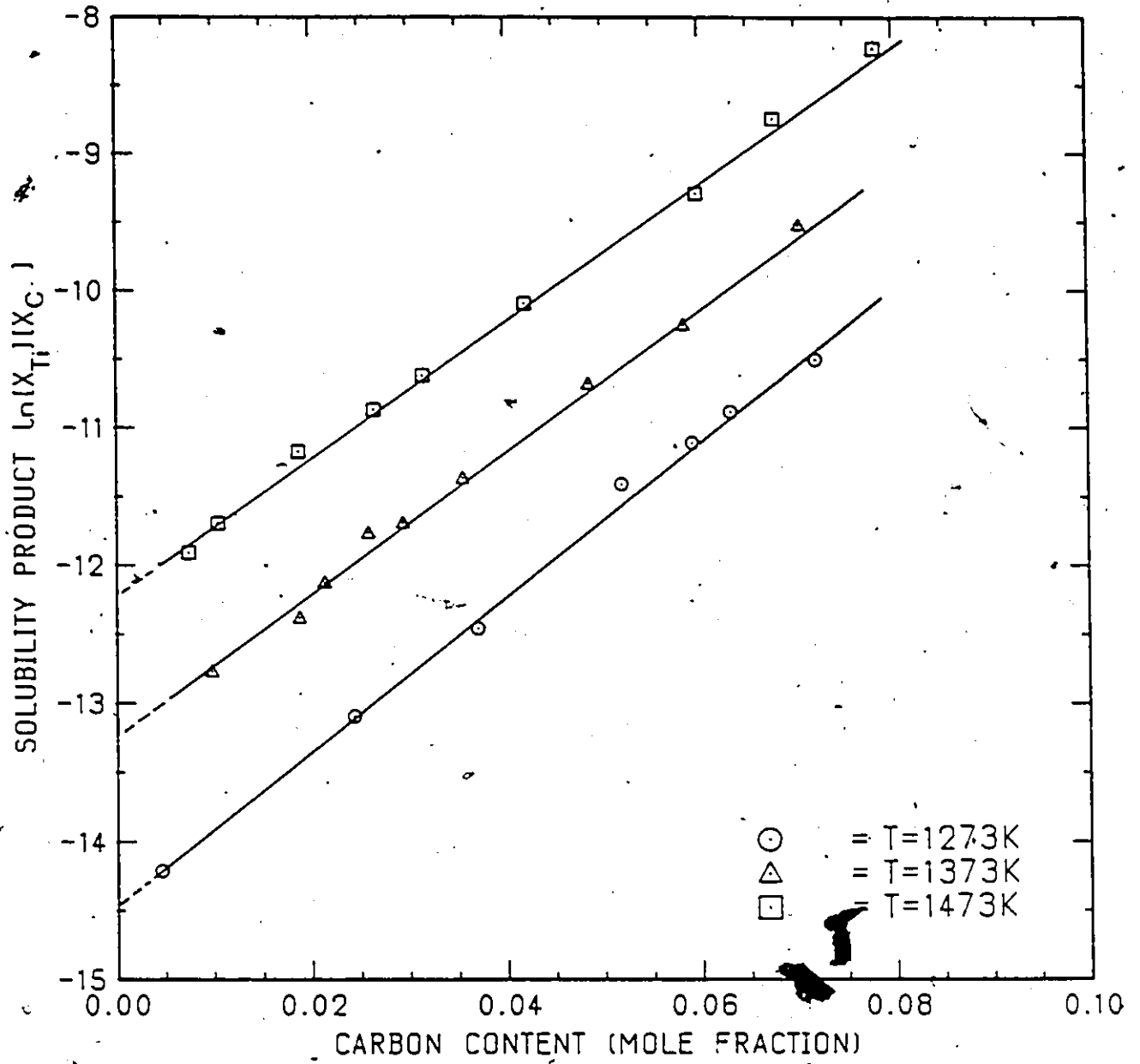


FIG. 4.8

VARIATION OF SOLUBILITY LIMIT OF TiC IN  
Fe-Ti-C AUSTENITE

Equation (4.1) is written up to the second order terms. In the present case, the errors are not large enough to warrant these terms and hence the first order approximation shall be used. Secondly, the relative error in the determination of Wt% C is very small, and therefore can be neglected. Thus the absolute error in the solubility product (expressed in the logarithmic form) is approximately equal to the relative error in the Ti or Nb content as shown below.

$$\Delta \log[\text{Wt}\% \text{M} \cdot \text{Wt}\% \text{C}] = \frac{1}{2.303} \frac{\Delta_e \text{Wt}\% \text{M}}{\text{Wt}\% \text{M}} \quad (4.2)$$

If the compositions are expressed in mole fractions, the magnitude of the solubility product (in absolute terms) increases by an order of magnitude; see Tables 4.7 and 4.8) but the absolute error does not change much as it is equal to the relative error in composition i.e.,

$$\Delta \ln[X_C X_M] = \frac{\Delta_e X_M}{X_M} = \frac{\Delta_e \text{Wt}\% \text{M}}{\text{Wt}\% \text{M}} \quad (4.3)$$

Therefore it is better to use the mole fraction units for curve fitting purposes. The errors associated with the solubility products are given in Tables 4.7 and 4.8 along with the other results. Figures 4.7 and 4.8 illustrate the linear variation of the solubility product of NbC and TiC in austenite with carbon content at 1273K, 1373K, and 1473K. The slope and the intercept will be related to the interaction parameter and the dissolution free energy of Ti or Nb in Chapter VI.

#### 4.3 Results for the Fe-Nb-N System

In this section the results obtained from nitrogen equilibration experiments will be presented. Unlike the aforementioned carbon

systems, the Fe-Nb-N system does not exhibit a solubility minimum or the increased solubility of the nitride. Even though the N-Nb interaction is strong, due to very low solubility of nitrogen, the pronounced effects seen in the carbon systems are absent in the austenite - niobium nitride equilibrium. Therefore the ternary interaction parameter had to be determined from the modest increases in nitrogen contents due to niobium additions.

The nitridation experiments were carried out on lines similar to the carburization of Fe-Ti-C and Fe-Nb-C alloys. Ten Fe-Nb alloys along with a pure Fe sample were 'simultaneously' equilibrated at various nitrogen potentials ranging from (760mm - 50 mmHg) in the temperature range 1373K-1573K. The solubility limit is obtained from these equilibration runs. It is to be noted that the solubility limit is sharply defined in this system unlike the carbon counterpart. Once this limit is known, three compositions lying in the single phase region were re-equilibrated individually for the accurate determination of the increase in the nitrogen content due to ternary additions. In chapter VI it will be shown that the maximum increase in nitrogen content at any given temperature is limited by the solubility product. These increases were almost negligible at 1373K and hence these individual equilibrations were done only at 1473K and 1573K. In order to amplify the difference in the nitrogen content between the binary and the ternary samples, large sample weights (10grams) were used along with the balance set to operate at the highest sensitivity (100 microgram weight change range). If a 10 gram sample is used, a 5 ppm difference between the binary and the ternary alloy will be recorded as 50 micrograms

within an error of 3-5 micrograms. If the total nitrogen in the binary is low, say 50 ppm, this 5ppm is a significant 10% change. Thus at lower partial pressures the relative increase in nitrogen is significant as a large amount of Nb is dissolved to impart its effect. The equilibration experiments were repeated at least three times to ensure reproducibility in results.

Tables 4.9 - 4.11 list the nitrogen contents obtained in Fe-N and Fe-Nb-N alloys at 1373K, 1473K and 1573K respectively. It can be seen that the maximum increase is limited at 1-2 ppm at 1373K, 4-5 ppm at 1473K and 9-10 ppm at 1573K. Since we are basically determining the difference between two numbers very close to each other, the error involved is high. At high nitrogen pressures where the nitrogen contents are about 150-250 ppm, the errors in the determination of the relative increases are as high as 30 percent. On the otherhand at lower partial pressures, the nitrogen levels are around 50-100 ppm and the relative increases are as high as 10-13 percent. The error at these levels are about 10-15 percent where the lower figure corresponds to the higher temperature 1573K. In Tables 4.9 - 4.11, the increases in nitrogen contents instead of total nitrogen contents were given for the ternary alloys, to illustrate the magnitude and the accuracies involved. It might be possible to improve the accuracies further at higher temperatures (>1573K). However, the Nb-N interaction parameter can be determined to within 15% accuracy from these results which is sufficient for most cases. Since the concentration of nitrogen is usually very small in many steels, further refinement in the determination of the interaction is not worthwhile. The nitrogen contents of equilibrated

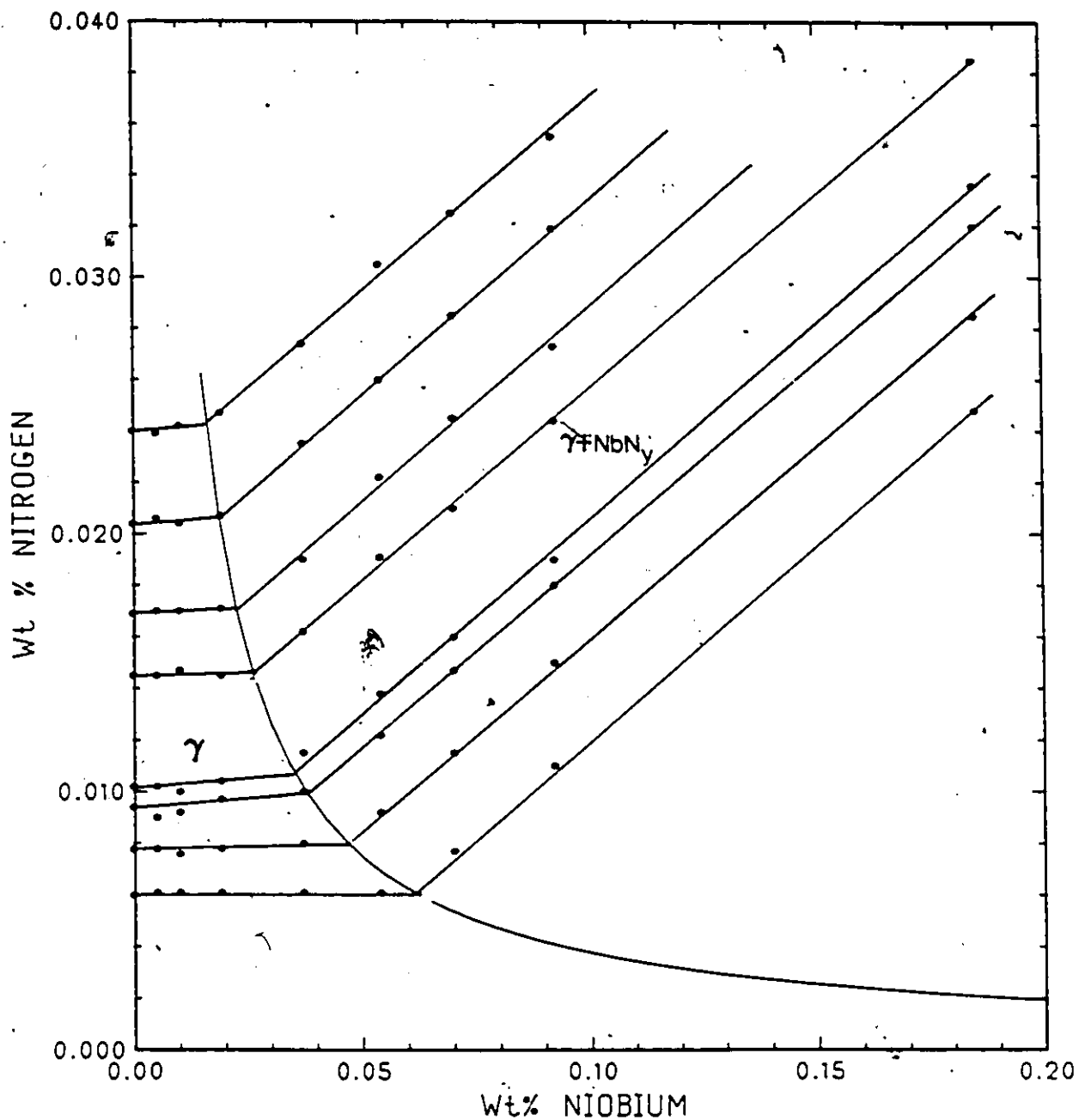


FIG. 4.9 NITROGEN CONTENTS OF EQUILIBRATED  
Fe-Nb-N ALLOYS (T=1373K)

(Note: As an expanded scale has been used data points corresponding to Wt% Nb > 0.20 and Wt% N > 0.04 given in Table 4.9 are not shown in this figure.)

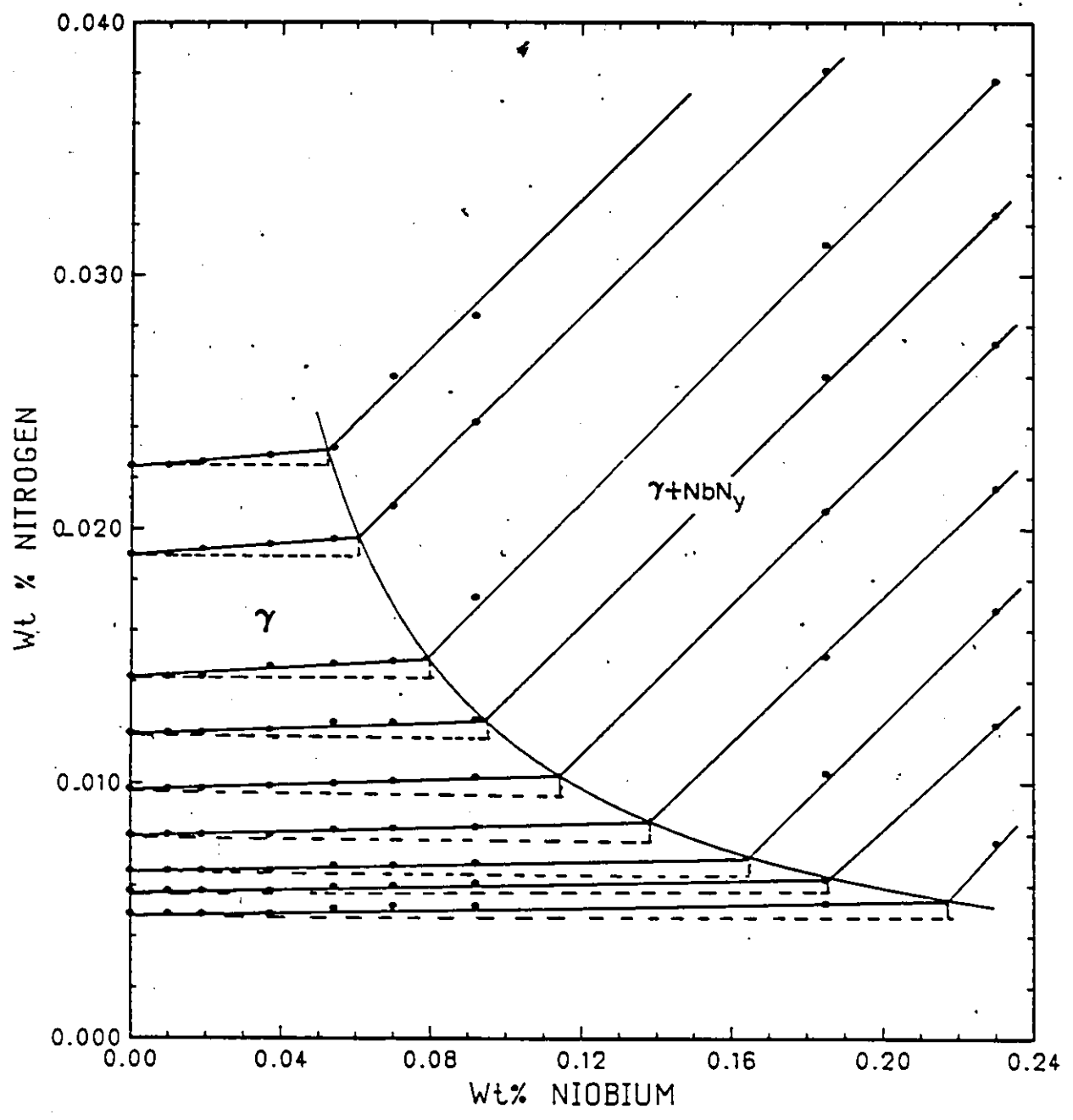


FIG. 4.10 NITROGEN CONTENTS OF EQUILIBRATED Fe-Nb-N ALLOYS (T=1473K)

(Note: As an expanded scale has been used data points corresponding to Wt% Nb > 0.24 and Wt% N > 0.04 given in Table 4.10 are not shown in this figure.)

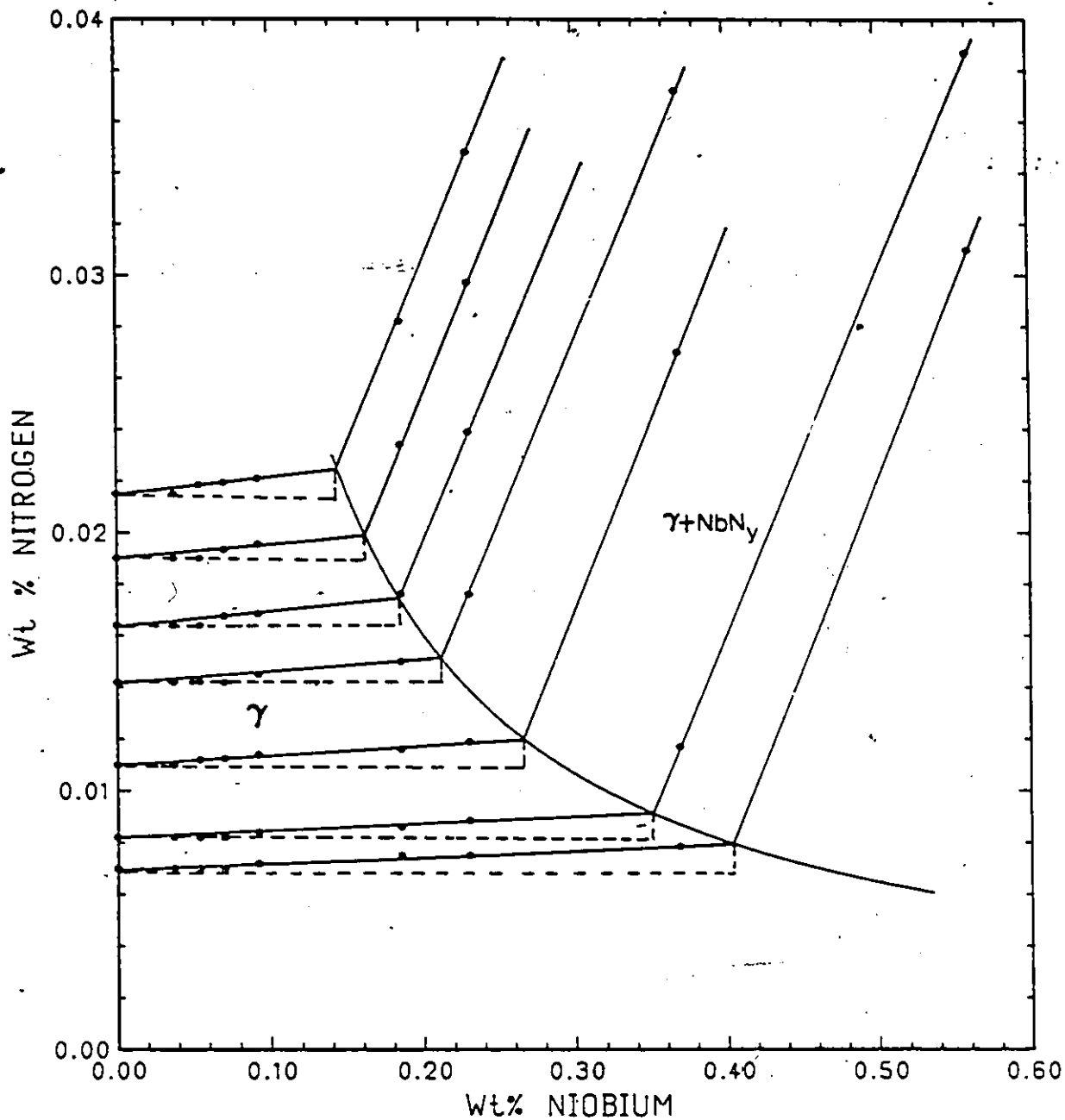


FIG. 4.11 NITROGEN CONTENTS OF EQUILIBRATED  
Fe-Nb-N ALLOYS (T=1573K)

(Note: As an expanded scale has been used data points corresponding to Wt% Nb > 0.60 and Wt% N > 0.04 given in Table 4.11 are not shown in this figure.)

Fe-Nb-N alloys are illustrated in Figures 4.9 - 4.11.

The solubility limit of NbN in austenite is fairly constant at any given temperature as shown in Table 4.12. As the change of slope in the isoactivity curves is very pronounced at the solubility limit, the errors involved in the determination of both nitrogen and niobium contents are very small. The maximum error in  $\log(\text{Wt}\% \text{N} \cdot \text{Wt}\% \text{Nb})$  is 0.052 which corresponds to about 12% error in the determination of the compositions ( $.12/2.303=0.052$ , see equation 4.2). The solubility limit of NbN in austenite as will be shown in Chapter VI is useful for obtaining a reliable value for the dissolution free energy of niobium in austenite.

#### 4.4 Results for $\text{NbC}_y$ and $\text{TiC}_y$ phases

The variation of carbon content in  $\text{NbC}_y$  and  $\text{TiC}_y$  phases as a function of the carbon potential has been determined using the hydrogen - methane mixtures at 1273K and 1473K. In order to achieve very low potentials, premixed gases containing very low levels of methane (see section 3.3.1) have been used. The lowest achievable composition corresponds to  $y=0.88$  in the case of  $\text{NbC}_y$  and  $y = 0.86$  in the case of  $\text{TiC}_y$ . As mentioned in Chapter III (section 3.4.4) very thin (10 microns) foils measuring 3cmx3cm were used for carburization. A Nb sample of these dimensions weighing nearly 90 mg picks up 12 mg of C at stoichiometry while a Ti sample of similar dimensions weighs 40-50 mg and picks up 12 mg of carbon. A weight change of 0.02mg translates to 0.0016 in the composition parameter  $y$ .

The variation of the carbon content in niobium and titanium

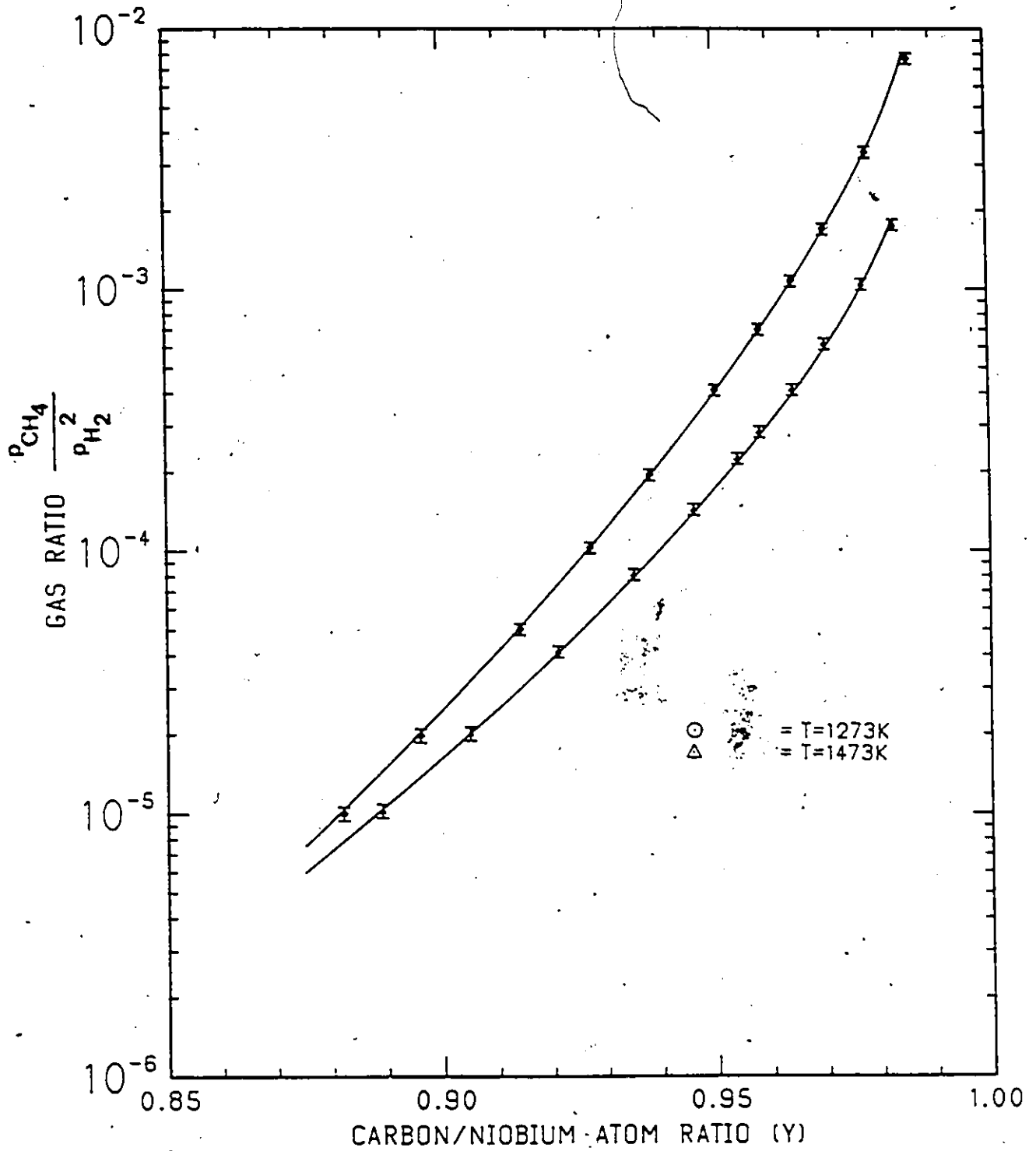


FIG. 4.12 VARIATION OF COMPOSITION OF NIOBIUM CARBIDE AS A FUNCTION OF GAS RATIO

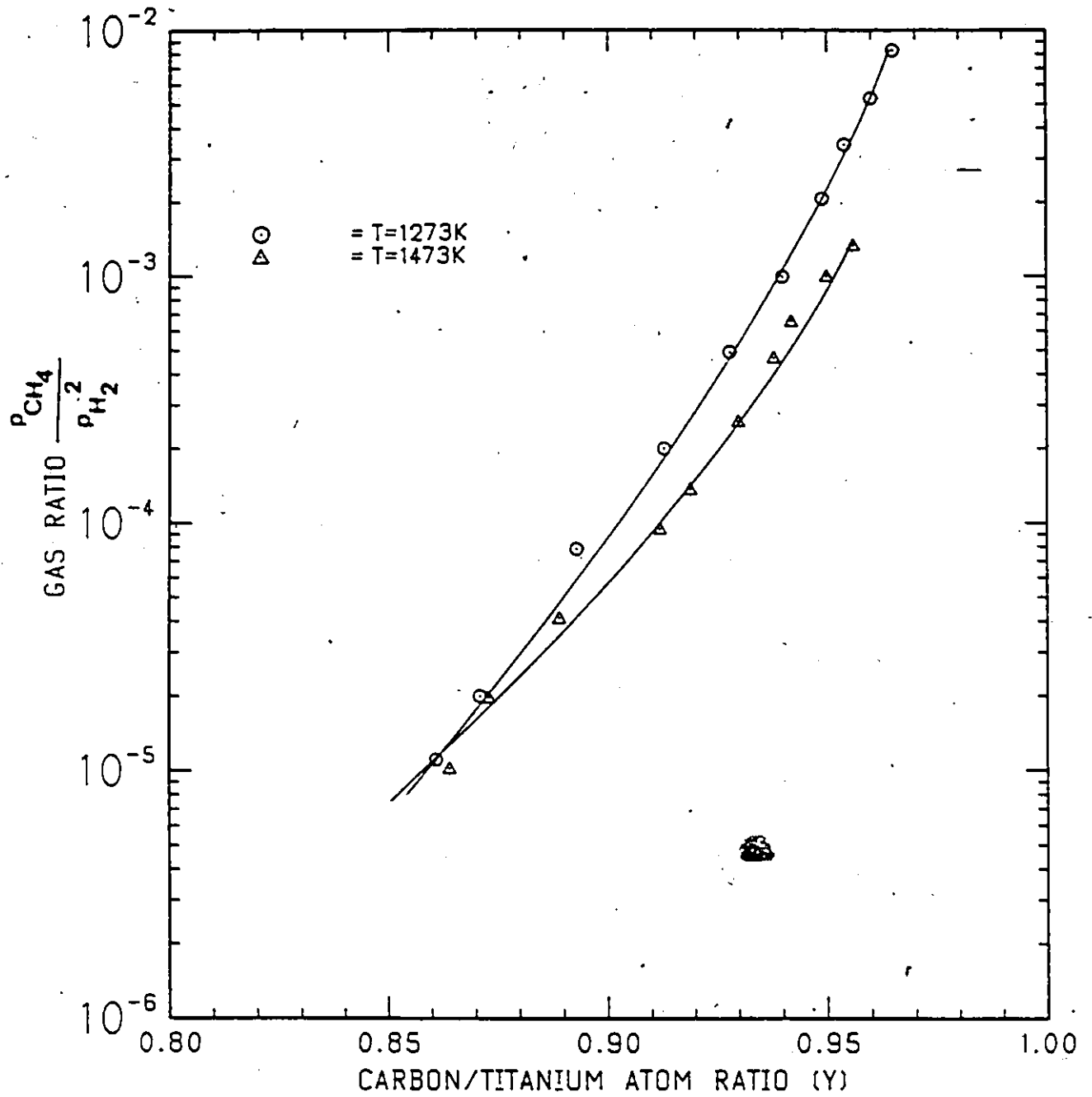


FIG. 4.13 VARIATION OF COMPOSITION OF TITANIUM CARBIDE AS A FUNCTION OF GAS RATIO

carbides\* as a function of the gas ratio shown in Figures 4.12 and 4.13 is listed in Tables 4.13 and 4.14. The error in the gas ratio is about 5 percent for ratios above  $1.0E-04$  and 10% for ratios below that value. As the logarithmic scale has been used for the axis depicting the gas ratio in Figures 4.12 and 4.13, the errors are compressed and hence are not discernible. The error in the determination of composition (expressed in terms of atom ratio  $y$ ) is about 0.0015 - 0.002.

#### 4.5 Results for the $NbN_y$ phase

The results of nitrogen equilibration experiments obtained for the  $NbN_y$  phase are illustrated in Figure 4.14 for 1573K, 1623K and 1673K. They are also listed Table 4.15. The partial pressures of nitrogen range from 760mm Hg to 25 mmHg and the nitrogen contents vary from 0.960 to 0.900 in this range at 1573K. For a given nitrogen potential, as the temperature is increased the nitrogen content decreases significantly. This implies that the partial molar entropy of nitrogen should be very significant unlike that of carbon in the carbides. The nitride-nitrogen phase boundary ( $y$  at 760mmHg) decreases with increasing temperature in line with the phase diagram in the literature (see Figure 2.7). The error involved in the control and measurement of partial pressure of nitrogen is negligible (less than 2%) as the pressures are fairly high. The error in the determination of nitrogen content is about the same as that of carbon in carbides. However, the changes in the composition of nitride with both temperature and pressure are pronounced compared to that in the carbides and hence the relative errors are smaller in the case of niobium nitride.

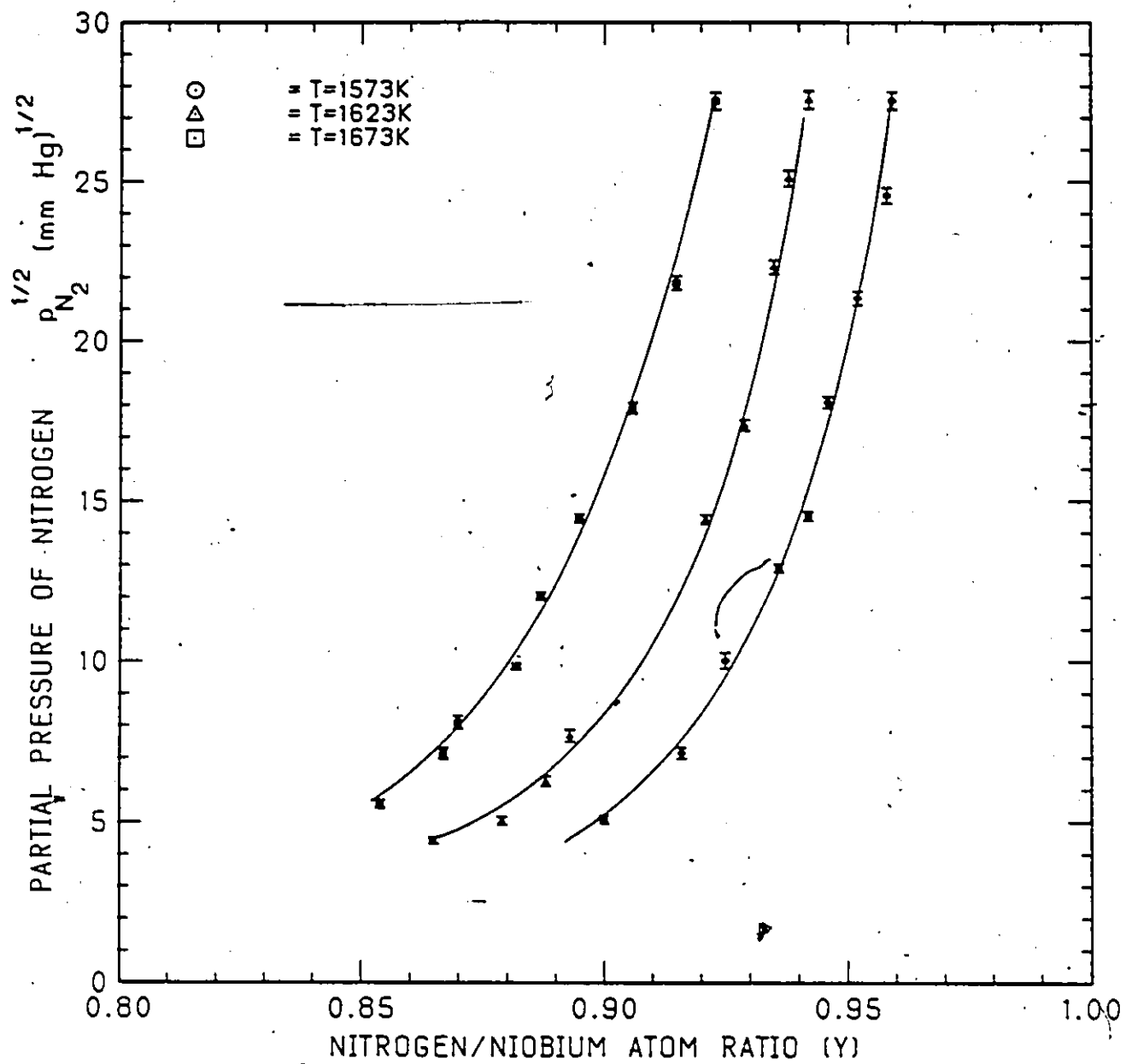


FIG. 4.14 VARIATION OF COMPOSITION OF NIOBIUM NITRIDE AS A FUNCTION OF PARTIAL PRESSURE OF NITROGEN

The experimental results given in this chapter will be analyzed in the subsequent chapters to obtain interaction parameters in the ternary austenites, the binary carbides of Ti and Nb and the niobium nitride. The thermodynamic models to be used for this analysis will be outlined in the next chapter.

TABLE 4.1

## Carbon Contents of Equilibrated Fe-C and Fe-Nb-C Alloys (T = 1273 K)

Gas Ratio $\times 10^3$	a <sub>c</sub>	wt% Nb						wt% C					
		0.0	0.005	0.010	0.019	0.037	0.054	0.070	0.092	0.185	0.368	0.560	
		0.196	0.197	0.196	0.197	0.199	0.203	0.203	0.207	0.220	0.238	0.265	
0.7	0.08	0.292	0.294	0.294	0.293	0.304	0.299	0.297	0.305	0.315	0.340	0.362	
1.05	0.11	0.416	0.415	0.419	0.417	0.421	0.424	0.424	0.427	0.440	0.461	0.482	
1.55	0.16	0.445	0.447	0.447	0.448	0.452	0.454	0.455	0.459	0.470	0.492	0.514	
1.75	0.19	0.517	0.515	0.514	0.519	0.522	0.522	0.524	0.528	0.539	0.562	0.581	
2.00	0.21	0.803	0.801	0.802	0.805	0.809	0.810	0.814	0.816	0.825	0.845	0.877	
3.35	0.36	1.094	1.094	1.097	1.100	1.101	1.102	1.107	1.110	1.118	1.141	1.163	
4.95	0.55	1.286	1.288	1.290	1.293	1.296	1.296	1.300	1.304	1.312	1.335	1.357	
6.10	0.65	1.522	1.525	1.523	1.527	1.534	1.536	1.539	1.541	1.551	1.574	1.589	
7.70	0.83												

TABLE 4.2

Carbon Contents of Equilibrated Fe-C and Fe-Nb-C Alloys (T=1373K)

Gas Ratio $\times 10^3$	$a_c$	wt% Nb						wt% C					
		0.0	0.010	0.019	0.037	0.054	0.070	0.092	0.185	0.230	0.368	0.560	
0.15	0.03	0.114	0.116	0.113	0.116	0.116	0.116	0.118	0.127	0.134	0.148	0.175	
0.43	0.086	0.303	0.298	0.302	0.303	0.307	0.311	0.322	0.326	0.342	0.367		
0.52	0.105	0.360	0.358	0.363	0.365	0.369	0.371	0.382	0.387	0.401	0.430		
0.69	0.14	0.461	0.461	0.465	0.468	0.470	0.472	0.484	0.489	0.503	0.530		
0.85	0.17	0.556	0.558	0.561	0.564	0.567	0.567	0.580	0.586	0.601	0.624		
1.45	0.29	0.880	0.883	0.887	0.890	0.890	0.894	0.905	0.911	0.925	0.951		
2.23	0.45	1.240	1.244	1.249	1.255	1.258	1.262	1.271	1.279	1.294	1.312		
2.70	0.54	1.435	1.438	1.442	1.447	1.452	1.456	1.469	1.475	1.489	1.511		
3.7	0.74	1.795	1.799	1.803	1.809	1.815	1.822	1.844	1.850	1.865	1.884		

TABLE 4.3

Carbon Contents of Equilibrated Fe-C and Fe-Nb-C Alloys (T=1473K)

Gas Ratio $\times 10^3$	$a_c$	Wt% Nb										
		0.0	0.037	0.054	0.070	0.092	0.185	0.230	0.368	0.560	0.740	0.930
		Wt% C										
0.14	0.049	0.226	0.226	0.228	0.231	0.235	0.240	0.245	0.263	0.284	0.308	0.332
0.22	0.077	0.345	0.346	0.348	0.348	0.352	0.368	0.369	0.387	0.411	0.429	0.455
0.28	0.098	0.429	0.433	0.431	0.436	0.440	0.452	0.457	0.475	0.500	0.516	0.540
0.35	0.118	0.509	0.507	0.513	0.518	0.521	0.531	0.537	0.554	0.578	0.599	0.619
0.41	0.142	0.605	0.608	0.608	0.610	0.616	0.625	0.633	0.647	0.672	0.690	0.715
0.61	0.212	0.849	0.854	0.854	0.857	0.866	0.881	0.885	0.901	0.926	0.943	0.965
1.05	0.360	1.304	1.312	1.310	1.315	1.322	1.345	1.352	1.370	1.389	1.411	1.425
1.34	0.460	1.574	1.585	1.590	1.594	1.601	1.627	1.637	1.661	1.677	1.701	1.719
1.46	0.510	1.688	1.696	1.700	1.703	1.711	1.734	1.748	1.778	1.795	1.819	1.835

TABLE 4.4

Carbon Contents of Equilibrated Fe-C and Fe-Ti-C Alloys (T=1273K)

Gas Ratio $\times 10^3$	$a_c$	Wt% Ti											
		0.0	0.004	0.009	0.017	0.030	0.041	0.061	0.084	0.102	0.200	0.530	
		Wt% C											
0.33	0.04	0.098	0.098	0.098	0.098	0.100	0.105	0.109	0.114	0.119	0.141	0.220	
2.0	0.22	0.528	0.528	0.534	0.533	0.537	0.541	0.546	0.552	0.555	0.575	0.658	
3.4	0.36	0.794	0.797	0.794	0.798	0.802	0.806	0.810	0.820	0.816	0.845	0.940	
5.3	0.56	1.161	1.159	1.166	1.172	1.174	1.175	1.181	1.185	1.190	1.220	1.265	
6.4	0.69	1.315	1.318	1.318	1.324	1.329	1.334	1.335	1.340	1.346	1.351	1.374	
7.0	0.75	1.405	1.409	1.415	1.418	1.427	1.429	1.435	1.440	1.440	1.465	1.538	
8.27	0.89	1.620	1.627	1.631	1.639	1.647	1.655	1.661	1.664	1.670	1.692	1.764	

TABLE 4.5

## Carbon Contents of Equilibrated Fe-Ti-C Alloys (T=1373K)

Gas Rat. to $\times 10^3$	$a_c$	Wt% Ti										
		0.0	0.009	0.017	0.030	0.041	0.061	0.084	0.102	0.200	0.530	0.840
		Wt% C										
0.29	0.06	0.208	0.209	0.209	0.212	0.216	0.219	0.228	0.228	0.254	0.330	0.397
0.59	0.12	0.400	0.405	0.410	0.413	0.417	0.418	0.425	0.426	0.452	0.528	0.600
0.68	0.14	0.460	0.457	0.464	0.468	0.473	0.477	0.479	0.486	0.510	0.579	0.653
0.85	0.17	0.561	0.566	0.563	0.570	0.570	0.577	0.582	0.583	0.607	0.684	0.759
0.99	0.20	0.635	0.635	0.642	0.647	0.647	0.653	0.658	0.661	0.688	0.762	0.834
1.24	0.25	0.775	0.774	0.780	0.784	0.790	0.790	0.797	0.802	0.826	0.893	0.974
1.83	0.36	1.064	1.062	1.072	1.080	1.087	1.093	1.095	1.103	1.114	1.190	1.265
2.35	0.47	1.271	1.275	1.280	1.287	1.295	1.309	1.314	1.318	1.340	1.410	1.486
2.95	0.59	1.526	1.534	1.541	1.545	1.557	1.573	1.590	1.601	1.618	1.696	1.762

TABLE 4.6

## Carbon Contents of Equilibrated Fe-Ti-C Alloys (T=1473K)

Gas Ratio $\times 10^3$	$a_c$	wt% Ti										
		0.0	0.017	0.030	0.041	0.049	0.061	0.084	0.102	0.200	0.530	0.840
0.093	0.032	0.153	0.153	0.156	0.154	0.158	0.160	0.162	0.166	0.188	0.265	0.335
0.135	0.047	0.217	0.221	0.223	0.225	0.225	0.231	0.235	0.256	0.335	0.400	
0.26	0.089	0.393	0.396	0.398	0.403	0.406	0.407	0.417	0.442	0.512	0.583	
0.37	0.130	0.565	0.568	0.571	0.575	0.578	0.581	0.586	0.615	0.692	0.762	
0.46	0.160	0.666	0.674	0.677	0.684	0.685	0.694	0.697	0.702	0.725	0.795	0.874
0.651	0.225	0.897	0.902	0.904	0.914	0.916	0.922	0.933	0.935	0.958	1.038	1.105
0.99	0.340	1.255	1.268	1.274	1.279	1.285	1.293	1.305	1.315	1.354	1.435	1.500
1.15	0.395	1.405	1.417	1.422	1.431	1.438	1.445	1.457	1.472	1.535	1.611	1.679
1.33	0.460	1.570	1.579	1.589	1.594	1.600	1.610	1.623	1.640	1.705	1.840	1.903

TABLE 4.7

Experimental ResultsSolubility of NbC in Fe-Nb-C Austenite

Wt%C	Wt%Nb	log K' K' = Wt%C.Wt%Nb	Error in log K'	ln K K = X <sub>Nb</sub> .X <sub>C</sub>	
1.3	0.033	- 1.37	0.015	- 11.42	
1.1	0.029	- 1.50	0.015	- 11.70	
0.81	0.025	- 1.71	0.015	- 12.16	
0.52	0.020	- 1.99	0.040	- 12.80	T = 1273K
0.45	0.019	- 2.07	0.050	- 12.98	
0.42	0.020	- 2.08	0.055	- 13.00	
0.30	0.023	- 2.17	0.030	- 13.20	
0.20	0.027	- 2.28	0.025	- 13.44	
1.84	0.162	- 0.53	0.015	- 9.52	
1.46	0.101	- 0.83	0.015	- 10.20	
1.26	0.081	- 0.99	0.020	- 10.56	
0.89	0.061	- 1.27	0.025	- 11.16	
0.56	0.055	- 1.51	0.040	- 11.69	T = 1373K
0.49	0.053	- 1.60	0.045	- 11.91	
0.37	0.053	- 1.71	0.050	- 12.14	
0.31	0.059	- 1.74	0.050	- 12.21	
0.12	0.110	- 1.89	0.030	- 12.53	
2.06	0.404	- 0.08	0.020	- 8.50	
1.77	0.294	- 0.28	0.025	- 8.96	
1.65	0.247	- 0.39	0.030	- 9.20	
1.35	0.194	- 0.58	0.040	- 9.62	
0.88	0.142	- 0.91	0.050	- 10.33	T = 1473K
0.62	0.123	- 1.12	0.055	- 10.80	
0.52	0.121	- 1.20	0.060	- 10.98	
0.45	0.124	- 1.26	0.060	- 11.11	
0.36	0.137	- 1.31	0.040	- 11.21	
0.24	0.170	- 1.39	0.030	- 11.40	

TABLE 4.8

Experimental ResultsSolubility of TiC in Fe-Ti-C Austenite

Wt%C	Wt%Ti	$\log K'$ $K' = \frac{\text{Wt}\%C \cdot \text{Wt}\%Ti}{\dots}$	Error in $\log K'$	$\ln K$ $K = X_{Ti} \cdot X_C$	
1.64	0.035	- 1.25	0.030	- 10.50	T = 1273K
1.43	0.027	- 1.42	0.035	- 10.90	
1.33	0.023	- 1.52	0.040	- 11.17	
1.16	0.019	- 1.65	0.040	- 11.41	
0.82	0.0093	- 2.12	0.065	- 12.46	
0.53	0.0075	- 2.40	0.065	- 13.10	
0.10	0.013	- 2.90	0.055	- 14.21	
1.60	0.095	- 0.82	0.015	- 9.52	T = 1373K
1.31	0.054	- 1.15	0.020	- 10.25	
1.08	0.042	- 1.34	0.030	- 10.68	
0.79	0.029	- 1.65	0.035	- 11.37	
0.65	0.025	- 1.79	0.040	- 11.70	
0.57	0.026	- 1.83	0.055	- 11.78	
0.47	0.022	- 1.99	0.060	- 12.15	
0.41	0.019	- 2.10	0.050	- 12.38	
0.21	0.025	- 2.27	0.030	- 12.77	
1.79	0.31	- 0.25	0.020	- 8.23	T = 1473K
1.54	0.21	- 0.48	0.030	- 8.74	
1.35	0.14	- 0.73	0.030	- 9.29	
0.93	0.087	- 1.09	0.040	- 10.10	
0.69	0.068	- 1.33	0.050	- 10.62	
0.58	0.063	- 1.44	0.060	- 10.87	
0.41	0.065	- 1.57	0.060	- 11.17	
0.23	0.068	- 1.81	0.040	- 11.69	
0.16	0.078	- 1.90	0.030	- 11.91	

TABLE 4.9

Nitrogen Contents of Equilibrated Fe-N and Fe-Mb-N Alloys (T=1373 K)

$P_{N_2}$ (mm Hg)	$a_N$	wt% Nb						N (ppm)									
		0.005	0.010	0.019	0.037	0.054	0.070	0.092	0.185	0.368	0.560						
760	1.0	239	242	247	274	304	325	355	498	770	1060						
555	0.85	206	204	207	235	260	285	319	467	734	1010						
375	0.70	168	170	170	190	222	245	273	420	690	980						
268	0.59	145	147	145	162	191	216	244	385	650	945						
154	0.45	102	100	104	115	138	160	190	335	605	890						
120	0.40	90	92	97	100	122	147	180	320	600	870						
80	0.33	79	76	78	80	92	115	150	285	560	844						
50	0.25	61	61	60	62	61	77	110	248	521	804						

TABLE 4.10

Nitrogen Contents of Equilibrated Fe-N and Fe-Nb-N Alloys (T=1473 K)

P <sub>H<sub>2</sub></sub> (mm Hg)	a <sub>N</sub>	Wt% Nb						Increase in N Content (ppm)			
		0.010	0.019	0.037	0.054	0.070	0.092				0.185
760	1.0	0	1-2	3-5	6-7	35	59	200	270	470	760
565	0.86	0	1-2	2-4	4-6	19	52	190	258	460	745
380	0.63	0	0	2-4	3-5	4-6	33	170	237	440	725
225	0.54	0	0	0	2-4	3-5	4-6	140	202	408	684
150	0.44	0	0	0	1-2	2-3	4-5	109	175	377	660
95	0.35	0	0	0	2	2-3	3	70	136	334	621
70	0.30	0	0	0	1-2	2	2-3	37	102	304	580
51	0.26	0	0	0	1-2	2	3	4.5	65	266	540
40	0.23	0	0	0	2	2-3	3	4	28	225	552

\* Error approximately 40% of the value

\*\* Error approximately 25% of the value

\*\*\* Error approximately 10-15% of the value



TABLE 4.12

Experimental ResultsSolubility of NbN in Fe-Nb-N Austenite

N (ppm)	Wt% Nb	log K'	
		K' = $\frac{\text{Wt}\% \text{N}}{\text{Wt}\% \text{Nb}}$	
240	0.0168	- 3.39	
205	0.0187	- 3.42	
169	0.0220	- 3.44	
145	0.0263	- 3.42	T = 1373K
102	0.0349	- 3.45	
95	0.0390	- 3.43	
80	0.0467	- 3.42	
62	0.0618	- 3.41	
		ave	- 3.42
230	0.054	- 2.90	
194	0.072	- 2.85	
147	0.081	- 2.92	
126	0.096	- 2.92	T = 1473K
103	0.110	- 2.95	
84	0.144	- 2.91	
69	0.162	- 2.95	
63	0.188	- 2.93	
54	0.219	- 2.93	
		ave	- 2.92
223	0.146	- 2.49	
197	0.172	- 2.47	
171	0.184	- 2.50	
149	0.204	- 2.52	T = 1573K
119	0.262	- 2.51	
91	0.350	- 2.49	
80	0.395	- 2.49	
		ave	- 2.50

TABLE 4.13

Experimental ResultsVariation of Composition with Carbon Potential  
in Niobium Carbide

Gas Ratio $\frac{P_{\text{CH}_4}}{(P_{\text{H}_2})^2}$	C/Nb Atom Ratio y	
7.68E-03	0.986	T = 1273K
3.35E-03	0.978	
1.70E-03	0.970	
1.07E-03	0.964	
6.98E-04	0.958	
4.10E-04	0.950	
1.95E-04	0.938	
1.02E-04	0.927	
5.02E-05	0.914	
2.00E-05	0.896	
1.00E-05	0.882	
1.75E-03	0.983	T = 1473K
1.04E-03	0.977	
6.15E-04	0.970	
4.10E-04	0.964	
2.83E-04	0.958	
2.24E-04	0.954	
1.43E-04	0.946	
8.10E-05	0.935	
4.12E-05	0.921	
2.00E-05	0.905	
1.00E-05	0.900	

TABLE 4.14

Experimental ResultsVariation of Composition with Carbon Potential  
in Titanium Carbide

Gas Ratio $\frac{P_{CH_4}}{(P_{H_2})^2}$	C/Ti Atom Ratio y	
8.27E-03	0.965	T = 1273K
5.30E-03	0.960	
3.40E-03	0.954	
2.05E-03	0.949	
1.00E-03	0.940	
4.90E-04	0.928	
1.95E-04	0.913	
7.80E-05	0.893	
2.00E-05	0.871	
1.10E-05	0.861	
1.32E-03	0.956	T = 1473K
9.95E-04	0.950	
6.50E-04	0.942	
4.60E-04	0.938	
2.55E-04	0.930	
1.35E-04	0.919	
9.40E-05	0.912	
4.10E-05	0.889	
2.00E-05	0.873	
1.00E-05	0.864	

TABLE 4.15

Experimental ResultsVariation of Composition with Nitrogen Potential  
in Niobium Nitride

Nitrogen Potential $P_{N_2}^{1/2}$ (mm Hg) <sup>1/2</sup>	N/Nb Atom Ratio y	
27.545	0.960	
24.56	0.958	
21.33	0.952	
18.06	0.946	
14.52	0.942	T = 1573K
12.90	0.936	
10.01	0.925	
7.13	0.916	
5.08	0.900	
27.545	0.942	
25.10	0.938	
22.31	0.935	
17.35	0.929	
14.42	0.921	T = 1623K
9.46	0.899	
7.67	0.893	
6.26	0.888	
5.03	0.879	
4.43	0.865	
27.545	0.923	
21.80	0.915	
17.90	0.906	
14.45	0.895	T = 1673K
12.02	0.889	
9.84	0.887	
8.10	0.872	
7.13	0.867	
5.55	0.854	

## CHAPTER V

### THERMODYNAMIC MODELS

#### 5.1 Introduction

In this chapter thermodynamic models relevant to the description of dilute ternary austenites and interstitial compounds like  $TiC_y$ ,  $NbC_y$  etc. will be outlined. Modified Wagner formalism for dilute solutions will be applied to Fe-Ti-C, Fe-Nb-C, Fe-Ti-N and Fe-Nb-N austenites. The correspondence between the modified Wagner formalism and the subregular solution expressions will be discussed in the light of determining the dissolution free energy (Henry's law coefficient) of Ti and Nb in fcc iron. Periodic correlations between the dissolution free energy on the one hand and the size factor and the atomic number of the transition metal solutes on the other are illustrated. The sublattice - subregular solution model proposed by Hillert and Staffansson is considered for the description of the thermodynamics of the binary carbides and nitrides of Ti and Nb. The parameters in the sublattice model will be related to the pair interaction energies in these compounds using statistical mechanical considerations. Finally, the limitations in applying the classical Schottky-Wagner Model for defect compounds to highly nonstoichiometric phases will be discussed.

#### 5.2 Modified Wagner Formalism for Dilute Fe-M-X Austenites

According to the modified Wagner formalism (18-21) the variation of chemical potentials of solutes in a ternary Fe-M-X austenite (M=Ti,Nb and X=C,N) can be written as

$$G_M = RT \ln a_M = RT \ln X_M + RT \left[ \ln^0 \gamma_M + \epsilon_M^M X_M + \epsilon_M^X X_X \right] - RT/2 \left[ \epsilon_M^M X_M^2 + \epsilon_X^X X_X^2 + 2\epsilon_X^M X_M X_X \right] \quad (5.1)$$

$$G_X = RT \ln a_X = RT \ln X_X + RT [\ln^0 \gamma_X + \epsilon_X^1 X_X + \epsilon_X^m X_X^m] - RT/2 [\epsilon_X^m X_X^2 + \epsilon_X^X X_X^2 + 2\epsilon_X^m X_X X_X] \quad (5.2)$$

and

$$RT \ln \gamma_{Fe} = - RT/2 [\epsilon_N^m X_N^2 + \epsilon_X^X X_X^2 + 2\epsilon_N^m X_N X_X] \quad (5.3)$$

where  $X_i$  and  $\gamma_i^0$  refer to the concentration (mole fraction) and Henry's law coefficient of solute  $i$  in austenite respectively. The  $\epsilon_i^i$ 's and  $\epsilon_i^j$ 's are the self- and the cross-interaction parameters of the solutes. Pure metals (bcc Ti, Nb), graphite, and nitrogen gas at one atmosphere are taken as standard states.

Equations (5.1) and (5.2) contain the extra term  $RT \ln \gamma_{Fe}$  which is a modification to the classical Wagner expressions. This term is necessary for overcoming two problems inherent in the classical expressions (19), namely, (i) inconsistency, i.e., the reciprocity relation  $\epsilon_i^j = \epsilon_j^i$  arising from the mathematical imperative

$$\frac{\partial}{\partial n_i} \left( \frac{\partial G}{\partial n_j} \right) = \frac{\partial}{\partial n_j} \left( \frac{\partial G}{\partial n_i} \right) \quad (5.4)$$

is satisfied only at infinite dilution and hence in general the classical expressions for the partial molar free energies are not consistent with equation (5.4).; (ii) the Gibbs-Duhem relation, the other imperative is also not satisfied by the classical expressions at finite concentration of solutes. Darken(19) proposed a 'quadratic' formalism which reduced to Wagner's expressions at infinite dilution but which is thermodynamically consistent at finite concentrations. Pelton and Bale(20) following the lines of Darken proposed the addition of an extra term ( $\ln \gamma_{Fe}$ ) to the partial molar free energies of solutes to overcome the inconsistency. These authors also extended this 'modified' Wagner formalism to encompass higher order interactions while preserving the

interaction parameter notation due to Wagner. A major advantage of this modification is that the existing compilations of the interaction parameters can be used directly in the modified formalism. Hillert(21) showed the correspondence between the modified formalism and the regular solution expressions. This correspondence will be used in the later sections to obtain the Henry's law coefficient and the self interaction parameters in the modified Wagner formalism from the regular (or sub-regular) solution expressions.

The Henry's law coefficient (infinitely dilute standard state) and the self interaction parameters are known to a high degree <sup>of</sup> accuracy for the interstitial solutes, carbon and nitrogen. The values as given by Chipman (25) and Hillert and Jarl (40) for Carbon and Nitrogen are

$$RT \ln^0 \gamma_C = 44184 - 17.7T \text{ Joules} \quad (5.5)$$

$$RT \ln^0 \gamma_N = -55520 - 69.87T \log T + 317.44T \text{ Joules} \quad (5.6)$$

$$RT \epsilon_C^C = 73925 \text{ Joules} \quad (5.7)$$

and

$$RT \epsilon_N^N = 52300 \text{ Joules} \quad (5.8)$$

Similar values are not readily available for Ti and Nb in austenite. However, due to the success of techniques such as computer coupling of phase diagrams and thermochemistry of many binary systems, these parameters can be established to a fair degree of accuracy. Kaufman (119) and the research group at the Royal Institute of Technology, Stockholm, Sweden have evaluated parameters describing the thermochemistry of phases for a number of iron based binary systems. The unknown parameters in the Wagner expression for the binary transition metal systems can be extracted from the excess free energy functions given by Kaufman and the Swedish group. The procedure is outlined below.

### 5.3 Interaction Parameters in Fe-M Systems

Within the Wagner approximation the excess free energy and the partial molar excess free energies of M and Fe in Fe-M austenite is written as

$$EG_m = RT \left[ X_M \ln \gamma_M + (1-X_M) \ln \gamma_{Fe} \right] \quad (5.9)$$

$$\bar{EG}_M = RT \ln \gamma_M = RT \ln \gamma_M^0 + RT \epsilon_M^M X_M - RT/2 [\epsilon_M^M X_M^2] \quad (5.10)$$

and

$$\bar{EG}_{Fe} = RT \ln \gamma_{Fe} = -RT/2 [\epsilon_M^M X_M^2] \quad (5.11)$$

where  $X_M$  refers to the mole fraction of the metal. The excess free energies according to the subregular model adopted by Kaufman is given by

$$EG_m = X_M(1-X_M) [g(1-X_M) + hX_M] \quad (5.12)$$

where  $g$  and  $h$  are the temperature dependent interaction parameters. The expression adopted by the Stockholm group is given by

$$EG_m = X_M(1-X_M) [A + B(X_M - X_{Fe})] \quad (5.13)$$

where  $A$  and  $B$  are the interaction parameters.  $A$  and  $B$  can be related to  $g$  and  $h$  and vice-versa as follows

$$A = (g+h)/2 \quad (5.14)$$

and

$$B = (h-g)/2 \quad (5.15)$$

The partial molar expressions as obtained from equation (5.13) are

$$\bar{EG}_M = (1-X_M)^2 [(A-B) + 4B X_M] \quad (5.16)$$

and

$$\bar{EG}_{Fe} = X_M^2 [(A-3B) + 4B X_M] \quad (5.17)$$

Equating the expressions as given in equations (5.9) and (5.10) with those given above in (5.16) and (5.17) one obtains the unknown parameters in the Wagner formalism as

$$RT \ln^0 \gamma_M = \lim_{X_M \rightarrow 0} RT \ln \gamma_M = \lim_{X_M \rightarrow 0} \left[ (1-X_M)^2 [(A-B) + 4B X_M] \right] \quad (5.18)$$

$$\text{and} \quad = (A-B) \quad (5.19)$$

$$\bar{E}_{Fe} = -RT/2 \left[ \epsilon_M^M X_M^2 \right] = X_M^2 [(A-3B) + 4B X_M] \quad (5.20)$$

Neglecting the higher order terms in equation (5.20) one obtains

$$RT \epsilon_M^M = -2(A-3B) \quad (5.21)$$

In general if the excess free energy function is given by a polynomial of the following form

$$\bar{E}_{GM} = X_M(1-X_M) [k_0 + k_1 X_M + k_2 X_M^2 + \dots] \quad (5.22)$$

The partial molar free energy of the solute M becomes

$$\bar{E}_{GM} = (1-X_M)^2 [k_0 + 2k_1 X_M + 3k_2 X_M^2 + \dots] \quad (5.23)$$

and correspondingly one obtains

$$RT \ln^0 \gamma_M = k_0 \quad (5.24)$$

and

$$RT \epsilon_M^M = -2(k_0 - k_1) \quad (5.25)$$

It is also necessary to add the free energy difference between the fcc and bcc forms of pure M as the bcc form of the solvent has been taken as standard state in the modified Wagner formalism. The  $(^0G_M^{fcc} - ^0G_M^{bcc})$  values have been taken from the compilation of Kaufman (10,20). Table 5.1 lists the lattice stability values and the interaction parameters given by Murray (2) for the Fe-Ti system and by Kaufman for the Fe-Ti and Fe-Nb systems.

The values given by Murray have been adopted as they reproduce the gamma loop in the Fe-Ti system better than those of Kaufman. Niobium, according to Kaufman's data, behaves ideally (with respect to fcc Nb) whereas a limited investigation by Hawkins (121) predicts negative deviations. The high solubility of niobium carbide at high carbon levels also points towards the dissolution free energy  $(RT \ln^0 \gamma_{Nb})$  of fcc Nb in fcc Fe being negative. The carbon niobium interaction,

which even though it is quite pronounced at high carbon levels, has been found to be insufficient to account for such high solubility of the carbide. Since vanadium and tantalum, belonging to the same group as niobium, also show substantial negative deviation from the ideality, niobium can be expected to behave in a similar fashion.

A reasonable value for the Henry's law coefficient, or a parameter describing the excess free energy of mixing of fcc Fe-Nb phase, has been obtained via suitable Periodic-Table correlations. Hume-Rothery (122) found rational correlations between the size, the electronegativity difference and the position of the solute in the periodic table on the one hand with the constitution of Fe-M systems on the other. The extent of the gamma phase, the tendency to form intermetallic phases, and the relative effects of solute in stabilizing alpha or gamma phase correlated well with the size factor and the position of the solute in the periodic table. A similar correlation can be shown to exist between the free energy of dissolution of the transition metal solute in fcc Fe and the aforementioned factors. The Henry's law coefficient determined from the excess energy expressions, given mostly by Kaufman and the Stockholm group via equations (5.18 - 5.25), are presented in Table 5.2. The correlation of these coefficients with the size factor and the position of the solute in the periodic table are shown in Figures 5.1 and 5.2. The correlation with the latter is very striking, and hence as a first approximation 'available' d shell electrons can be considered to be the predominant factor controlling the thermodynamics of dissolution of various solutes. Niobium belongs to the same group as vanadium (Group V B) and its size factor (i.e. atomic diameter calculated for coordination number 12) is closer to that of titanium. Hence an average

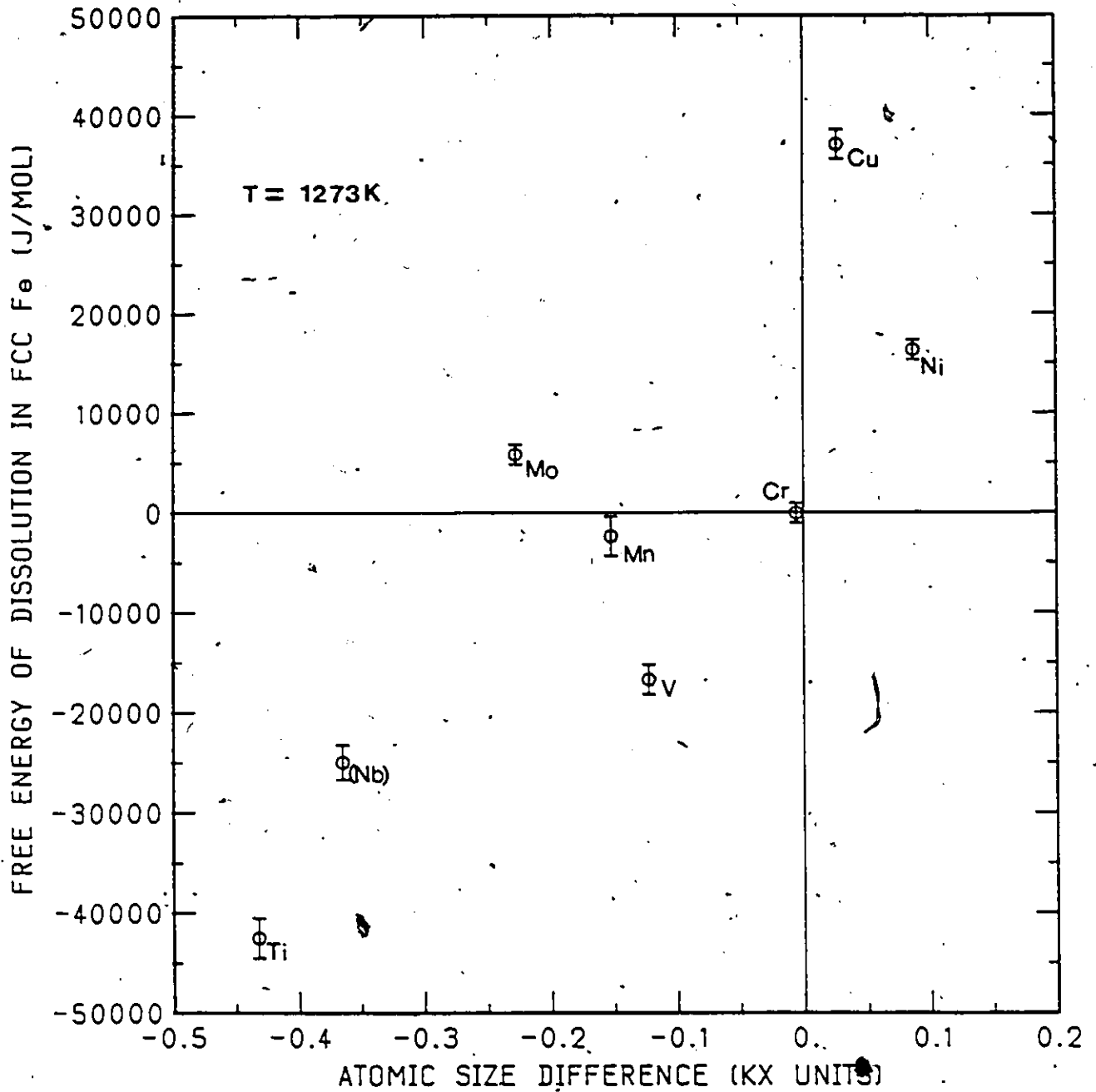


FIG. 5.1

## CORRELATIONAL RELATIONSHIP

FREE ENERGY OF DISSOLUTION OF SOLUTE IN FCC Fe  
vs ATOMIC SIZE DIFFERENCE

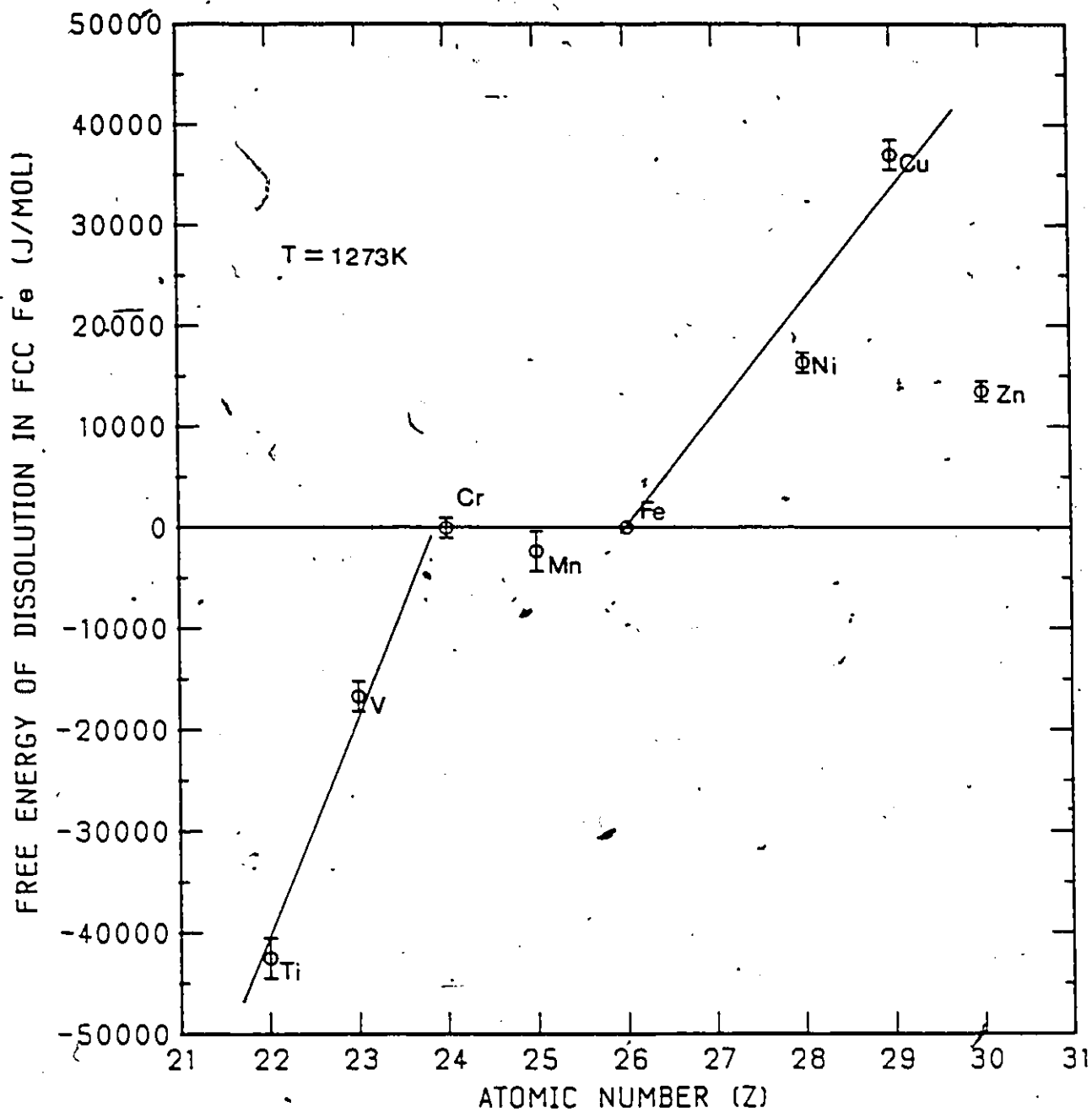


FIG. 5.2

## CORRELATIONAL RELATIONSHIP

FREE ENERGY OF DISSOLUTION OF SOLUTE IN FCC Fe  
vs ATOMIC NUMBER OF THE SOLUTE

of the values for titanium and vanadium should be a reasonable estimate for the dissolution free energy of niobium.

#### 5.4 Thermodynamics of Nonstoichiometric Monocarbides and Nitrides

##### 5.4.1 Introduction

In this section expressions for the partial molar free energies of transition metal and nonmetal are obtained from statistical mechanical considerations applied to interstitial solutions. The pair interaction energies are then related to the parameters in the sublattice-subregular model introduced by Hillert and Staffansson.

##### 5.4.2 Assumptions

In the following, it is assumed that nonstoichiometry is due to structural vacancies in the interstitial sublattice, the metal lattice is completely filled and interstitial atoms and vacancies mix randomly.

##### 5.4.3. Theory

With Guggenheim (132) the system of  $n_1$  metal atoms with  $n_2$  nonmetal atoms existing in the NaCl lattice can be regarded as a united 'ensemble' with the following properties :

(a) Any configuration of such an ensemble can be described by specifying the number of geometrical locations of occupiable sites and the number of sites actually occupied.

(b) The interaction between atoms that are not near neighbors may be neglected and the Helmholtz free energy of the system can be expressed as the sum of the free energies of interaction of the nearest atoms. The grand partition function of such an ensemble is

$$Q = \sum \frac{n_1!}{n_2!(n_1 - n_2)!} a_1^{n_1} a_2^{n_2} \exp\left[\frac{-F}{kT}(n_1, n_2, V, T)\right] \quad (5.26)$$

where  $a_1$ ,  $a_2$  are the activities of the components and  $F(n_1, n_2, V, T)$  is a

modified Helmholtz free energy for the system. Pure metal and pure non-metal are taken as the standard states. The free energy  $F$  which appears in equation (1) is composed of the total internal energy and the vibrational component of the entropy only.  $F(n_1, n_2, V, T)$  can be expressed as the sum of interaction free energies in the following way :

$$F(n_1, n_2, V, T) = (n_1 F_1 + n_2 F_2) + \left[ \frac{n_1}{2} F_{11} + \frac{n_2^2}{2n_1} F_{22} + n_2 F_{12} \right] \quad (5.27)$$

where  $F_1$  and  $F_2$  are free energies required to transfer the metal and the nonmetal from the pure substance state to the NaCl structure.  $F_{11}$  is the change in the M-M interaction free energy due to addition of the non-metal.  $F_{12}$  and  $F_{22}$  are the free energies of interaction between M-X and X-X atoms, respectively. It should be noted that the functions and formulas derived depend on the choice of variables used in constructing the partition function. The Helmholtz free energy function that is used to define the states in our partition function accounts for all the vibrational quantum states that are accessible to the system. Now, by following the methodology of Guggenheim (132), the chemical potentials can be obtained as

$$kT \ln a_1 = kT \ln \frac{n_1 - n_2}{n_1} + \frac{\partial F}{\partial n_1} \quad (5.28)$$

and

$$kT \ln a_2 = kT \ln \frac{n_2}{n_1 - n_2} + \frac{\partial F}{\partial n_2} \quad (5.29)$$

From equations (5.27 - 5.29), identifying  $n_1$  and  $n_2$  as mole rather than atom numbers, we obtain

$$\bar{F}_1 = \left\{ F_1 + \frac{F_{11}}{2} \right\} - \frac{F_{22}}{2} \left( \frac{n_2}{n_1} \right)^2 + RT \ln \frac{n_1 - n_2}{n_1} \quad (5.30)$$

and

$$\bar{F}_2 = (F_2 + F_{12}) + F_{22} \left( \frac{n_2}{n_1} \right) + RT \ln \frac{n_2}{n_1 - n_2} \quad (5.31)$$

It is interesting to note that as  $n_2 \rightarrow 0$  in equation (5.30) the chemical potential for the metal becomes  $(F_1 + F_{11}/2)$ .  $F_1$  is defined as the free energy to transfer a mole of metal from pure substance (bcc state) to NaCl structure (fcc) i.e.  $(G_M^{fcc} - G_M^{bcc})$ . Since the term  $F_{11}/2$  represents the change in the interaction free energy between metal atoms in the compound phase, it should reduce to zero when all the nonmetal atoms are removed ( $n_2 \rightarrow 0$ ). When equation (5.30) is applied to the experimental results in the Nb-C system a large value of 80-100KJ/Mol Nb is obtained for the  $(F_1 + F_{11}/2)$  term. The value for this term from lattice stability compilations (10) is a much lower 8-15KJ/Mol Nb. Such a large observed value will correspond to an 'expanded' fcc reference state which does not reflect the realistic situation.

A better understanding of the interactions of metal and nonmetal atoms in the NaCl lattice can be obtained by considering investigations (133-138) on the nature of bonding in these carbides and nitrides. These studies reveal a partly ionized state of atoms in the structure. The ionization arises due to non-metal solutes contributing "electrons" to the transition metals like Ti and Nb in order to facilitate bonding. It has also been reported (136-138) that the degree of ionicity (electron transfer from nonmetal to metal atoms) increases as the non-metal content of the compound increases. This would mean that the pair interaction energies should vary with composition. Thus a physical model incorporating the above characteristics should reflect a more realistic picture.

As a first approximation, pair interaction energies with linear dependence on non-metal to metal atom ratio can be considered. Thus one can write

$$F_{ij} = {}^0F_{ij} + \left(\frac{n_2}{n_1}\right) {}^1F_{ij} \quad (5.32)$$

where  ${}^0F_{ij}$  and  ${}^1F_{ij}$  are constants. As  $F_{11}$  should vanish as  $n_2 \rightarrow 0$ ,  ${}^0F_{11}$  is zero. Substituting equation (5.32) into equation (5.27) and going through the same procedure one can obtain expressions more general than those in equations (5.30) and (5.31) viz.

$$\bar{F}_1 = A_0 + A_2 \left(\frac{n_2}{n_1}\right)^2 + A_3 \left(\frac{n_2}{n_1}\right)^3 + RT \ln \frac{n_1 - n_2}{n_1} \quad (5.33)$$

and

$$\bar{F}_2 = B_0 + B_1 \left(\frac{n_2}{n_1}\right) + B_2 \left(\frac{n_2}{n_1}\right)^2 + RT \ln \frac{n_2}{n_1 - n_2} \quad (5.34)$$

where

$$A_0 = \left\{ F_1 + \frac{{}^0F_{11}}{2} \right\}; \quad A_2 = -\frac{1}{2} ({}^0F_{22} + 2{}^1F_{12}); \quad A_3 = -{}^1F_{22} \quad (5.35)$$

$$B_0 = \left\{ F_2 + {}^0F_{12} + \frac{{}^1F_{11}}{2} \right\}; \quad B_1 = -2A_2 = ({}^0F_{22} + 2{}^1F_{12})$$

$$B_2 = -\frac{3}{2} A_3 = \frac{3}{2} {}^1F_{22} \quad (5.36)$$

Now let  $x$  be the mole fraction of non-metal in the compound and by definition

$$\frac{n_2}{n_1 + n_2} = x; \quad \frac{n_1}{n_1 + n_2} = 1 - x \quad \text{and} \quad \frac{n_2}{n_1} = \frac{x}{1-x} \quad (5.37)$$

Next let

$$\frac{x}{1-x} = y \quad (5.38)$$

Substituting relations (5.37) and (5.38) into equations (5.33) and (5.34) we finally obtain,

$$RT \ln a_1 = A_0 + A_2 y^2 + A_3 y^3 + RT \ln(1-y) \quad (5.39)$$

and

$$RT \ln a_2 = B_0 + B_1 y + B_2 y^2 + RT \ln \left(\frac{y}{1-y}\right) \quad (5.40)$$

Equations (5.39-5.40) describe the variation of chemical potential as a function of composition and temperature. The parameters  $A_0$ ,  $A_2$ , etc. are related to the various free energy interactions and hence are composed of energetic and entropic(vibrational) components.

In equation (5.39) as  $y \rightarrow 0$ , the chemical potential of the metal is given by  $A_0 = F_1 + {}^0F_{11}/2$ . Since  ${}^0F_{11}$  is zero, the chemical potential corresponds to that of the pure substance standard state ( $F_1$ ) i.e., fcc. Referring back to the physical model outlined in the previous paragraph we can establish the sign of the various interaction energies. Since the atoms are partly ionized in the binary transition metal carbides and nitrides, the metal-metal interaction and the nonmetal-nonmetal interactions would be repulsive and hence positive values can be anticipated for the  $F_{11}$  and the  $F_{22}$  terms. The metal-nonmetal interaction ( $F_{12}$ ) is attractive in character. Since the degree of ionicity increases with the nonmetal content, both  ${}^0F_{12}$  and  ${}^1F_{12}$  in  $F_{12} = {}^0F_{12} + (y F_{12})$  should take negative values.

#### 5.4.4 Hillert - Staffansson Model

In this section, the sublattice-subregular model suggested by Hillert and Staffansson (29) will be outlined and the parameters in the model related to the pair interaction energies described in the previous section.

In this sublattice model the metal atoms occupy one lattice and the non-metal atoms and vacancies occupy the interstitial sublattice. The free energy of such a system can be written as

$$G_m = y {}^0G_{nz} + (1-y) {}^0G_{nv_a} + RT[y \ln y + (1-y) \ln(1-y)] + y(1-y)[L_0 + L_1[y - (1-y)]] \quad (5.41)$$

where  $y$  refers to the fraction of nonmetal in the interstitial subla-

lattice (which is same as  $y$  in the formula  $MX_y$ ),  ${}^0G_{MX}$  is the free energy of the stoichiometric compound and  $L_0$  and  $L_1$  are the interaction parameters describing the excess free energy of the system.  ${}^0G_{MVA}$  (Va=vacancy) refers to the free energy of system when the interstitial lattice is completely vacant i.e., the free energy of the metal in the pure fcc state. The partial quantities are obtained as

$$\bar{G}_x = ({}^0G_{MX} - {}^0G_M^{fcc}) + RT \ln\left(\frac{y}{1-y}\right) + \bar{E}G_x \quad (5.42)$$

and

$$\bar{G}_M = {}^0G_M^{fcc} + RT \ln(1-y) + \bar{E}G_M \quad (5.43)$$

where  $\bar{E}G_x$  and  $\bar{E}G_M$  refer to partial molar excess free energies which are given below.

$$\bar{E}G_x = -L_0(2y-1) - L_1(6y^2+6y-1) \quad (5.44)$$

and

$$\bar{E}G_M = y^2 [(L_0 - L_1) + 2L_1(2y-1)] \quad (5.45)$$

It is to be noted that the functions multiplying the interaction parameters in equation (5.44) are the first and second order Legendre polynomials in  $y$  and are orthogonal in the range zero to one ( $0 \leq y \leq 1$ ) and hence are ideally suited for curve fitting. In equation (5.45) the so called  $\alpha$  function  $\bar{E}G_M/(y^2)$  is also expressed in terms of Legendre polynomials. The constant term  $(L_0 - L_1)$  becomes the coefficient of the zeroth order polynomial,  $p_0 = 1$ , while  $2L_1$  is the coefficient of the first order polynomial  $p_1 = (2y-1)$ . Orthogonal polynomials remove the ill-conditioning associated with curve-fitting procedures and the coefficients determined are also uncorrelated (145). Moreover, the predominant contributions come from the leading terms unlike the case wherein the excess free energies are expressed as an ordinary power series. Hence it is advantageous to rearrange the chemical potential

expressions obtained in the earlier section in terms of orthogonal polynomials. In fact such a rearrangement gives a direct correspondence between the pair interaction energies and the interaction parameters in the Hillert-Staffansson model. Even though there are six parameters  $A_0$ ,  $A_2$ ,  $A_3$ ,  $B_0$ ,  $B_1$  and  $B_2$  describing the variations of chemical potentials in equations (5.39) and (5.40), they can be reduced to only two parameters. By virtue of the Gibbs-Duhem relation  $B_1 = -2A_2$  and  $B_2 = -(3/2)A_3$  as shown in equation (5.36).  $A_0$  refers to the reference state for the metal which is the same as  ${}^0G_M^{fcc}$  in the Hillert-Staffansson model. If the bcc state is taken as reference then the difference  ${}^0G_M^{fcc} - {}^0G_M^{bcc}$  is to be used instead of  ${}^0G_M^{fcc}$ .  $B_0$ , which refers to the infinitely dilute standard state for the nonmetal, is to be solved as a constant in the Gibbs-Duhem integration. In order to achieve compatibility with the Hillert-Staffansson model, the free energy of formation of the stoichiometric compound ( $y=1$ ) has to be used for that purpose, i.e.,

$$\Delta G_{MX}^0 = A_0 + B_0 + (A_2 + B_1) + (A_3 + B_2) \quad (5.46)$$

Since  $B_1 = -2A_2$  and  $B_2 = (-3/2)A_3$ ,

$$B_0 = \Delta G_{MX}^0 - A_0 + A_2 + \frac{A_3}{2} \quad (5.47)$$

where  $\Delta G_{MX}^0$  refers to the free energy of formation of the stoichiometric compound from the component elements. Thus for a carbide, if the bcc state for the metal and graphite are taken as component elements, then  $G_{MX}$  refers to the free energy change of the following reaction :



$$\Delta G_{MC}^0 = {}^0G_{MC} - {}^0G_M^{bcc} - {}^0G_{gr} \quad (5.49)$$

This  $\Delta G_{MC}^0$  has to be used in conjunction with  $A_0 = {}^0G_M^{fcc} - {}^0G_M^{bcc}$  in equation (5.47). Thus only two parameters  $A_2$  and  $A_3$  (or  $B_1$  and  $B_2$ ) have

to be determined. These two parameters can be related to the interaction parameters in the Hillert-Staffansson model and vice-versa by equating the coefficients of like powers of  $y$  in equations (5.39) and (5.40), and (5.42) and (5.43). Thus one obtains

$$A_0 = {}^0G_M^{\text{fcc}} \quad \text{or} \quad {}^0G_M^{\text{fcc}} - {}^0G_M^{\text{bcc}} \quad (5.50)$$

$$A_2 = -B_1/2 = L_0 - 3L_1 \quad (5.51)$$

$$A_3 = -(2/3)B_2 = 4L_1 \quad (5.52)$$

and

$$B_0 = \Delta G_{MX}^0 - A_0 + A_2 + (1/2)A_3 \quad (5.47)$$

$$= (\Delta G_{MX}^0 - A_0) + (L_0 - L_1) \quad (5.53)$$

### 5.5 Limitation of the Schottky-Wagner Model for Defect Compounds

In the last two sections, we considered the nonstoichiometric compound to be made up of (a) an ensemble of  $n_1$  moles of metal atoms and  $n_2$  moles of nonmetal atoms, and (b) as a solid solution of  $n_2$  moles of stoichiometric compound and  $(n_1 - n_2)$  moles of metal atoms (Hillert-Staffansson model). It has also been shown that if the stoichiometric compound is to taken as a reference state for the nonmetal with the former case, the two approaches are equivalent. As an alternative to these approaches, one can envision with Schottky and Wagner (80) an equivalent solid solution of  $n_1$  moles of stoichiometric compound and  $(n_1 - n_2)$  moles of interstitial vacancies. Now the Helmholtz (Gibbs) free energy of such a solid solution can be written as

$$F_{MX} = n_1 {}^0F_{MX} + (n_1 - n_2) \Delta F_{Va} + RT \ln \frac{(n_1 - n_2)! n_2!}{n_1!} \quad (5.54)$$

where

${}^0F_{MX}$  = free energy of a mole of pure stoichiometric compound

and

$\Delta F_{Va}$  = free energy change due to formation of a mole of vacancies.

Equation (5.54) is closely related to the free energy expression given by Schottky-Wagner for defect compounds. The term  $\Delta F_{Va}$  in equation (5.53) includes the internal energy and the vibrational entropy of formation of a mole of interstitial vacancies. In order that this formalism be equivalent to the other two approaches, it is clear that  $\Delta F_{Va}$  cannot be composition independent as assumed by Schottky and Wagner. The assumption of constant  $\Delta F_{Va}$  is a fairly good one in the case of defect compounds with very little deviations from stoichiometry. However in case of large deviations as in the present one,  $\Delta F_{Va}$  should depend on composition. Indeed one can obtain a good estimate of the functional dependence of  $\Delta F_{Va}$  on composition by referring to the expressions obtained via the statistical mechanical approach.

From equation (5.30) and (5.31) one can write

$$F = n_1 \bar{F}_1 + n_2 \bar{F}_2 \quad (5.55)$$

$$= n_1 \left[ \left( F_1 + \frac{F_{11}}{2} \right) - \frac{F_{22}}{2} \left( \frac{n_2}{n_1} \right)^2 \right] + n_2 \left[ \left( F_2 + F_{12} \right) + F_{22} \left( \frac{n_2}{n_1} \right) \right] + RT \ln \frac{n_2! (n_1 - n_2)!}{n_1!} \quad (5.56)$$

Rearranging the terms in equation (5.56) we obtain

$$F = n_1 \left[ F_1 + F_2 + F_{12} + \frac{(F_{11} + F_{22})}{2} \right] - (n_1 - n_2) \left[ F_2 + F_{12} + F_{22} \left( \frac{n_2}{n_1} \right) + F_{22} \frac{(n_1 - n_2)}{n_1} \right] + RT \ln \frac{n_2! (n_1 - n_2)!}{n_1!} \quad (5.57)$$

Comparing equations (5.54) and (5.57), and being reminded that all  $F_i$  and  $F_{ij}$  are dependent of temperature and independent of composition, we note that

$${}^0 F_{n \times 1, 0} = \left[ F_1 + F_2 + F_{12} + \frac{(F_{11} + F_{22})}{2} \right] \quad (5.58)$$

and

$$\Delta F_{va} = - \left\{ F_2 + F_{12} + F_{22} \left( \frac{n_2}{n_1} \right) + F_{22} \frac{(n_1 - n_2)}{2n_1} \right\} \quad (5.59)$$

Reflecting the consistency of the construction, equation (5.58) can be obtained from equation (5.27) by substituting  $n_2 = n_1$  (stoichiometry). The chemical potentials of the stoichiometric compound  $\text{MX}_{1.0}$  and vacancies can now be obtained from equation (5.57) by taking the partial derivatives of  $F$  with respect to  $n_1$  and  $(n_1 - n_2)$ . Thus

$$\frac{\partial F}{\partial n_1} \Big|_{(n_1 - n_2)} = \bar{F}_{\text{MX}_{1.0}} = \left\{ F_1 + F_2 + F_{12} + \frac{(F_{11} + F_{22})}{2} \right\} - \frac{(n_1 - n_2)^2}{2n_1^2} F_{22} + RT \ln \left( \frac{n_2}{n_1} \right) \quad (5.60)$$

and

$$\frac{\partial F}{\partial (n_1 - n_2)} \Big|_{n_1} = \bar{F}_{va} = - (F_2 + F_{12}) + F_{22} \left( \frac{n_2}{n_1} \right) + RT \ln \frac{(n_1 - n_2)}{n_1} \quad (5.61)$$

Combining equation (5.58) with equation (5.60) we obtain for the partial molar quantities

$$\bar{F}_{\text{MX}_{1.0}} = {}^0F_{\text{MX}_{1.0}} - \left\{ \frac{(n_1 - n_2)^2}{2n_1^2} \right\} F_{22} + RT \ln \left( \frac{n_2}{n_1} \right) \quad (5.62)$$

and

$$\bar{F}_{va} = {}^0F_{va} - \left( \frac{n_2}{n_1} \right) F_{22} + RT \ln \frac{(n_1 - n_2)}{n_2} \quad (5.63)$$

where

$${}^0F_{va} = - (F_2 + F_{12}) \quad (5.64)$$

These necessarily satisfy the Gibbs-Duhem equation. From equation (5.63) we conclude that the composition dependence of  $\Delta F_{va}$  arises out of various interactions. Writing

$$F = n_1 \bar{F}_{\text{MX}_{1.0}} + (n_1 - n_2) \bar{F}_{va} \quad (5.65)$$

substituting the relevant expressions from equations (5.62) and (5.63) into equation (5.65) and rearranging the terms we obtain

$$F = n_1 {}^0F_{MX_{1.0}} + (n_1 - n_2) {}^0F_{Va} - F_{22} \left\{ \frac{n_2(n_1 - n_2)}{n_1} + \frac{(n_1 - n_2)^2}{2n_1} \right\} + RT \ln \frac{n_2!(n_1 - n_2)!}{n_1!} \quad (5.66)$$

where  ${}^0F_{MX_{1.0}}$  and  ${}^0F_{Va}$  are constants as defined in equations (5.58) and (5.64) respectively.

The two terms multiplied by  $F_{22}$  in equations (5.66) which is our correction to the Schottky-Wagner expression can be explicitly identified with the free energy change due to nonmetal-vacancy and vacancy-vacancy interactions, respectively.

If in line with our most general statistical mechanical calculation leading to relations (5.33) and (5.34), we release the requirement of constancy on the  $F_{ij}$ , allowing them to become linear in  $n_2/n_1$ , we can arrive at even more general expressions corresponding to equations (5.58) and (5.59) viz.

$${}^0F_{MX_{1.0}} = \left[ F_1 + F_2 + ({}^0F_{12} + {}^1F_{12}) + \frac{1}{2} ({}^0F_{11} + {}^1F_{11}) + \frac{1}{2} ({}^0F_{22} + {}^1F_{22}) \right] \quad (5.67)$$

$$\begin{aligned} \text{and} \quad \Delta F_{Va} = - & \left[ \left[ F_2 + {}^0F_{12} + {}^1F_{12} + \frac{1}{2} ({}^0F_{22} + {}^1F_{22}) + \frac{1}{2} {}^1F_{11} \right] \right. \\ & \left. + \frac{1}{2} \left[ ({}^0F_{22} + {}^1F_{22} + 2{}^1F_{12}) \left( \frac{n_2}{n_1} \right) \right] + \frac{1}{2} {}^1F_{22} \left( \frac{n_2}{n_1} \right)^2 \right] \quad (5.68) \end{aligned}$$

$$= p_0 + p_1 \left\{ \frac{n_2}{n_1} \right\} + p_2 \left\{ \frac{n_2}{n_1} \right\}^2 \quad (5.69)$$

where  $p_0$ ,  $p_1$  and  $p_2$  stand for the various interaction terms in the brackets.

The chemical potentials of the stoichiometric compound and vacancy in the pseudo-binary solid solution can now be written as

$$\bar{F}_{MX_1 \cdot 0} = {}^0F_{MX_1 \cdot 0} - \frac{(n_1 - n_2)^2}{n_1^2} \left\{ \frac{1}{2} ({}^0F_{22} + {}^1F_{22} + 2{}^1F_{12}) \left( \frac{n_2}{n_1} \right) \right\} + RT \ln \frac{n_2}{n_1} \quad (5.70)$$

and

$$\bar{F}_{Va} = {}^0F_{Va} - \frac{n_2}{n_1} \left\{ \frac{1}{2} ({}^0F_{22} + 2{}^1F_{12}) + \frac{3}{2} {}^1F_{22} \left( \frac{n_2}{n_1} \right) \right\} + RT \ln \frac{(n_1 - n_2)}{n_2} \quad (5.71)$$

where

$${}^0F_{Va} = - (F_2 + {}^0F_{12} + {}^1F_{11}/2) \quad (5.72)$$

The overall free energy expression becomes

$$\begin{aligned} \bar{F}_{MX_1 \cdot 0} &= n_1 {}^0F_{MX_1 \cdot 0} + (n_1 - n_2) {}^0F_{Va} \\ &\quad - \frac{n_2(n_1 - n_2)}{n_1} \left[ ({}^0F_{22} + {}^1F_{22} + 2{}^1F_{12}) + \frac{1}{2} {}^1F_{22} \left( \frac{n_2}{n_1} \right) \right] \\ &\quad - \frac{(n_1 - n_2)^2}{2n_1} \left[ {}^0F_{22} + {}^1F_{22} + 2{}^1F_{12} \right] + RT \ln \frac{n_2!(n_1 - n_2)!}{n_1!} \end{aligned} \quad (5.73)$$

where  ${}^0F_{MX_1 \cdot 0}$  and  ${}^0F_{Va}$  are constants given by equations (5.67) and (5.72), respectively. The third and the fourth terms in the above expression will still be interpreted as the free energy changes due to nonmetal-vacancy and vacancy-vacancy interactions, respectively. Comparing equations (5.73) and (5.66) it is seen that the energy parameters in the latter are necessarily composition dependent.

TABLE 5.1

Excess Free Energies of fcc Phases in Fe-Ti and Fe-Nb Systems

$$E_G = X_M (1-X_M) [A + B(X_M - X_{Fe})] \text{ Joules/Mole}$$

System	A	B	$G_M^{fcc}$	$G_M^{bcc}$	Ref.
Fe-Ti	-31000	11506	-1004	+ 3.76T	Murray(2)
	-21966	11506			Kaufman(10)
Fe-Nb	0	0	9000	+ 3.56T	Kaufman(10)

TABLE 5.2

Excess Free Energies of fcc Phases in Fe-H Systems

$$EG = X \left( \frac{1-X}{H} \right) [A + B(X - X_H) + C(X - X_H)^2] \text{ Joules/Hole}$$

System	A	B	$RT \ln \gamma_H^0$	$\gamma_H^0$	$\Delta G_G^{\text{fcc}}$	$\Delta G_G^{\text{bcc}}$	Ref.
Fe-Zn	6940+5.16T	0	6940+5.16T	-	1045+0.84T	-	(123)
Fe-Cu	48205-8.45T 53360-12.63T	-5920+5.02T 11512-7.10T	54125-13.46T 41850-5.53T	-	6275+3.35T	-	(124) (125)
Fe-Ni	18300-5.15T 14240-2.82T	-14310+7.66T -10630+4.41T	32610-12.81T 24870-7.235T	-	5650-3.35T	-	(124) (126)
Fe-Cr	10830-7.45T	1410	9420-7.45T	-	10460+0.63T	-	(128)
Fe-Mn	-5980+2.64T	0	-5980+2.84T	-	1800+1.28T	-	(129)
Fe-V	-18180+1.16T	0	-18180+1.16T	-	9000+3.56T	-	(130)
Fe-Ti	-31000 -21966	11506 11506	-42506 -33372	-	1005+3.76T	-	(2) (10)
Fe-Ilc	28347-17.7T	0	28347-17.7T	-	10460+0.63T	-	(128)
Fe-IId	0	0	0	-	9000+3.56T	-	(10)

TABLE 5.3

Calculated Atomic Diameters (Coordination Number = 12)

Metal	Crystal Structure	Lattice * Parameter (KX Units)	Atomic Diameter (KX Units)	d - d Fe M (KX Units)
Cu	fcc	3.6074	2.5508	+ 0.0226
Ni	fcc	3.5166	2.4866	+ 0.0868
Co	fcc	3.5370	2.5010	+ 0.0724
		3.5540	2.5130	+ 0.0604
Fe	fcc	3.6394	2.5734	0.0
	bcc	2.8606	2.4473	
	bcc (1394K)	2.9263	2.5342	
Mn	fcc (1368K)	3.8546	2.7256	- 0.1522
	bcc (1407K)	3.0744	2.7424	
Cr	bcc	2.8788	2.5679	- 0.0055
V	bcc	3.0286	2.6956	- 0.1222
Ti	bcc (1173K)	3.3065	2.9435	- 0.3701
	hcp	2.9504(a)	3.0054	- 0.4320
		4.6833(c)	3.0623	- 0.4889
Mo	bcc	3.1405	2.8013	- 0.2279
Nb	bcc	3.2940	2.9382	- 0.3648
W	bcc	3.1586	2.8174	- 0.2440

\* Taken from

A Handbook of Lattice Spacings and Structures of Metals and Alloys, Ed. W.B. Pearson, Pergamon Press, (1958) page 21 and Table 7.

## CHAPTER VI

### ANALYSIS AND DISCUSSION

#### 6.1 Introduction

In this chapter the thermodynamic results obtained for Fe-Ti-C, Fe-Nb-C, and Fe-Nb-N austenites and  $TiC_y$ ,  $NbC_y$ , and  $NbN_y$  compound phases will be analyzed using the models outlined in the previous chapter. Following the treatment of Smith and Kirkaldy(139), the minimum observed in the solubility of titanium and niobium carbide in Fe-Ti-C and Fe-Nb-C austenites respectively, has been related to the ternary interaction parameter, viz,  $\epsilon_c^{Ti}$  and  $\epsilon_c^{Nb}$ . Starting with an approximate value for the interaction parameter obtained from the solubility minimum, a better value has been evaluated by considering the increase in the carbon content due to Nb or Ti additions. A correction term which depends on the ternary interaction parameter is given to describe the increased solubility of the carbides at higher carbon levels. The solubility relations and the interaction parameters obtained in this study are compared with those obtained by Ohtani et al.(41,42) in a parallel investigation. Some periodic table trends in the variation of the interaction parameters of the solutes in ternary austenites have also been established.

The thermodynamics of dilute ternary austenites as shown in the previous chapter can be satisfactorily described using the modified Wagner formalism. The unknowns in that description were the ternary (cross) interaction parameters,  $\epsilon_c^{Ti}$  and  $\epsilon_c^{Nb}$ . Moreover only an approximate value of the Henry's law coefficient for Nb in fcc Fe is

known. In the following sections the experimental data obtained from isoactivity measurements in Fe-Ti-C and Fe-Nb-C systems will be analyzed to obtain these parameters.

## 6.2 Analysis of Fe-Nb-C and Fe-Ti-C Austenites

The isoactivity equilibration measurements done in this study in principle allow one to obtain (i) the solubility limit as the locus of composition coordinates at which the slope of carbon isoactivity curve changes significantly and (ii) the ternary interaction parameter from the increase in carbon content due to Nb or Ti additions. Regarding the solubility limit, one finds the change of slope to be significant at high carbon levels (greater than 0.6 wt%C) but less pronounced for isoactivity curves near the minimum (around 0.5 wt%C). The error in the determination of the solubility limit as mentioned in Chapter IV is significant only near the minimum (see Figures 4.1-4.6). This is due to the error involved in the determination of Nb or Ti content being higher.

Regarding ternary interactions, the effect of Ti and Nb on carbon activity is significant enough to be measured accurately as the increase in carbon content only when the solubility limits are higher, a case obtained at higher carbon levels (greater than 0.5 wt%) and/or at higher temperatures (1373-1573K) as shown in Figures 4.1-4.6 and Tables 4.1-4.6. The solubility minimum which occurs around 0.4-0.5 wt%C and the increased solubility of the carbide at high carbon levels are also manifestations of strong solute interactions and these effects can be quantitatively related to the ternary interaction parameter as will be

shown in the subsequent sections. Thus the parameter defining the carbon-transition metal solute interactions is in principle determinable from three sources, namely, (i) the solubility minimum (ii) the increase in the amount of dissolved carbon in austenite at constant carbon activity due to the addition of Nb or Ti, and (iii) the variation of solubility product with carbon content at higher carbon concentrations. The solubility minimum, though not accurately determinable from experiments, nevertheless provides a quick estimate which can be improved by considering the other options.

#### 6.2.1 Solubility Minima and Ternary Interactions

In the following section the solubility minimum observed in austenite-carbide equilibrium is related to the ternary interaction parameter following the methodology of Smith and Kirkaldy. Let phase I be the ternary austenite phase to which the modified Wagner formalism for dilute solutions can be applied and let phase II be the carbide phase which is in thermodynamic equilibrium with phase I. At constant temperature and pressure the Gibbs-Duhem equations for phases I and II in equilibrium are

$$X_C^I du_C + X_M^I du_M + X_{Fe}^I du_{Fe} = 0 \quad (6.1)$$

$$X_C^{II} du_C + X_M^{II} du_M + X_{Fe}^{II} du_{Fe} = 0 \quad (6.2)$$

where  $X_i$ 's are the mole fractions and  $\mu$ 's are the chemical potentials. Recalling that  $\sum X_i = 1$  and subtracting equation (6.2) from (6.1) one obtains

$$(X_C^{II} - X_C^I)(du_C - du_{Fe}) + (X_M^{II} - X_M^I)(du_M - du_{Fe}) = 0 \quad (6.3)$$

According to the modified Wagner approximation:

$$\frac{d\mu_C}{RT} = \frac{dX_C}{X_C} + \epsilon_C^C dX_C + \epsilon_C^M dX_M + d\ln\gamma_{Fe} \quad (6.4)$$

$$\frac{d\mu_M}{RT} = \frac{dX_M}{X_M} + \epsilon_M^C dX_C + \epsilon_M^M dX_M + d\ln\gamma_{Fe} \quad (6.5)$$

$$\frac{d\mu_{Fe}}{RT} = -dX_C - dX_M + d\ln\gamma_{Fe} \quad (6.6)$$

Substituting these three equations into equation (6.3) results after simplification, in the differential equation

$$[a/X_C - bX_C - cX_M + d]dX_C + [e/X_M - fX_M - cX_C + g]dX_M = 0 \quad (6.7)$$

where

$$a = X_C^I ; \quad e = X_M^I \quad (6.8a)$$

$$b = (1 + \epsilon_C^C) ; \quad f = (1 + \epsilon_M^M) \quad (6.8b)$$

$$c = (1 + \epsilon_C^M) = (1 + \epsilon_M^C) \quad (6.8c)$$

$$d = (1 + \epsilon_C^C)X_C^I + (1 + \epsilon_M^M)X_M^I - 1 \quad (6.8d)$$

and

$$g = (1 + \epsilon_M^M)X_M^I + (1 + \epsilon_C^C)X_C^I - 1 \quad (6.8e)$$

where  $X_i = X_i^I$  as a shorthand notation. The optima in the solubility of the carbide if they exist are defined by:

$$\frac{dX_C}{dX_M} = 0 ; \quad \frac{dX_M}{dX_C} = 0 \quad (6.9)$$

and are obtained directly from equation (6.7) as

$$\frac{dX_C}{dX_M} = \frac{(e/X_M - fX_M - cX_C + g)}{(a/X_C - bX_C - cX_M + d)} = 0 \quad (6.10)$$

and

$$\frac{dX_M}{dX_C} = - \frac{(a/X_C - bX_C - cX_M + d)}{(e/X_M - fX_M - cX_C + g)} = 0 \quad (6.11)$$

By definition in binary transition metal carbides

$$X_C^{II} + X_M^{II} = 1 ; \quad \frac{X_C^{II}}{X_M^{II}} = y \quad (6.12)$$

Depending on the approximations that can be made with regard to concentrations of the solutes  $X_C$  and  $X_M$ , one can make further simplifications to expressions in equations (6.10) and (6.11). The first approximation that can be made is that  $X_C$  is small in comparison to  $X_M$  (by three orders of magnitude) when  $dX_C/dX_M$  is zero; and the reverse is true when  $dX_M/dX_C$  is zero. Thus neglecting the term containing  $X_C$  in equation (6.10) and  $X_M$  in equation (6.11) one obtains quadratic relations in  $X_M$  and  $X_C$  respectively which can be solved for  $(X_M)_{opt}$  and  $(X_C)_{opt}$ , respectively. Thus  $(X_M)_{opt}$  and  $(X_C)_{opt}$  can be expressed as a function of the interaction parameters and the composition of the carbide  $y$  as given below.

$$(X_M)_{opt} = - \frac{e}{g} \left[ 1 - \frac{ef}{g^2} \right] \quad (6.13)$$

and

$$(X_C)_{opt} = - \frac{a}{d} \left[ 1 - \frac{ab}{d^2} \right] \quad (6.14)$$

Depending on the relative contribution of the second term in the brackets, one should decide on the merits of neglecting of that term in comparison to 1.0. In Fe-Nb-C and Fe-Ti-C systems these terms, namely  $ef/(g^2)$  and  $ab/(d^2)$ , are generally small compared to 1.0 and hence can

be ignored to obtain the following simpler relations.

$$(X_M)_{opt} = -\frac{e}{g} = -\frac{1}{y\epsilon_M^C + \epsilon_M^N} \quad (6.15)$$

and

$$(X_C)_{opt} = -\frac{a}{d} = -\frac{y}{\epsilon_C^N + y\epsilon_C^C} \quad (6.16)$$

and the optimum will exist if  $e/g$  and/or  $a/d$  is negative.

The ternary interaction parameter  $\epsilon_C^M$  can also be obtained from equations (6.10) and (6.11) in terms of  $(X_M)_{opt}$  and  $(X_C)_{opt}$ , respectively, by rearranging the terms as given below.

$$\epsilon_M^C = -\frac{1}{y(X_M)_{opt}} \left[ 1 + \epsilon_M^N (X_M)_{opt} - f(1+y)(X_M)_{opt}^2 \right] \quad (6.17)$$

and

$$\epsilon_M^C = -\frac{y}{(X_C)_{opt}} \left[ 1 + \epsilon_C^N (X_C)_{opt} - \frac{b}{y} (1+y)(X_C)_{opt}^2 \right] \quad (6.18)$$

If the contribution from the quadratic terms are not very significant and if the carbide is assumed to be close to stoichiometry (an approximation valid only when  $dX_M/dX_C = 0$ ) one obtains simpler relations corresponding to the above equations as

$$\epsilon_M^C = -\frac{1}{y(X_M)_{opt}} \left[ 1 + \epsilon_M^N (X_M)_{opt} \right] \quad (6.19)$$

and

$$= -\frac{1}{(X_C)_{opt}} \left[ 1 + \epsilon_C^N (X_C)_{opt} \right] \quad (6.20)$$

In Fe-Ti-C and Fe-Nb-C systems the optimum corresponding to  $dX_M/dX_C = 0$  exists while the other optimum lies beyond the stability

region of austenite-carbide equilibria and hence is not experimentally attainable. The solubility minimum  $((X_c)_{opt})$  in these two systems could be determined only to a limited accuracy and hence should be used only for a first estimate of the ternary interaction parameter. The solubility minimum occurs between 0.4Wt%C and 0.5Wt%C in Fe-Nb-C system and between 0.35Wt% and 0.45Wt%C in the Fe-Ti-C system. From equation(6.20) the C-Nb ternary interaction parameter can be determined to be around -50 and the C-Ti interaction parameter to be around -60. It is difficult to estimate the temperature dependence of these parameters as the minimum is not sharply defined. Further improvements in the value of the interaction parameters can be made using the other options as will be shown in the subsequent sections.

### 6.2.2 Increase in Carbon Content and Ternary Interactions

The parameter  $\epsilon_c^M$  can be determined to a fair degree of accuracy from the increase in carbon contents due to niobium or titanium additions at constant carbon activity, as shown below. The carbon activity in a ternary Fe-M-C alloy within the modified Wagner formalism is written as

$$\ln a_c = \ln X_c + \ln^0 \gamma_c + \epsilon_c^c X_c - \frac{1}{2} [\epsilon_c^c (X_c)^2 + \epsilon_M^M (X_M)^2] + \epsilon_c^M X_M \quad (6.21)$$

Rearranging the terms in equation (6.21) we obtain

$$[\ln \gamma_c - \ln^0 \gamma_c] - [\epsilon_c^c X_c - 1/2 \{ \epsilon_c^c (X_c)^2 + \epsilon_M^M (X_M)^2 \}] = \epsilon_c^M X_M \quad (6.22)$$

where  $\gamma_c$  refers to the activity coefficient of carbon in ternary austenite.  $\gamma_c$  is known from the experimental isoactivity curves. Only

those Nb compositions that lie in the single phase austenitic region are to be considered for the determination of  $\epsilon_c^M$  using equation (6.22) which requires an a priori knowledge of the phase boundary. Even though equation (6.22) is directly applicable to the experimental results in this study, there is an inherent problem in using this expression. A close scrutiny would reveal that the product ( $\epsilon_c^M X_M$ ) is small (around  $1.0E-02$ ) by virtue of  $X_M$  being small and this small value is obtained as a second difference of positive terms, shown in square brackets in equation (6.22). Therefore the error involved in the determination of  $\epsilon_c^M$  would be high. A better procedure would be to obtain expressions for evaluating the ternary interaction parameter that can directly use the increase in carbon contents measured in this study. The procedure will be outlined in the following paragraphs.

At constant carbon activity, the expressions for the carbon activities in the binary Fe-C alloy and ternary single phase Fe-M-C alloys can be equated to obtain,

$$\begin{aligned} \ln a_c &= \ln X_c^B + \ln^0 \gamma_c + \epsilon_c^C X_c^B - \frac{1}{2} \epsilon_c^C (X_c^B)^2 \\ &= \ln X_c^T + \ln^0 \gamma_c + \epsilon_c^C X_c^T - \frac{1}{2} [ \epsilon_c^C (X_c^T)^2 + \epsilon_M^M (X_M)^2 + 2\epsilon_c^M X_c^T X_M ] + \epsilon_c^M X_M \end{aligned} \quad (6.23)$$

where  $X_c^B$  and  $X_c^T$  refer to the carbon contents in binary and ternary alloys and  $\epsilon_c^C$ ,  $\epsilon_M^M$  and  $\epsilon_c^M$  are the interaction parameters. Equation (6.24) allows us to cancel the large contribution in  $\ln^0 \gamma_c$  from both sides and on rearranging the terms and denoting the increase in carbon content as  $\Delta X_c$  we obtain

$$\frac{\ln\left[1 + \frac{\Delta X_c}{X_c^B}\right] + \Delta X_c \varepsilon_c^C \left[1 - \frac{\Delta X_c}{2(1-X_c^B - \Delta X_c)}\right] - \frac{1}{2} \varepsilon_M^M (X_M)^2}{(1 - X_c^B - \Delta X_c)} = -\varepsilon_c^M X_M \quad (6.24)$$

Equation (6.24) has been arranged in a form such that the left hand side(LHS) contains only the compositions and the binary interaction parameters and a graph of LHS vs  $X_M$  should yield the ternary interaction parameter as its slope. This expression can be simplified to various degrees depending on the "diluteness" of the solutes and the relative magnitudes of the self interaction parameters. If the concentration of the alloying element M is small compared to that of carbon as in the present case ( $X_M < 1.0E-02 * X_c$ ) then one can neglect the contribution due to the second order term ( $\varepsilon_M^M \cdot X_M^2$ ). As the atomic weights of Nb and Ti are large in comparison to that of carbon, the contribution from this term is negligible even at concentrations as high as 1.0 wt%Nb ( $X=6E-03$ ) and 0.5 wt%Ti ( $X=5.0E-03$ ). Typical values of the various terms in the above equation applicable to Fe-Ti-C and Fe-Nb-C systems are given below.

$$X_c^T, X_c^B \approx 4-8 \times 10^{-2} \quad ; \quad \Delta X_c \approx 1-5 \times 10^{-3}$$

$$\frac{\Delta X_c}{X_c^B} \approx 5 \times 10^{-2} \quad ; \quad \frac{\Delta X_c}{(1-X_c^T)} \approx 5 \times 10^{-3}$$

Since the relative increase in carbon content, i.e.,  $\Delta X_c / X_c$  is of the order of 0.02-0.05, the logarithmic term can be expanded up to second order using a Taylor series. Similar expansion can be made for the term

$1/(1-X_c-\Delta X_c)$  as  $X_c+\Delta X_c$  is less than 1.0. Incorporating these simplifications into equation (6.24) and ignoring the cubic terms in  $(\Delta X_c/X_c)$  we get

$$-\epsilon_c^N X_N = \frac{\Delta X_c}{X_c^B} \left[ 1 + X_c^B + \epsilon_c^C X_c^B \right] - \left\{ \frac{\Delta X_c}{X_c^B} \right\}^2 \left[ 1 - X_c^B + \epsilon_c^C (X_c^B)^2 + \epsilon_c^C (X_c^B)^3 \right] \quad (6.25)$$

$$-\epsilon_c^N X_N = \frac{\Delta X_c}{X_c^B} \left[ 1 + X_c^B + \epsilon_c^C X_c^B \right] - \left\{ \frac{\Delta X_c}{X_c^B} \right\}^2 \quad (6.26)$$

Thus the ternary interaction parameter is directly related to the relative increase in carbon content and the binary interaction parameters. Further simplification is possible, as in most cases the contribution from the quadratic term is less than 3-5% of the leading term. Thus neglecting the quadratic term in equation (6.26) we get

$$-\epsilon_c^N X_N = \frac{\Delta X_c}{X_c^B} \left[ 1 + X_c^B + \epsilon_c^C X_c^B \right] \quad (6.27)$$

Simplifications in the leading can be made only if the carbon content and the contribution from the  $\epsilon_c^C X_c^B$  term are small (less than  $1.0E-02$ ) compared to 1.0. The carbon levels used for the determination of the ternary interaction parameter in this study are high viz.,  $1.0 < \text{wt}\%C < 2.0$ , i.e.,  $0.04 < X_c < 0.08$  and since  $\epsilon_c^C$  is around 6.5, the contribution from  $X_c$  and  $\epsilon_c^C X_c^B$  are as high as 0.4 compared to 1.0 and hence further simplification is not valid. In the case of the Fe-Nb-N system one can simplify further as the nitrogen contents are two orders of magnitude smaller than the carbon levels in corresponding carbon austenites. These simplifications will be discussed in section 6.3.1 which deals with the determination of the Nb-N interaction parameter.

### 6.2.3 The Niobium-Carbon Interaction Parameter

In this section we determine the niobium-carbon interaction parameter by applying equation (6.27) to the experimental data outlined in chapter IV. Equation (6.27) is ideally suited for the determination of  $\epsilon_c^{\text{Ni}}$  (rather  $-\epsilon_c^{\text{Ni}}$ ) for the following reasons; (i) all the terms inside the brackets are positive and hence  $-\epsilon_c^{\text{Ni}}$  is evaluated as a sum of positive terms of similar magnitude rather than difference between two large or two small terms as mentioned in the earlier section, (ii) these terms ( $X_c$  and  $\epsilon_c^{\text{C}}$ ) are known to a high degree of accuracy and (iii) the error in the value of  $\epsilon_c^{\text{Ni}}$  is directly proportional to the error in the determination of  $\Delta X_c$  and therefore higher weights can be given to the data corresponding to larger values  $\Delta X_c$  which are obtained at higher temperatures and higher carbon contents.

A graph depicting the variation of  $-\Delta X_c / X_c [1 + X_c + \epsilon_c^{\text{C}} \cdot X_c]$  (the right hand side of equation (6.27)) with  $X_{\text{Nb}}$  is shown in Figures 6.1-6.3 for three temperatures investigated in this study. It can be seen that the slope which is negative and equal to  $\epsilon_c^{\text{Ni}}$  is accurately determinable at 1373K and 1473K. The solubility is very low at 1273K and hence the accuracy is reduced for that temperature. However, one can extrapolate the values obtained at 1373K and 1473K to 1273K and cross-check it with the value obtained from isoactivity curves at high carbon levels (>1.0wt%C) at 1273K. From the values obtained at these three temperatures it can be noted that the variation of the interaction parameter (when expressed as  $RT\epsilon_c^{\text{Ni}}$ ) with temperature is very small and therefore the entropic part of the interaction parameter should not be very significant. The free energy of formation of these carbides which

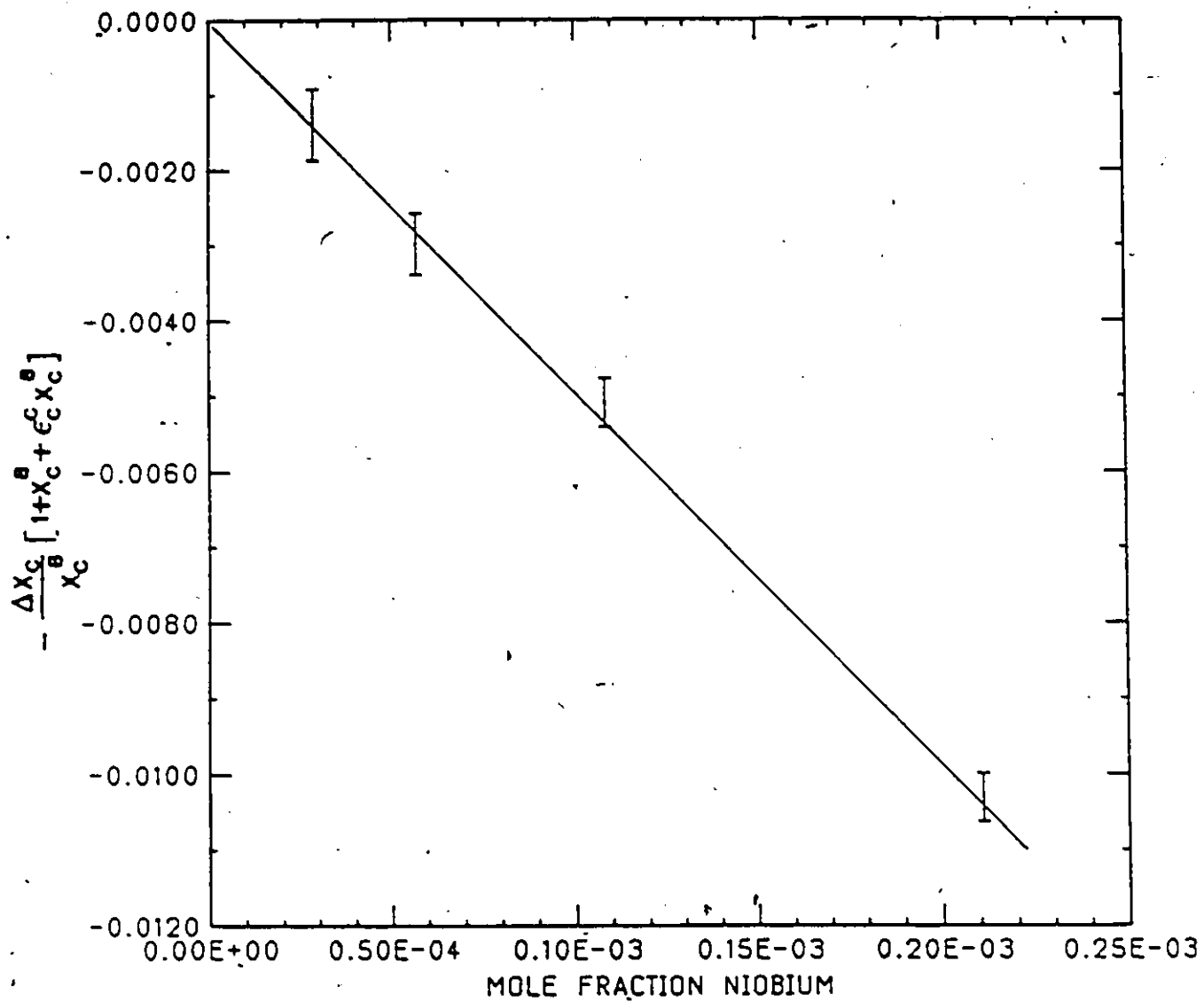


FIG. 6.1 DETERMINATION OF NIOBIUM-CARBON INTERACTION PARAMETER IN Fe-Nb-C AUSTENITE (T=1273K)

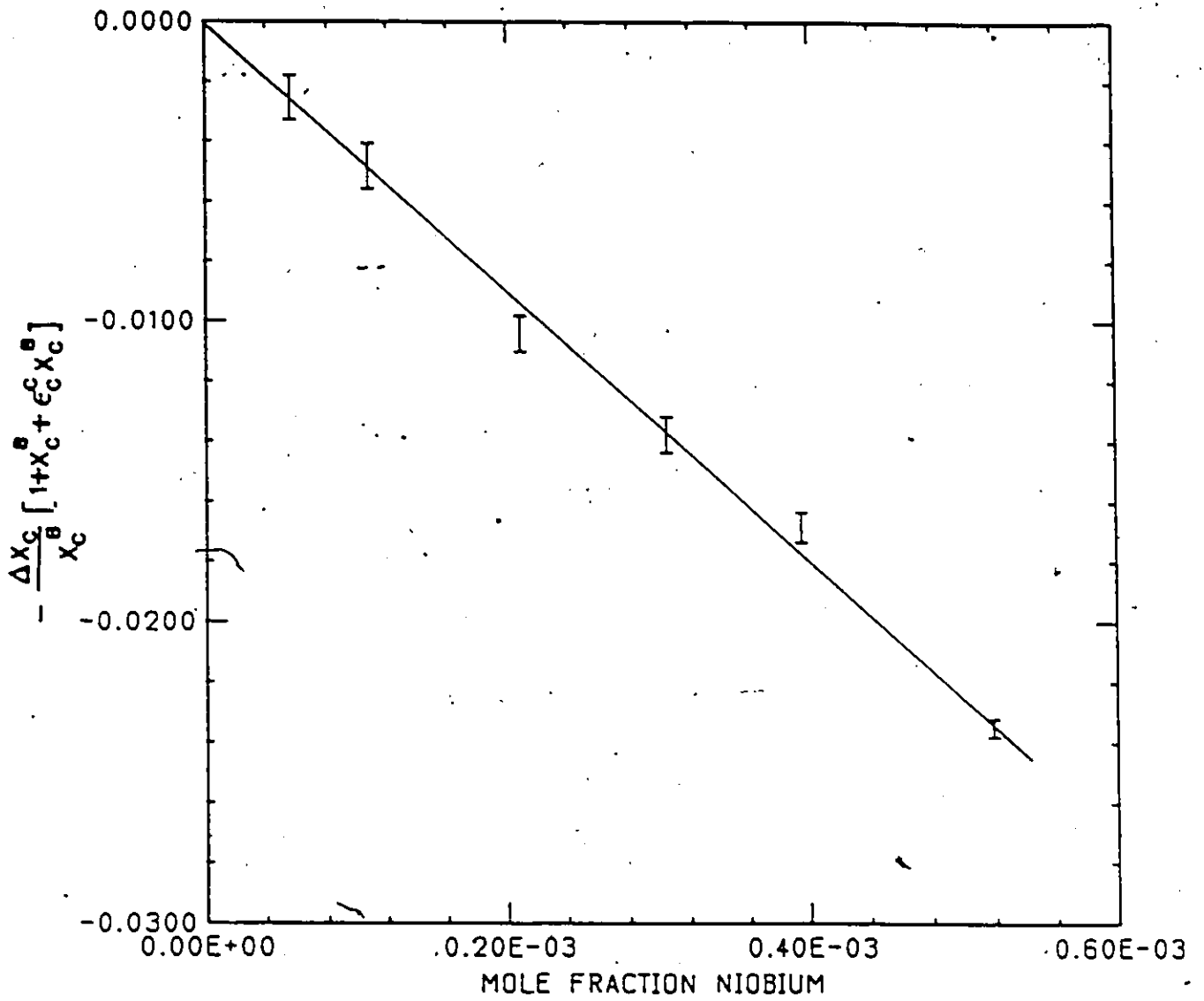


FIG. 6.2 DETERMINATION OF NIOBIUM-CARBON INTERACTION PARAMETER IN Fe-Nb-C AUSTENITE (T=1373K)

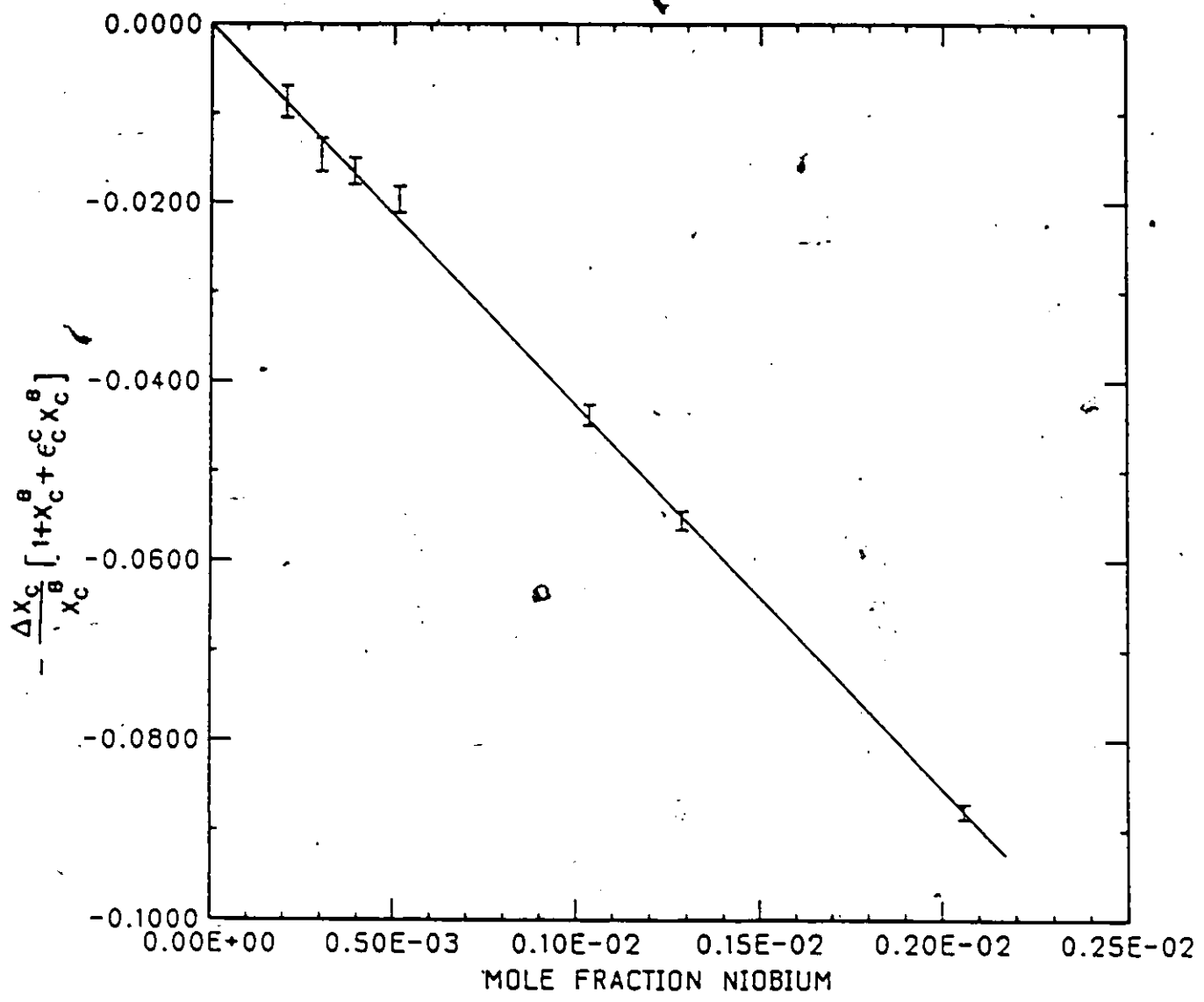


FIG. 6.3 DETERMINATION OF NIOBIUM-CARBON INTERACTION PARAMETER IN Fe-Nb-C AUSTENITE (T=1473K)

is a good measure of the interaction between carbon and the transition metals, as will be shown later, correlates well with the ternary interaction parameters ( $RT\epsilon_c^M$ , M=transition metal), in austenite. The small change in interaction parameter with temperature is in agreement with the low entropy of formation observed for these carbides. The C-Nb interaction parameter is determined as

$$\epsilon_C^{Nb} = - \frac{(65350 \pm 4000)}{T} + 2.5 \quad (6.28)$$

#### 6.2.4 The Titanium-Carbon Interaction Parameter

The approximate ternary titanium-carbon interaction obtained from the solubility minimum has been improved by considering the increase in carbon contents of equilibrated Fe-Ti alloys at high carbon and/or high temperatures similar to the Fe-Nb-C austenite outlined in the earlier section. Figures 6.4-6.6 show the variation of the right hand side of equation (6.27) with  $X_{Ti}$  for three temperatures 1273K, 1373K, and 1473K. The variation is similar in magnitude to the niobium-carbon interaction but the slope ( $\epsilon_c^{Ti}$ ) is more negative for the titanium case. This is in line with the free energy of formation of TiC being more negative compared to that of NbC. The temperature dependence of  $RT\epsilon_c^{Ti}$  like  $RT\epsilon_c^{Nb}$  is also very small, the reason being the same as outlined in the earlier section. The C-Ti interaction parameter is given by

$$\epsilon_C^{Ti} = - \frac{(85400 \pm 5000)}{T} + 5.0 \quad (6.29)$$

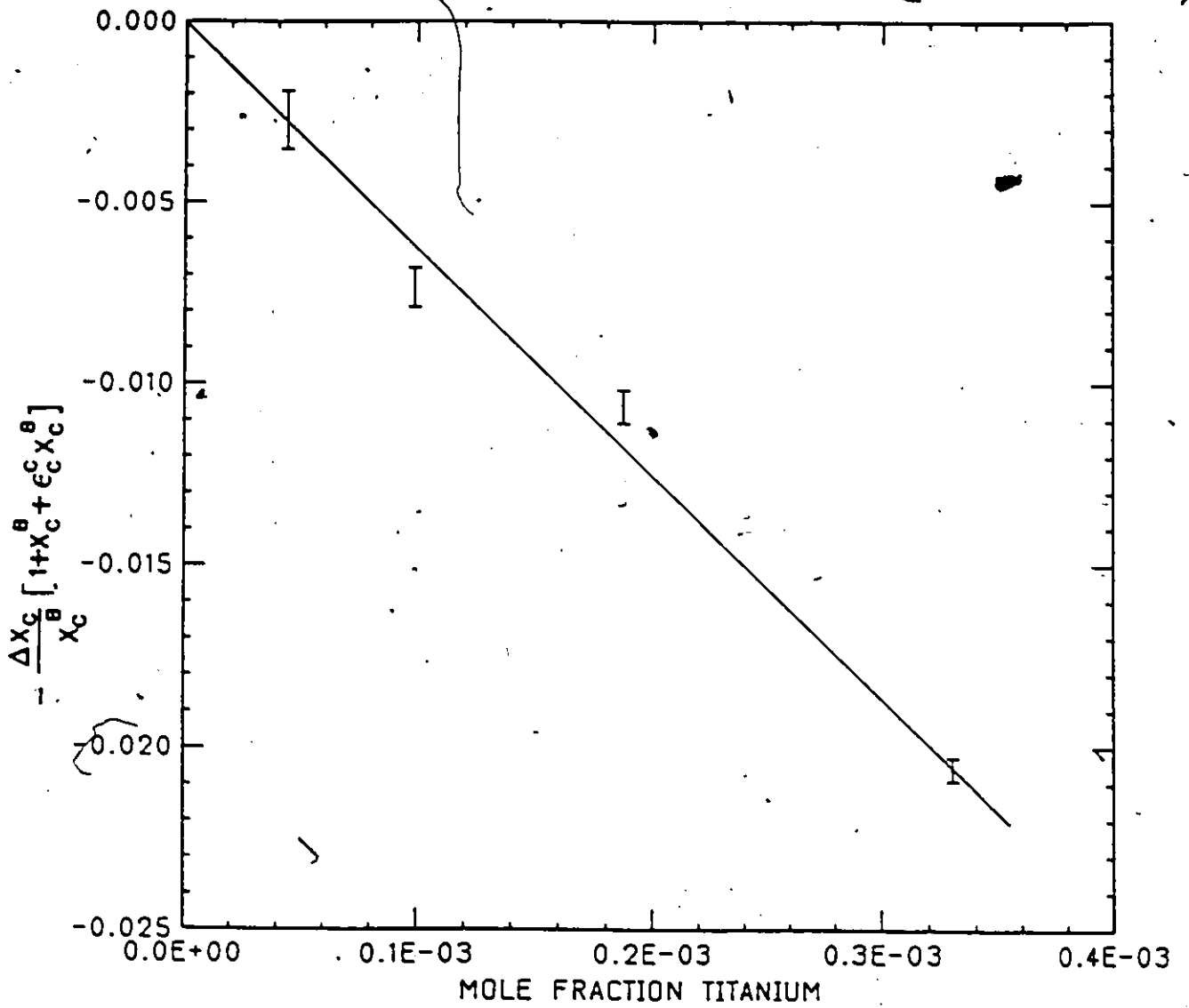


FIG. 6.4 DETERMINATION OF TITANIUM-CARBON INTERACTION PARAMETER IN  $F_{\theta}$ -Ti-C AUSTENITE (T=1273K)

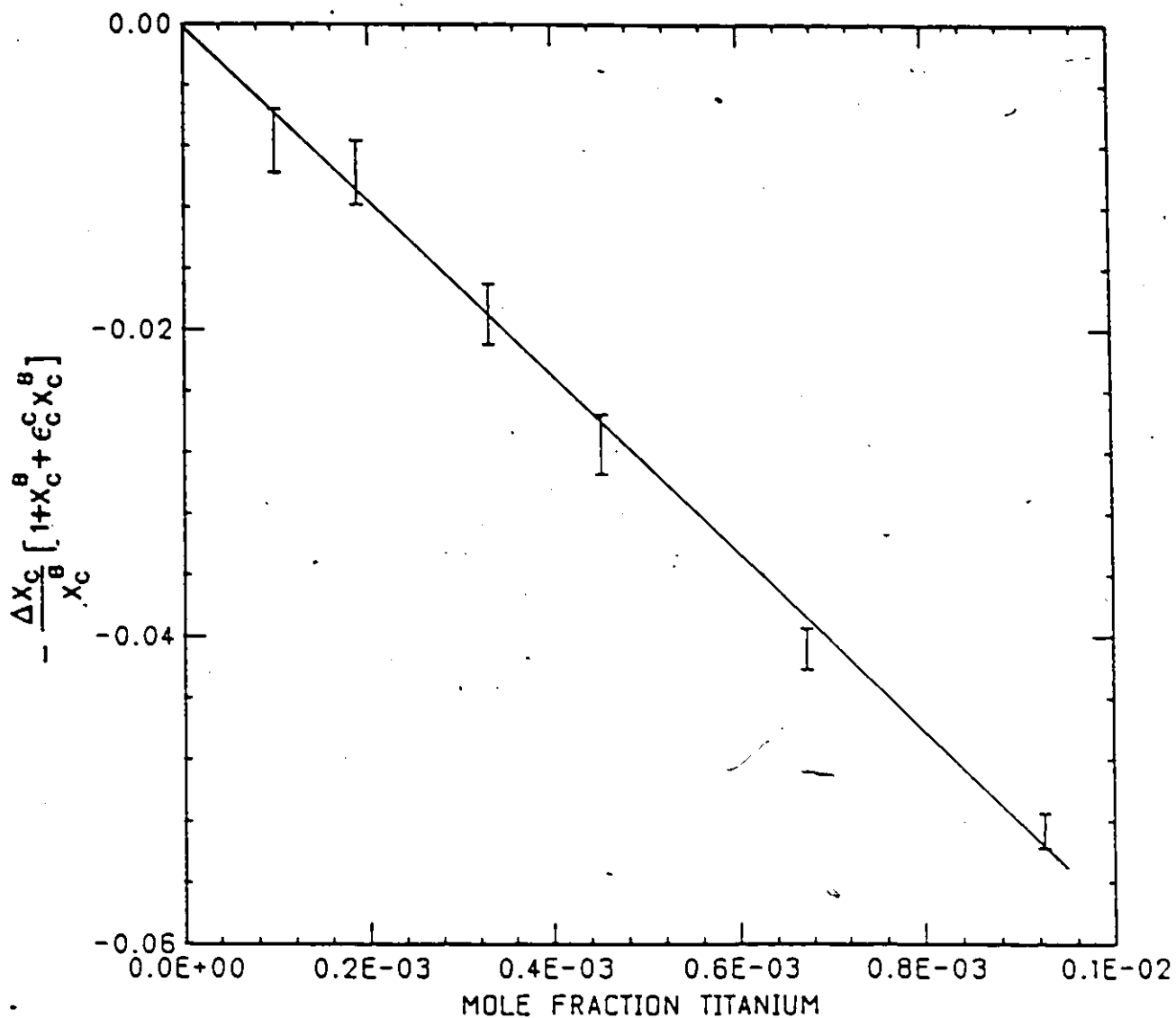


FIG. 6.5 DETERMINATION OF TITANIUM-CARBON INTERACTION PARAMETER IN Fe-Ti-C AUSTENITE (T=1373K)

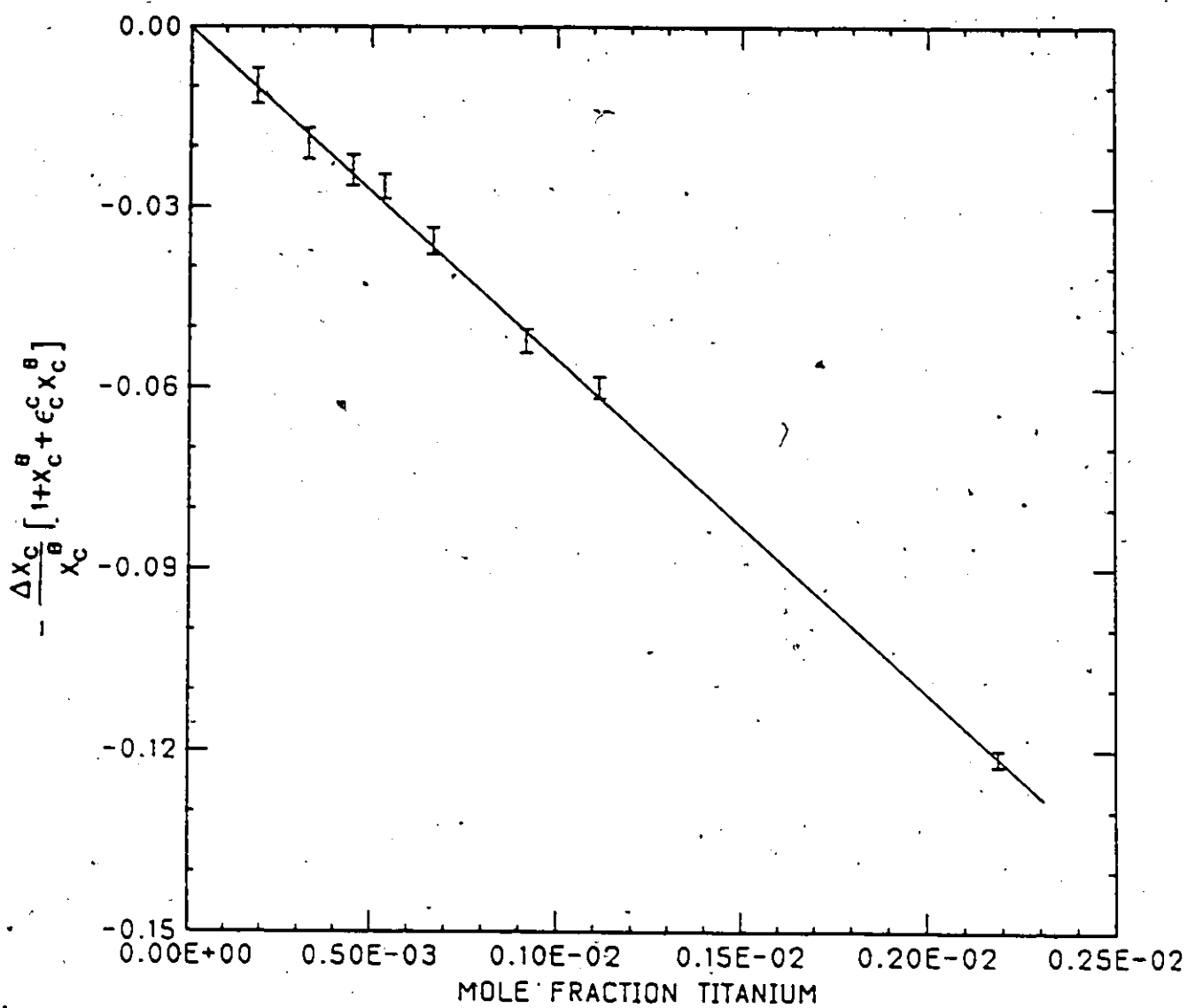


FIG. 6.6 DETERMINATION OF TITANIUM-CARBON INTERACTION PARAMETER IN Fe-Ti-C AUSTENITE (T=1473K)

### 6.2.5 The Carbide Solubility and Ternary Interactions

In this section the increased solubility of the carbide at high carbon levels will be described using an additional term to the classical solubility relationship. This additional term is dependent on the ternary interaction parameter and therefore serves as a means for checking the consistency in the experimental results. The classical part of the solubility product relation will be used to obtain the free energy of dissolution of Nb or Ti at infinite dilution (Henry's law coefficient). It has been noted in the earlier chapters that the mass action law approach is not feasible for the analysis of the austenite - nonstoichiometric carbide equilibria. However, if the composition of the carbide can be considered as being close to stoichiometry (a condition realised at high carbon levels), then one can use the mass action law to obtain simpler expressions for the solubility of the carbide.

The mass action law for the austenite - stoichiometric carbide equilibrium can be written as



$$\Delta G_{MC}^{\circ} = RT \ln[a_M a_C] = RT [\ln(X_M X_C) + \ln(\gamma_M \gamma_C)] \quad (6.31)$$

where  $\Delta G^{\circ}$  refers to the free energy of formation of the stoichiometric carbide MC,  $a_M$  and  $a_C$  are the activities of Ti (or Nb) and carbon respectively.  $\gamma_M, \gamma_C, X_M, X_C$  are the activity coefficients and the mole fractions of Ti (or Nb) and carbon, respectively. Assuming the modified Wagner expansion for the activities of the solutes we obtain the solubility product from equation (6.31) as

$$\ln(X_M X_C) = \left[ \frac{\Delta G_{M,C}^U}{RT} \right] - \left[ \ln({}^0 Y_M {}^0 Y_C) \right] - \left[ \epsilon_C^C (1-X_C) + \epsilon_C^M (1-X_M) \right] X_C - \left[ \epsilon_M^M (1-X_M) + \epsilon_M^C (1-X_C) \right] X_M \quad (6.32)$$

The classical solubility product is given by the first two terms on the right hand side of equation (6.32) and hence the correction terms due to solute interactions at high carbon and metal contents are given by the succeeding terms. At high carbon levels the concentration of transition metal solute is low in comparison and hence the last term in equation (6.32) can be neglected. As  $\epsilon_C^M$  is an order of magnitude larger than  $\epsilon_C^C$  some simplifications in the third term are possible. The maximum carbon content in austenite is about 2.0Wt% ( $X=0.08$ ) and since  $\epsilon_C^M$  is an order of magnitude larger than  $\epsilon_C^C$ , neglecting  $X_C$  in comparison to 1.0 will introduce no more than 1.0% error in the third term. The error due to neglecting  $X_M$ , which is less  $5.0E-03$  in comparison to 1.0, will be even smaller. Incorporating these simplifications in the above equation one obtains the modified solubility product as

$$\ln(X_M X_C) = \ln K - \left[ \epsilon_C^C + \epsilon_M^C \right] X_C \quad (6.33)$$

where K refers to the classical solubility product derived from the first two terms in equation (6.32). Equation (6.33) can be written in terms of wt%C and Wt%M by using the following conversion expressions.

$$X_C = \frac{(\text{Wt}\%C)}{21.5} (1 - 0.04\text{Wt}\%C) = \frac{(\text{Wt}\%C)}{21.5} \quad (6.34a)$$

$$X_{Nb} = \frac{(\text{Wt}\%Nb)}{166.35} ; \quad X_{Ti} = \frac{(\text{Wt}\%Ti)}{85.77} \quad (6.34b)$$

It can be seen that the linear transformation from mole fraction to

Weight percent and vice versa is valid only for the transition metal solutes and for carbon contents less than 0.5 wt%. Carbon contents higher than 0.5Wt%C carbon introduce an error in the slope of solubility vs Wt%C curves proportional to the concentration. In the range of 1-2 Wt%C the slope is underestimated by 5-8% if the linear approximation is used for converting carbon concentrations. Within this approximation the variation of solubility product with Wt%C can be related to the ternary interaction parameters as given below.

$$\log[(\text{Wt}\%M)(\text{Wt}\%C)] = \log K - \left[ \frac{(\epsilon_C^C + \epsilon_M^C)}{(21.5)(2.303)} \right] (\text{Wt}\%C) \quad (6.35)$$

The solubility limit obtained from the change in slope of the isoactivity curves can be fitted to the equation (6.33) in order (i) to cross-check the value of the ternary interaction parameter and (ii) to determine the leading term defining the classical solubility product. Thus a graph of  $\ln[X_M X_C]$  vs  $X_C$  is a straight line with  $\ln K$  as intercept and the slope is directly related to the interaction parameters as given in equation (6.33).

It was noted in Chapter IV that the accuracy of determination of the Ti or Nb content is less near the minimum, but actual error entering the left hand side of equation (6.33) is very small. This is due to the concentrations being expressed in mole fraction units. Moreover the ternary interaction parameter  $\epsilon_C^M$  is in consonance with the Wagner expansion only in mole fraction units. Therefore equation (6.33) is better suited for the determination of the interaction parameter rather than equation (6.35). Ohtani et al. (41,42) expressed their results in the form of equation (6.35) to illustrate the variation of the

solubility product observed in their study. Equation (6.35) has been derived in this section to illustrate the approximations and the attendant errors involved. Within 8-10% error margin equation (6.35) facilitates comparison of results from this study with those of Ohtani et al. The variation of the  $\ln[X_{Nb} \cdot X_C]$  with  $X_C$  and  $\ln[X_{Ti} \cdot X_C]$  with  $X_C$ , respectively were given in Chapter IV in Figures 4.7 and 4.8.

#### 6.2.6 Comparison with Results of Ohtani

Ohtani et al. (41,42) in a parallel study reported increased solubility of the carbide at high carbon concentrations in Fe-Ti-C and Fe-Nb-C systems. These authors considered the austenite and the carbide to be isostructural (NaCl) and analyzed their solubility data in terms of the sublattice model. The two principal results of their investigation, namely, (i) the solubility limit and (ii) the ternary interaction parameter can be compared with the results obtained in this study. Ohtani et al. expressed solubility limits in an expression similar to equation (6.35). Therefore the ternary interaction parameter can be extracted from the correction term in equation (6.35). The results from this study and those of Ohtani are given in Table 6.1. The solubility limits obtained at 1373K and 1473K in this study for Fe-Nb-C and Fe-Ti-C systems have been compared with those of Ohtani et al in Figures 6.7-6.10.

##### 6.2.6.1 Comparison of the Results in Fe-Nb-C System

It can be seen from Table 6.1, that the ternary interaction parameter for niobium-carbon obtained from the results of Ohtani are

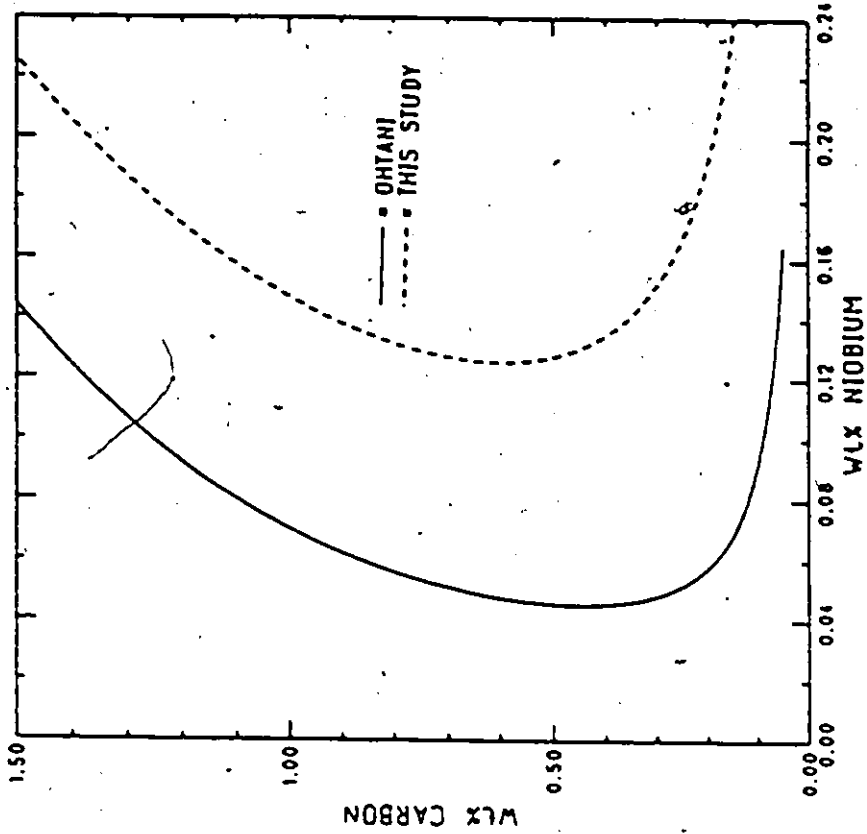


FIG. 6.8 SOLUBILITY LIMIT OF NbC IN AUSTENITE (T=1473K)

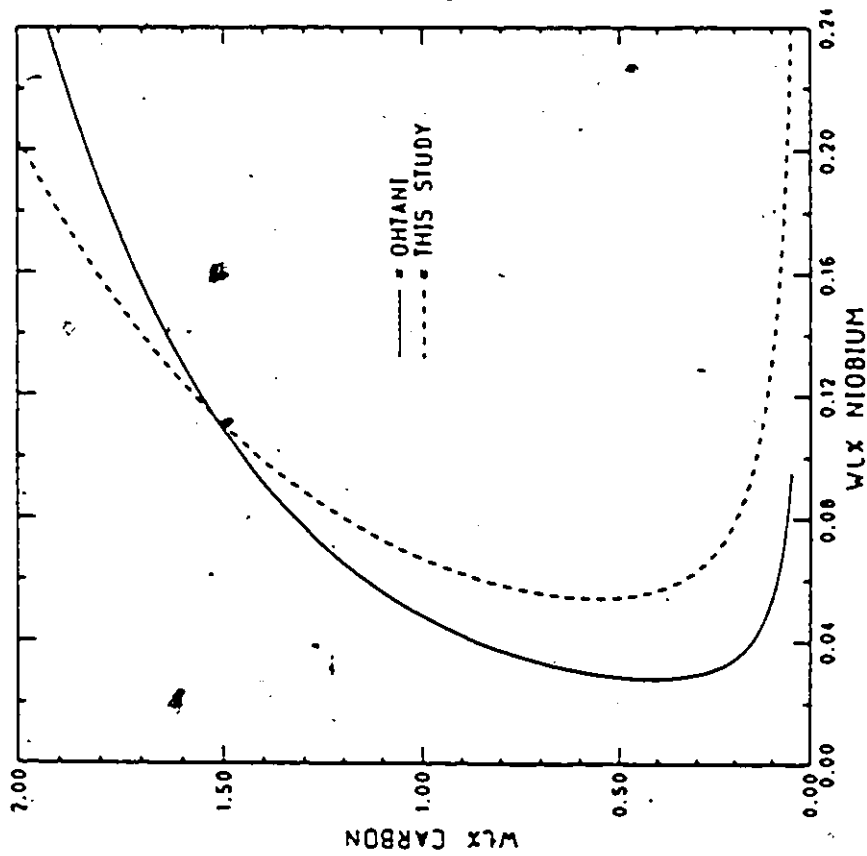


FIG. 6.7 SOLUBILITY LIMIT OF NbC IN AUSTENITE (T=1373K)

slightly more negative compared to the value obtained in this study but the values are well within 10% of each other. It is also worth noting that the entropic component of the interaction parameters are very small in both investigations. The solubility limits which are compared in Figures 6.7 and 6.8 show fair agreement at lower temperatures (1373K and below) but the difference between the two data sets widen with increasing temperature. The solubility as given by Ohtani are smaller than that obtained in this study. The reason for this is to be found in the leading term in equation 6.33 which defines the classical solubility product expression that neglects the solute interactions. On comparing the value for this term from the two studies (Table 6.1), it can be seen that Ohtani's result  $[(-4880/T)+1.18]$  is marked by smaller (absolute value) enthalpic and entropic contributions compared to those obtained in this study, viz.,  $[(-8030/T)+3.89]$ . This value is composed of three components, namely, (i) the free energy of formation of the stoichiometric carbide and (ii) the free energy of dissolution of carbon and (ii) and free energy of dissolution of niobium in austenite. The contributions from the first two components are the same in both the studies and therefore the difference in the solubility product values should result in different values for the free energy of dissolution of Nb in fcc Fe. The free energy of dissolution ( $RT \ln \gamma_{Nb}^{\circ}$ ) determined in the two studies are given in Table 6.1 along with the solubility products and the interaction parameters. It can be seen that the  $RT \ln \gamma_{Nb}^{\circ}$  values evaluated from Ohtani's results are more positive compared to the values obtained in this study, in line with the solubility differences observed in the two studies, i.e., the lower the

solubility the more positive is the free energy of dissolution. Further analysis of this value is required for resolving this discrepancy and it shall be taken up in the section subsequent to the comparison of the results in Fe-Ti-C system.

#### 6.2.6.2 Comparison of the Results in Fe-Ti-C System

The solubility limits and the interaction parameters in the Fe-Ti-C system from this study and those of Ohtani et al. are given in Table 6.1 along with the results for the Fe-Nb-C system. The titanium-carbon interaction parameter extracted from Ohtani's result given in the form of equation (6.35) is smaller compared to both the value obtained in this study as well as the niobium-carbon parameter. However the solubility limits (taken from Figures 3, 6c in ref.42) given by these authors are in very close agreement with the limits obtained in this study as shown in Figures 6.9 and 6.10. Therefore the expression for the solubility product given by Ohtani et al. from which the interaction parameter was extracted could be in error. This expression is also shown in Figures 6.9 and 6.10. This small discrepancy between the expression and the actual solubility limit could be due to ill-conditioning effects that arise during curve fitting. The interaction parameter value obtained by refitting the solubility limits given by Ohtani is in excellent agreement with that determined in this study. The classical solubility product values (leading term in equation (6.35)) are also in good agreement.

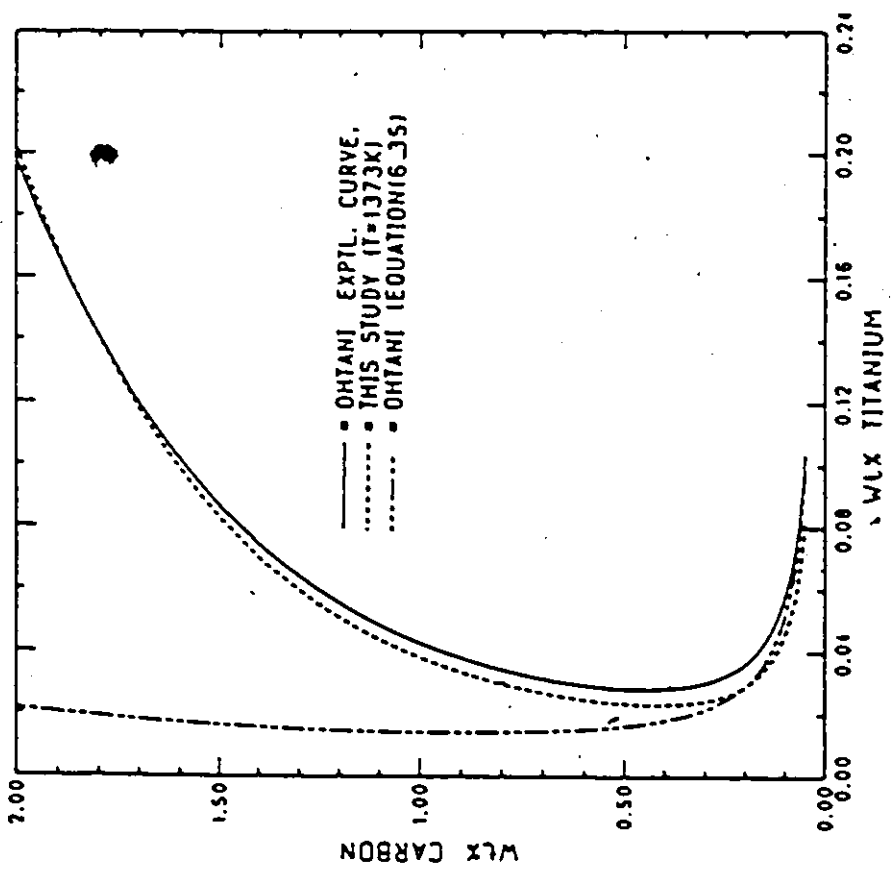


FIG. 6.9 SOLUBILITY LIMIT OF TiC IN AUSTENITE (T=1373K)

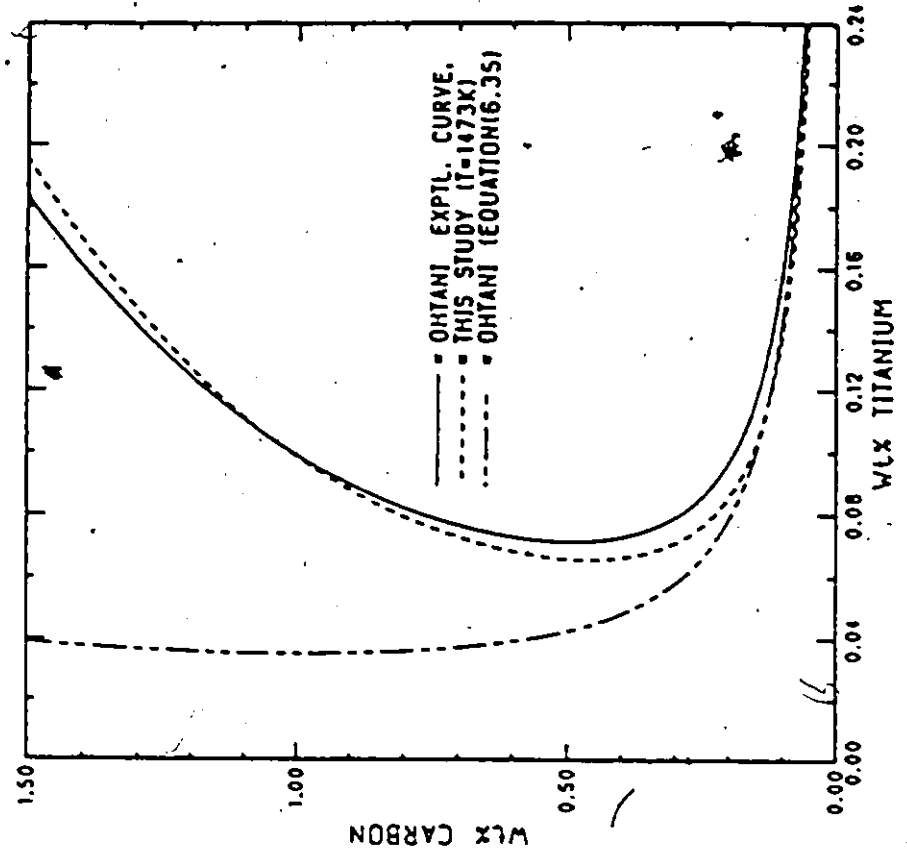


FIG. 6.10 SOLUBILITY LIMIT OF TiC IN AUSTENITE (T=1473K)

### 6.2.7 Free Energy of Dissolution of Nb and Ti In FCC Iron

In this section the discrepancy in the value of free energy of dissolution of Nb noted in the earlier section will be examined further. It was also noted that the free energy of dissolution of Nb in fcc iron could be obtained from the classical solubility product relationship involving NbC and NbN in austenite. Thus this value can be extracted from the solubility values given by various investigators listed in Tables 2.4 and 2.5 in the literature review. The results obtained from such an exercise together with the values obtained by Ohtani et al. and those obtained in this study are given in Table 6.2.

It can be seen from Table 6.2 that values ranging from -12KJ/mole to +18KJ/mole are obtained. Ohtani's results range from -5KJ/mole to +8KJ/mole while the present study gives -10(+1.5)KJ/mole in the temperature range 1273K-1473K. Few other features can be inferred from the results illustrated in Table 6.2. Firstly, both the enthalpic and entropic components exhibit a wide range of values and secondly the values determined from the NbN solubility are more consistent than those determined from the NbC solubility. In fact the Fe-Nb-N system, as will be shown in a later section, satisfies all the assumptions made in the derivation of the classical solubility relationship. Most of the studies including the present one were done close to and at one atmosphere nitrogen and hence the precipitate is close to stoichiometry, while only studies done at very high carbon levels like the present one satisfy this requirement in the Fe-Nb-C system. The contributions arising from solute interactions are minimal due to very low concentrations of N in austenite and hence the solubility limits in

Fe-Nb-N austenite reflect the dissolution characteristics of N and Nb to a greater degree than the corresponding carbon austenite. Moreover, the NbN solubility can be accurately determined as the change of slope in the variation of nitrogen content with niobium at constant nitrogen potential is very pronounced. Therefore the values obtained from NbN studies should be more reliable. Thus the dissolution free energy of niobium in iron should be around -10 to -15 KJ/mole in the temperature range 1273K-1473K.

In the previous chapter we noted the periodic table variation of the dissolution free energies of transition metal solutes in the first long period. As niobium belongs to the same group(VA) as vanadium and since its size factor is closer to that of titanium, it was also noted that its free energy of dissolution should lie between those of titanium and vanadium. The value obtained from such a correlation is around -15KJ/Mole which is closer to the values determined from the NbN solubility data. The values obtained in this study from both the NbC and NbN solubility lie around -8 to -12 KJ/Mole and hence there is overall consistency in the experimental results. The following average of the values obtained from the NbN solubility results of various investigations including the present study is recommended as the free energy of dissolution of Nb(bcc) in fcc iron.

$$RT \ln a_{\text{Nb}} = -25500 + 10.9T \text{ Joules/Mol} \quad (6.36)$$

The dissolution free energy of titanium in fcc iron has also been analyzed on similar lines. Table 6.3 lists the dissolution free energy values obtained from various investigations (Table 2.4) on the

solubility of TiC in austenite. It can be seen from Table 6.3 that the agreement in the values from all the investigations is good, barring some minor discrepancies. The value determined from Narita's(106) solubility data becomes more negative with increasing temperature (positive entropy of dissolution) while all other data sets show the opposite trend. The value taken from Irvine's(107) data shows a stronger dependence on temperature compared to the other three data sets. The following average of the values obtained from the results of the other three investigations namely, Ohtani(42), this study and Sharaiwa(108) is recommended as the free energy of dissolution of Ti in fcc iron.

$$RT \ln \gamma_{Ti}^0 = -60590 + 14.08T \text{ Joules/Mol} \quad (6.37)$$

In the previous chapter we also determined this value from the independent assessment of thermodynamics and phase diagram data of the Fe-Ti system by Murray(2) to be  $-43.5 + 3.76E-03 * T$  KJ/Mole. It is encouraging to note that this value, though slightly lower, is still fairly close (+2KJ/Mole) to the value given above in equation (6.37).

### 6.3 Analysis of Fe-Nb-N Austenite

In this section the results obtained from the nitrogen equilibration experiments will be analyzed to obtain the ternary niobium-nitrogen interaction parameter and the solubility limit of NbN in austenite. As mentioned in earlier chapters Fe-Nb-N system does not show any minimum in the solubility limit nor does the solubility of NbN increase at high nitrogen contents. Therefore the ternary interaction

to parameter has been determined from the increase in nitrogen content due to addition of niobium. In the following section the ternary interaction parameter in the Fe-Nb-N will be determined following the procedure outlined in section 6.2.2.

### 6.3.1 The Niobium - Nitrogen Interaction parameter

In section 6.2.2 we derived the relation between the ternary interaction parameter and the relative increase in the carbon content at constant carbon activity. Various approximations were given depending on the concentration of the solutes and the contributions due to the binary interaction parameter  $\epsilon_c^c$ . The nitrogen levels are two orders of magnitude smaller than carbon and therefore an expression simpler than the one applicable to the carbon austenites can be used for determining the interaction parameter. Rewriting equation (6.26) for the Fe-Nb-N system we get

$$-\epsilon_N^N X_{Nb} = \frac{\Delta X_N^I}{X_N^I} \left[ 1 + X_N^I + \epsilon_N^I X_N^I \right] - \left[ \frac{\Delta X_N^I}{X_N^I} \right]^2 \quad (6.38)$$

where  $X_N^I$  and  $\Delta X_N^I$  refer to the binary nitrogen content and the increase in the nitrogen content due to Nb additions, respectively. Typical values of the relevant terms in this equation are

$$X_N^I, X_N^I = 2-8 \times 10^{-4} \quad ; \quad \Delta X_N^I = 1-4 \times 10^{-5}$$

$$\frac{\Delta X_N^I}{X_N^I} (\text{max}) = 0.15 \quad ; \quad \epsilon_N^I = 6$$

The quadratic terms in equation (6.38) contribute a maximum of 5 percent of the leading term and since the error associated with the

determination of the relative increase in nitrogen content  $\Delta X_N / X_N$  is around 5-8 percent, the quadratic term can be ignored. The largest contributions due to  $X_N + \epsilon_N^N \cdot X_N$  in the leading term is  $1.0E-02$  and hence can be neglected in comparison to 1.0. Incorporating these simplifications in equation (6.38) we obtain

$$-e_N^N X_{Nb} = \frac{\Delta X_N}{X_N^B} \quad (6.39)$$

Thus the relative increase in nitrogen content is directly related to the ternary interaction parameter. It immediately follows that the error in the determination of the interaction parameter is directly proportional to the error in the relative increase in nitrogen. In the case of carbon austenites we were able to achieve high accuracies in the determination of the relative increase in carbon at concentrations greater than 1.0wt%C. In the case of Fe-Nb-N austenite at 1373K, the highest attainable nitrogen content corresponds to 240ppm at  $p_{N_2} = 1$  atm. The amount of dissolved niobium is limited by the solubility product and the increase in nitrogen content due to niobium at 1 atm. is an insignificant 1-2ppm which corresponds to 0.5 percent of the binary concentration. In order to increase the relative increase in composition ( $\Delta X_N / X_N$ ) as mentioned in Chapter IV, equilibration at higher temperatures and lower partial were performed.

By rearranging equation (6.39) we find that the ternary interaction parameter is determined within 10 percent error by the following simple relationship with the solubility product  $K_{NbN}$ .

$$-e_N^N = \frac{\Delta X_N}{X_N^B X_{Nb}^Y} = \frac{\Delta X_N}{K_{NbN}} \quad (6.40)$$

At any given temperature the solubility product and  $\epsilon_N^{Nb}$  are constant and thus from the above equation it follows that there is an approximate limit on the value of  $\Delta X_N$ . The solubility limit varies exponentially with temperature whereas the interaction parameter typically varies as  $1/T$ . Therefore  $\Delta X_N$  should increase substantially with temperature. The limit on  $\Delta X_N$  increases from 2 ppm at 1373K to 9 ppm at 1573K and therefore measurements made at 1473K and 1573K are useful in the determination of the interaction parameter. As we noted in the previous paragraph the relative increase is more important than the actual increase in nitrogen content. Since the upper limit on  $\Delta X_N$  is more or less fixed for any given temperature, it necessarily follows that the overall nitrogen content has to be smaller for improving accuracy. Thus equilibration at lower partial pressures (25-50mm Hg) gives more accurate results. At 1573K and 85mm Hg partial nitrogen pressure an increase of 8-9 ppm at 70 ppm level (12 percent increase) is observed and this has been measured fairly accurately using large sample weights (10grams). Thus a reasonable value of the interaction parameter can be obtained by giving higher weights to the data obtained near the solubility limit at lower nitrogen potentials. The N-Nb interaction parameter determined using equation (6.39) from the most reliable of the data at 1473K and 1573K are given below.

$$\epsilon_N^{Nb} (1473K) = -70 \pm 8 \quad (6.41)$$

$$\epsilon_N^{Nb} (1573K) = -52 \pm 6 \quad (6.42)$$

The entropy of formation of nitrides is very large (80-85 J/mole/K) and hence a significant entropic component in  $RT\epsilon_N^{Nb}$  can be anticipated.

Since we have values at only two temperatures, there could be significant error in the temperature coefficient of  $RT\epsilon_N^{Nb}$ . The expression for  $\epsilon_N^{Nb}$  obtained from the values at these two temperatures is given below.

$$\epsilon_N^{Nb} = - \frac{(406240 \pm 20000)}{T} + 206 \quad (6.43)$$

### 6.3.2 Solubility of NbN in Fe-Nb-N Austenite

The solubility of NbN obtained in this study at 1373K-1573K can be adequately represented by the classical solubility product relationship. The correction term analogous to the one given for the carbon austenites contributes less than 1.0 percent to the solubility product and hence does not affect the classical solubility relationship significantly. The dissolution free energy of niobium that can be extracted from this solubility product has been discussed in section 6.2.7. The solubility limit of NbN in austenite is given below.

$$\log[\text{Wt}\% \text{Nb} \cdot \text{Wt}\% \text{N}] = 3.82 - \frac{9940}{T} \quad (6.44)$$

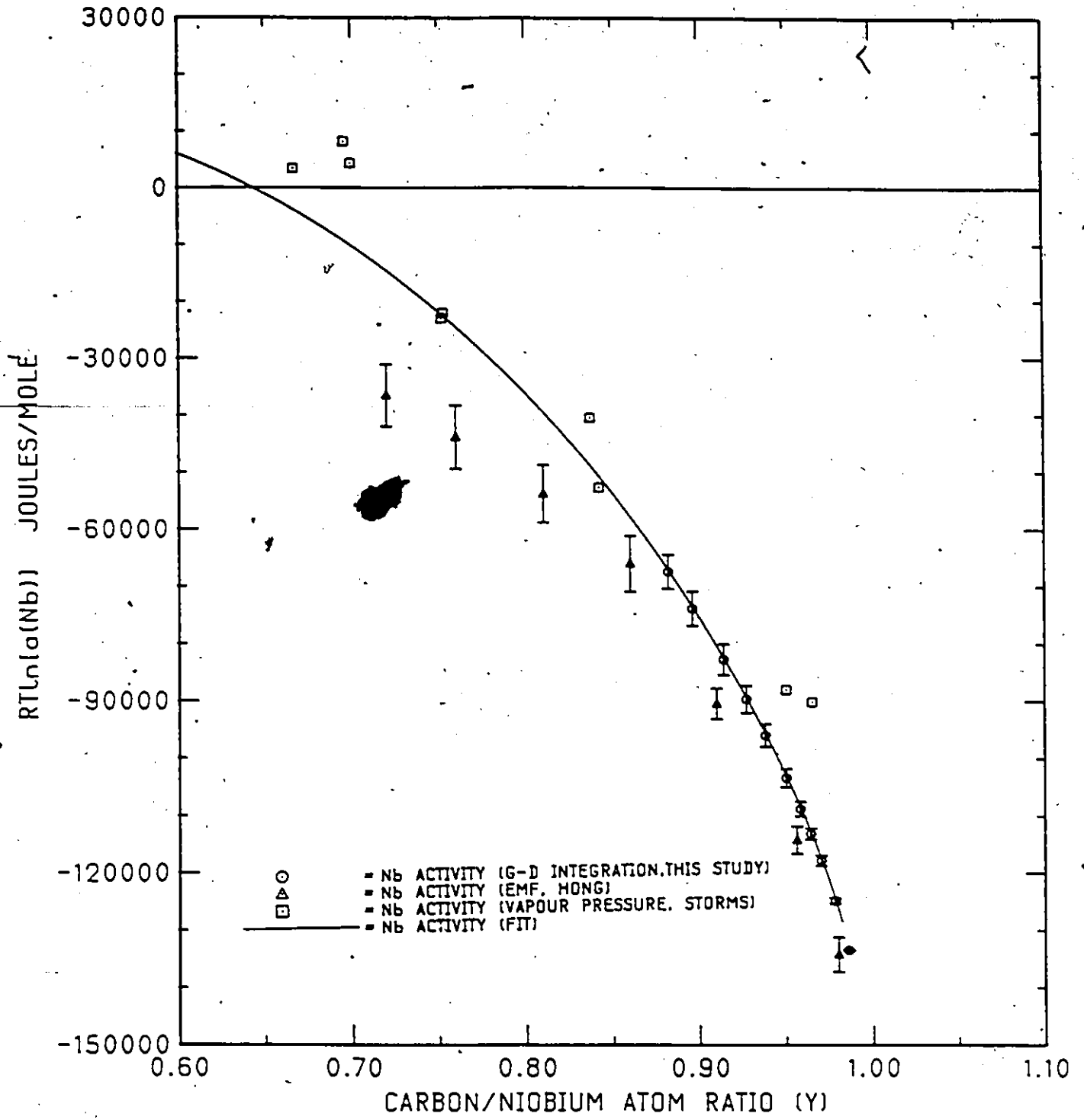
In the last few sections we have extensively analyzed the thermodynamics of the ternary Fe-Nb-C, Fe-Ti-C, and Fe-Nb-N austenites using modified Wagner formalism in order to determine the ternary interaction parameters, the solubility limits of NbC, TiC, and NbN in their respective austenites, and the dissolution free energies of Nb and Ti in fcc iron. It has all along been assumed that the precipitating carbides and the nitride were close to stoichiometry. This assumption is valid for the Fe-Nb-N system and at high carbon levels in the carbon

ternaries. At lower carbon contents (<0.1wt%) and at higher temperatures the composition of these compounds deviate from stoichiometry and it is necessary to investigate the effect of this on the solubility of these precipitates. This would require knowledge about the thermodynamics of these compound phases. In the following sections the sublattice-subregular model outlined in the previous chapter will be used to analyze these compound phases.

#### 6.4 Analysis of NbC<sub>y</sub> Phase

As mentioned in the chapter on literature review, and apart from this study, there have been only two experimental investigations pertaining to the variation of partial molar free energies, namely, the high temperature (2300K-2500K) vapour pressure measurements by Storms et al.(90) and the EMF study by Hong et al.(91) in the temperature range 1100K-1350K. The carbon activity-composition measurements made in this study complement the niobium activities determined in the other two studies. The results from all three data sets have been used in optimising the parameters in the sublattice model as will be shown below.

Figures 6.11-6.13 show the variation of partial molar free energies of niobium at 1273K, 1600K and 2400K. The EMF results have been extrapolated to 2400K while the vapour pressure measurements were extrapolated to 1273K. These widely differing temperatures have been chosen to help understanding the behaviour of partial molar entropy of niobium as well as to illustrate the limitations in extrapolating over large temperature ranges. It can be seen that the EMF measurements



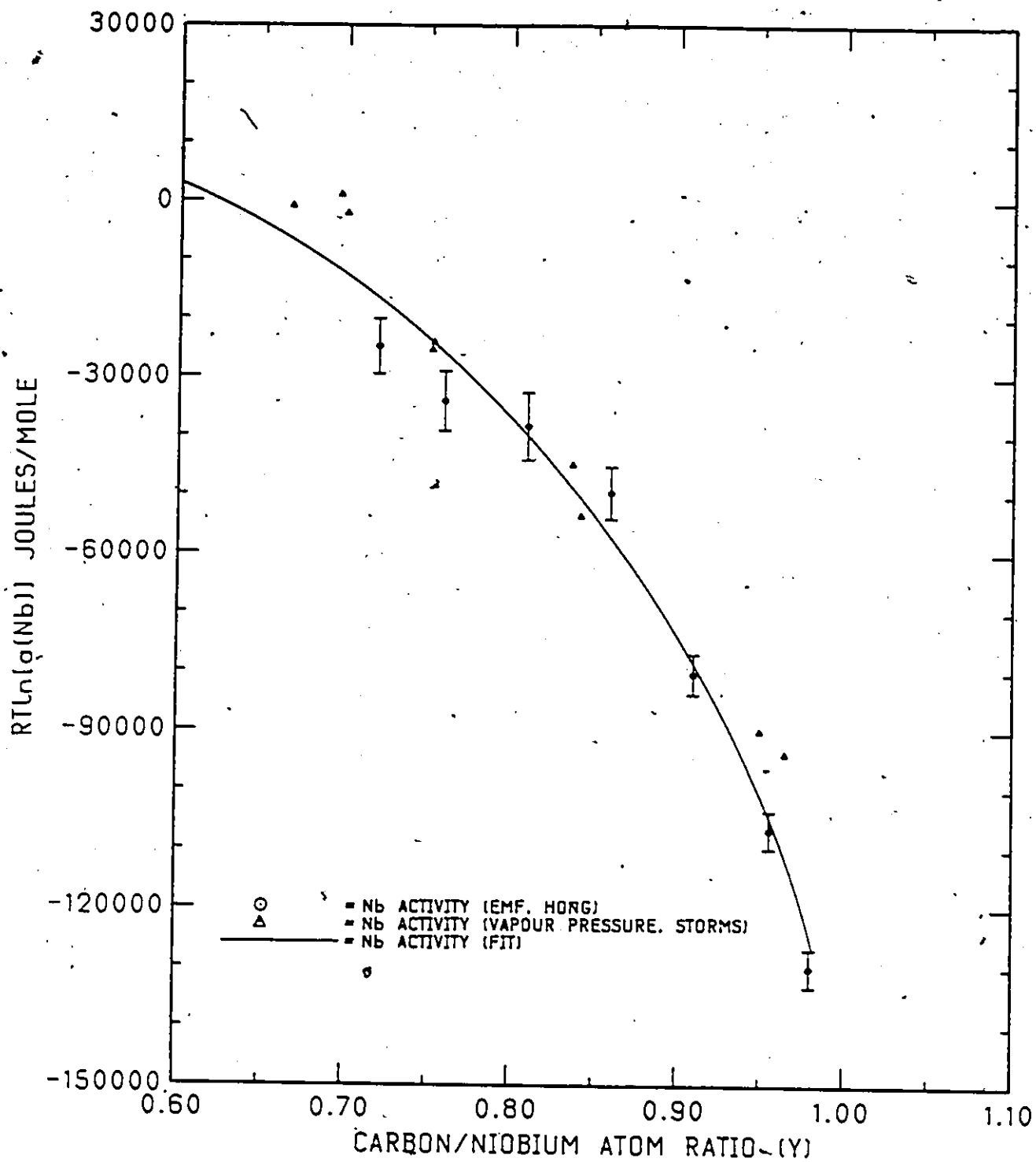


FIG. 6.12 VARIATION OF PARTIAL MOLAR FREE ENERGY OF NIOBIUM IN NbC (T=1600K)

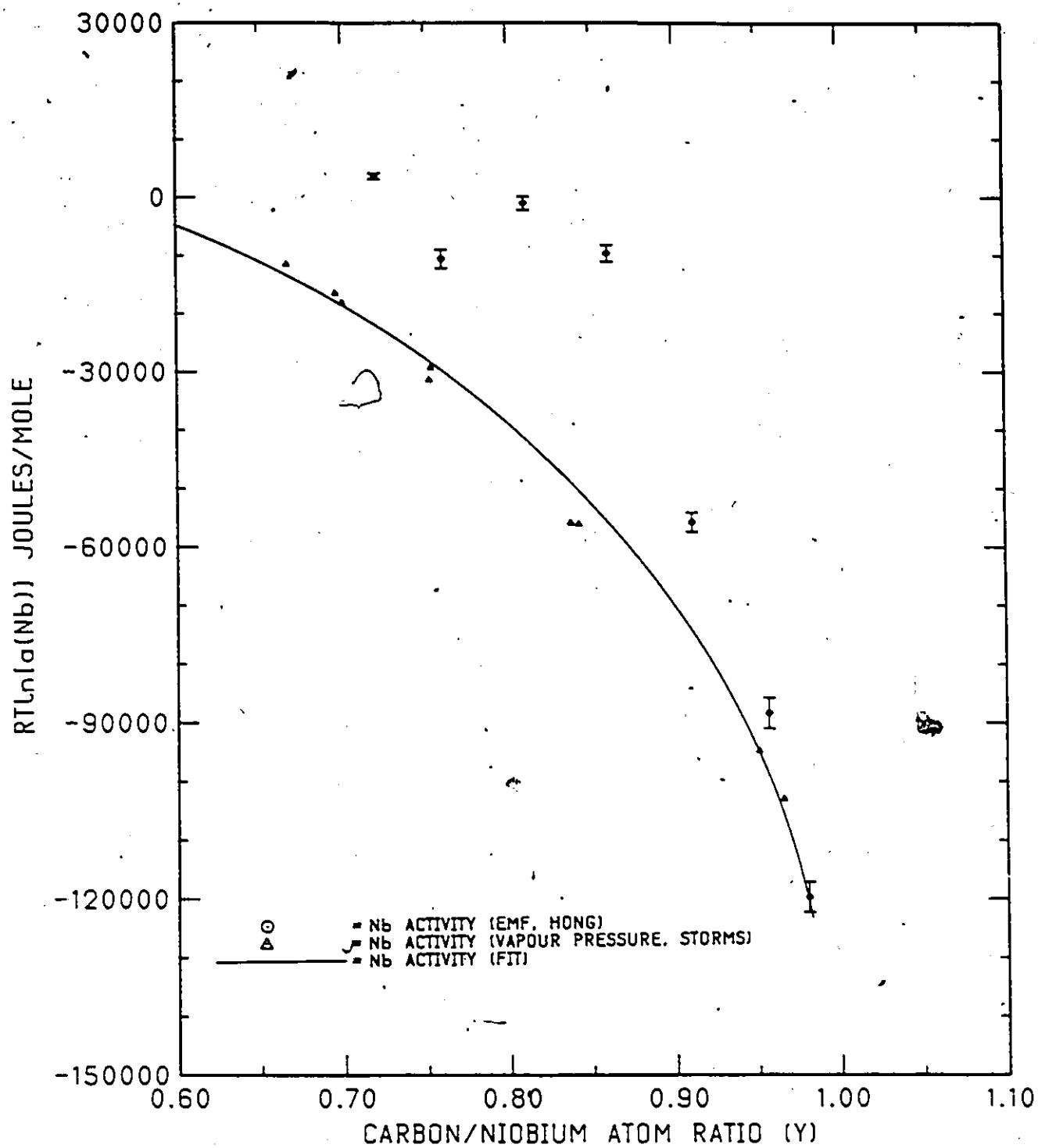


FIG. 6.13 VARIATION OF PARTIAL MOLAR FREE ENERGY OF NIOBIUM IN NbC (T=2400K)

cannot be extrapolated very much beyond 2400K as the partial molar free energy of niobium goes above the reference value ( ${}^{\circ}G_{\text{Nb}}^{\text{fcc}} - {}^{\circ}G_{\text{Nb}}^{\text{bcc}}$ ) for compositions less than  $y=0.86$ . This may be due to the partial molar entropy being in error for these compositions. The partial molar entropy which shows a minimum in composition (see Table 6.4) is negative for all compositions investigated in the EMF study. On the otherhand, vapour pressure studies show the partial molar <sup>excess</sup> entropy of niobium to be negative for compositions above and positive below  $y=0.8$ . This kind of behaviour is also seen in the case of  $\text{TiC}_y$  and hence the partial molar values obtained in the EMF study for compositions below  $y=0.86$  may be in error. Since only compositions greater than 0.85 are accessed in the present study using gas equilibration methods, the carbon activity below  $y=0.85$  could not be obtained to reinforce the partial molar entropic values of niobium. The results from the EMF study corresponding to compositions below  $y=0.86$  have not been used in optimising the parameters.

The  $\text{NbC}_y$  phase is in equilibrium with pure graphite at the carbon rich boundary. The carbon rich phase boundary is determined as  $y=0.99+0.005$  at 1273K in this study using the hydrogen-methane gas mixture. The partial molar free energy of niobium at that boundary should be very close to the free energy of formation of the stoichiometric compound which is known from independent calorimetric studies to be  $-137650 + 1.79T$  Joules/Mol Nb. The EMF study gives a good agreement with the calorimetric value for the composition  $y=0.98$  while the vapour pressure measurement over  $\text{NbC} + \text{C}$  by Storms gives a slightly more negative value as shown in Table 6.4.

The carbon activity measurements were made at 1273K and 1473K in this study. These measurements could not be used independently to determine the parameters as the temperature dependence of various parameters could not be satisfactorily evaluated from this limited data. The  $\text{NbC}_y$  phase is stable up to 4000 C and hence it is necessary to include the only available high temperature vapour pressure data in the evaluation of the parameters. The parameters in the sublattice model (equations (5.39-40)) were evaluated at three temperatures, 1273K, 1600K and 2400K using selected data from all the investigations. A linear temperature dependence of these parameters was then obtained from the evaluations at these three temperatures. For 1273K data from all the investigations except those corresponding to  $y=0.72, 0.76$  from the EMF study were used, the reason for their deletion being the uncertainty over the partial molar entropies as mentioned in the preceding paragraphs. At 1600K, there is good agreement between the two niobium data sets and hence all the data points were used. At 2400K, only the vapour pressure data was used as most of EMF measurements could not be satisfactorily extrapolated from 1200K to 2400K. The evaluated parameters are listed in Table 6.6.

### 6.5 Analysis of $\text{TiC}_y$ Phase

There have been a few low temperature (1050-1473K) studies and one high temperature (1900K) vapour pressure measurement by Storms(47) on the partial molar free energies of carbon and titanium as given in Table 2.3 in the literature review. The thermodynamics of this phase has been analyzed by Uhrenius(83), Teyssandier et al.(77), and Kaufman

and Agren(82). Teyssandier et al. used the substitutional regular solution model with Redlich-Kister expansion for the excess free energy while Uhrenius and Agren used the sublattice subregular model suggested by Hillert and Staffansson for analyzing the  $TiC_y$  phase. Of all the available experimental results, vapour pressure measurements by Storms and the low temperature EMF measurements by Koyama(89) have been found to be consistent with the phase diagram in the assessments by the above-mentioned authors. As there was insufficient data at high temperatures, Kaufman and Agren used the high and low carbon phase boundaries of the  $TiC_y$  phase together with Storms data at 1900K to evaluate the parameters.

The carbon activity as a function of temperature and composition has been measured using the gas equilibration technique by Alekseev(87) and Grieveson(86). The activity values of Grieveson are very high compared to those of Alekseev and both these data sets give higher values compared to the results in this study. One of reasons for this discrepancy could be insufficient time for equilibration and possible sintering of the powder compacts used as samples in those studies which reduce the permeability of the gas mixture. It has been found that nearly 30-50 hours are required for the carburization of a 100mg foil of about 10 microns thick. Secondly, large changes in chemical potential of carbon are required to give significant changes in composition. As the carbon potential in the gas decreases, the equilibration time increases and therefore the accuracy of gas equilibration technique is limited at lower carbon levels. Long equilibration times (up to 120 hours) were allowed in this study and approach to equilibrium could be

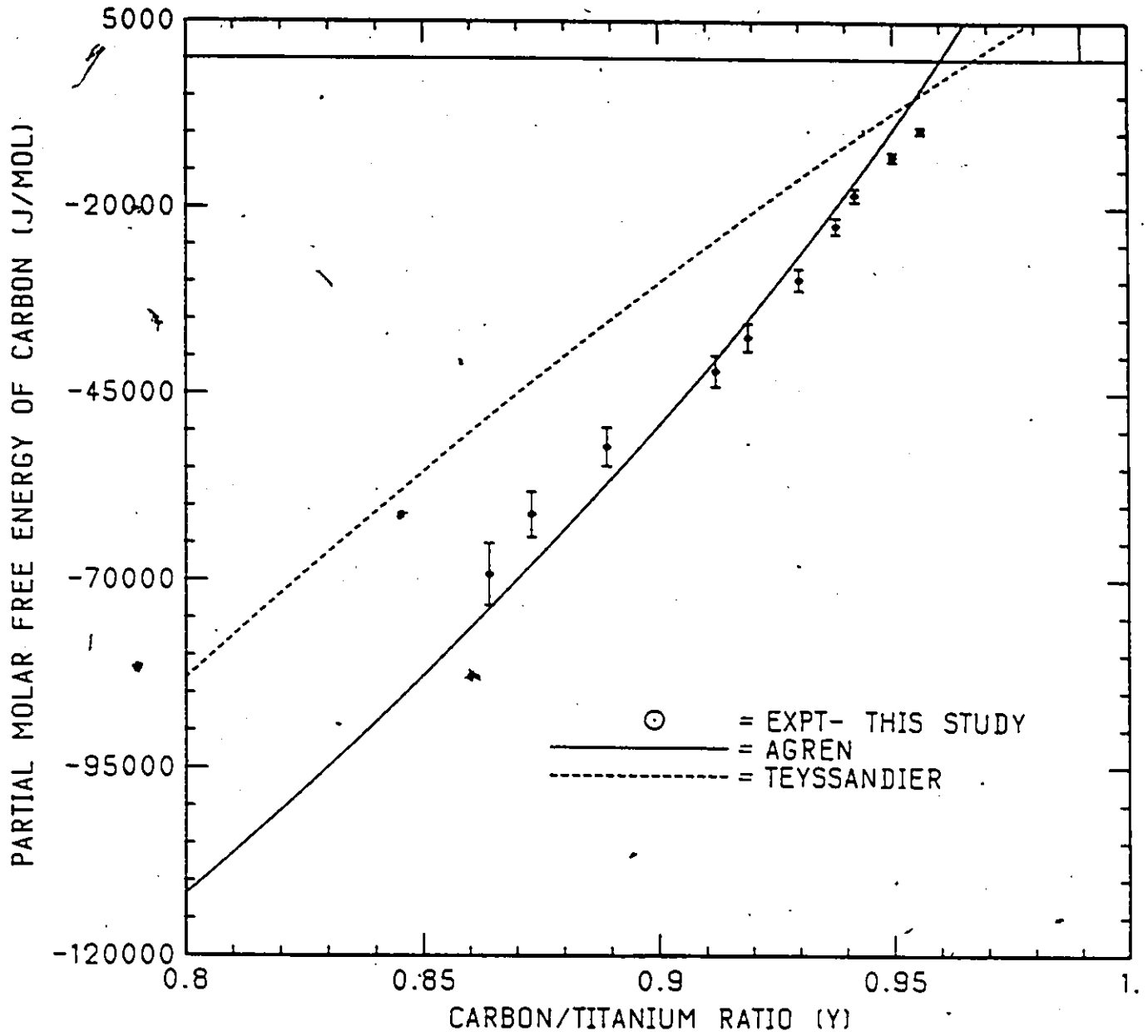


FIG. 6.14

VARIATION OF PARTIAL MOLAR FREE ENERGY  
OF CARBON IN  $TiC$  ( $T=1473K$ )

monitored continuously by the dynamic weight changes recorded by the electrobalance. The data obtained in this study is been found to be adequately described by Agren's parameters within the experimental errors. The experimental results and the prediction by Kaufman and Agren(82) are shown in Figure 6.14 .

### 6.6 Analysis of $NbN_y$ Phase

In this section the variation of nitrogen content in the  $NbN_y$  phase with partial pressure of nitrogen measured in this study at 1573K, 1623K and 1673K will be analyzed to obtain the parameters in the sublattice model. As mentioned in the literature review, apart from this study, there has been only one investigation on the partial molar properties of the  $NbN_y$  phase. Shchurik et al.(94) measured the dissociation pressure of nitrogen in this phase in the temperature range 1523K - 1853K. These authors also analyzed their results in terms of a sublattice lattice - regular solution model and represented their results in the following form.

$$\log [p_{N_2}(\text{mmHg})]^{1/2} = \left[ -6.39 + \frac{8510}{T} \right] + \left[ 13.13 - \frac{18950}{T} \right] y_n + \log \left[ \frac{y_n}{(1-y_n)} \right] \quad (6.45)$$

The first term in the above expression represents the heat of solution of nitrogen in an infinitely dilute fcc niobium alloy while the second term represents the change in this quantity with increasing nitrogen content. Rewriting equation (6.45) for the partial molar free energy of nitrogen these two terms can be identified with  $(\Delta G^\circ + L_0)$  and  $2L_0$  in the Hillert-Staffansson model, i.e.,

$$\Delta G^\circ + L_0 = 162935 - 149.92T \quad \text{Joules} \quad (6.46)$$

$$2L_0 = 362820 - 251.39T \quad \text{Joules} \quad (6.47)$$

where  $\Delta G^0$  represents the free energy of formation of stoichiometric niobium nitride from fcc Nb and nitrogen gas at one atmosphere, and  $L_0$  is the regular solution parameter. The free energy of formation of NbN from bcc Nb and 1 atm. nitrogen from independent calorimetric measurements as given by the compilations of Schick(141) is  $-236400 + 83.7T$  Joules per mole of Nb. Considering the lattice stability values given by Kaufman(10) for fcc Nb we obtain the free energy of formation of NbN from fcc Nb as

$${}^0G_{\text{NbN}} - {}^0G_{\text{Nb}}^{\text{fcc}} - \frac{1}{2} {}^0G_{\text{N}_2} = -245395 + 77.14T \text{ Joules (calorimetry)} \quad (6.48)$$

$$= -18475 - 24.23T \text{ Joules (Shchurik)} \quad (6.49)$$

Thus it is evident that the  $\Delta G^0$  value extracted from the expression given by Shchurik does not agree with the above mentioned value. It is therefore necessary to reanalyze the results of Shchurik et al. The experimental data given by Shchurik has been fitted to equation (5.45) in order to obtain the regular solution parameter ( $L_0$ ) and the subregular parameter ( $L_1$ ). It was not possible to describe these results using just one parameter as it gives an inconsistent free energy of formation. The experimental results of Shchurik together with the fit to the sublattice model are shown in Figure 6.15. The parameters  $L_0$  and  $L_1$  are given below.

$$L_0 \text{ (Shchurik)} = -191065 + 43.8T \text{ Joules} \quad (6.50)$$

and

$$L_1 \text{ (Shchurik)} = 87780 - 23.43T \text{ Joules} \quad (6.51)$$

Figure 6.16a shows the results obtained in this study as variation of excess free energy of nitrogen with the modified

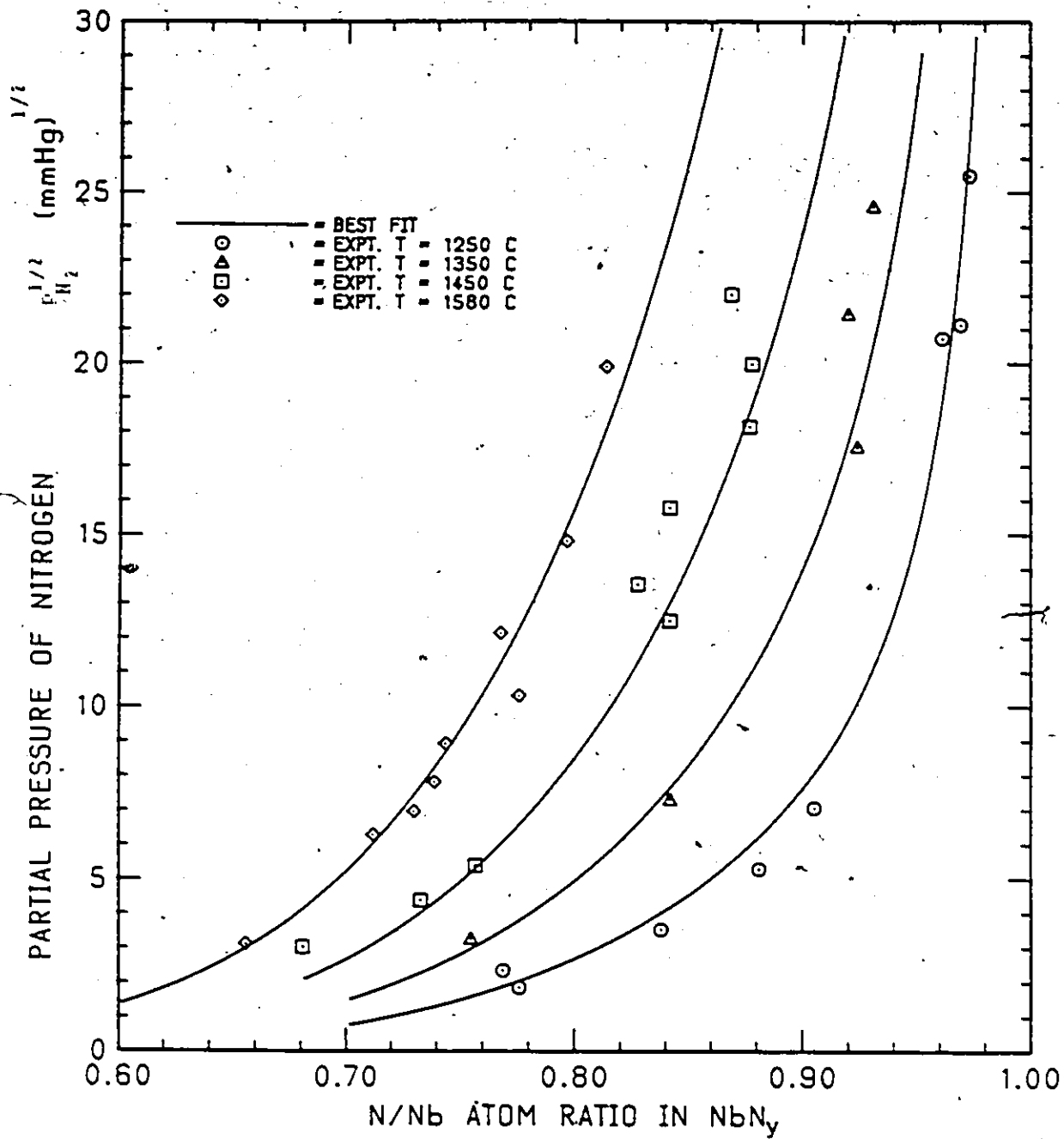


FIG. 6.15 EXPERIMENTAL RESULTS IN  $NbN$  PHASE (SHCHURIK) FITTED TO SUBLATTICE MODEL

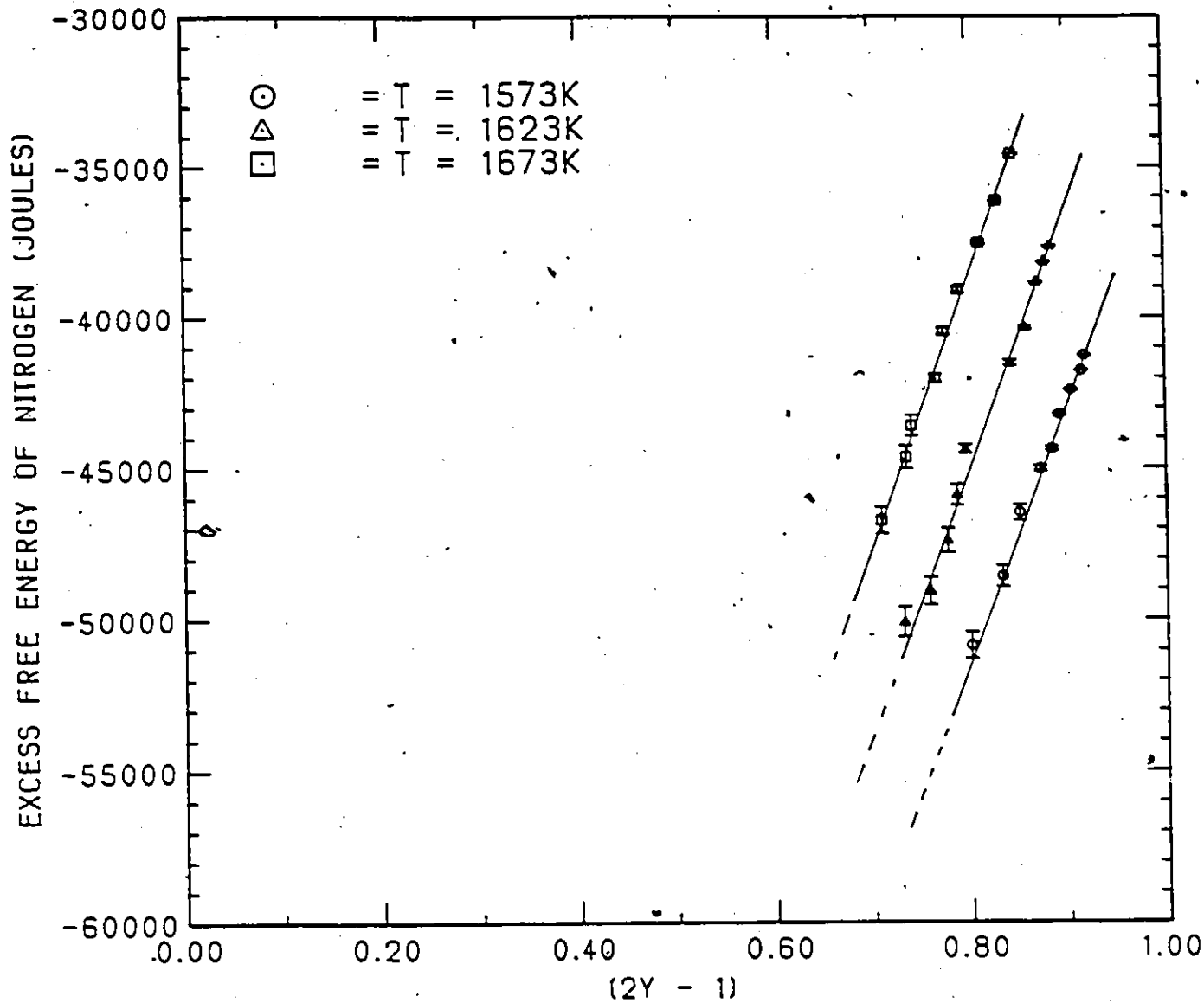


FIG. 6.16a DETERMINATION OF INTERACTION PARAMETER IN THE NbN PHASE (RESULTS THIS STUDY)

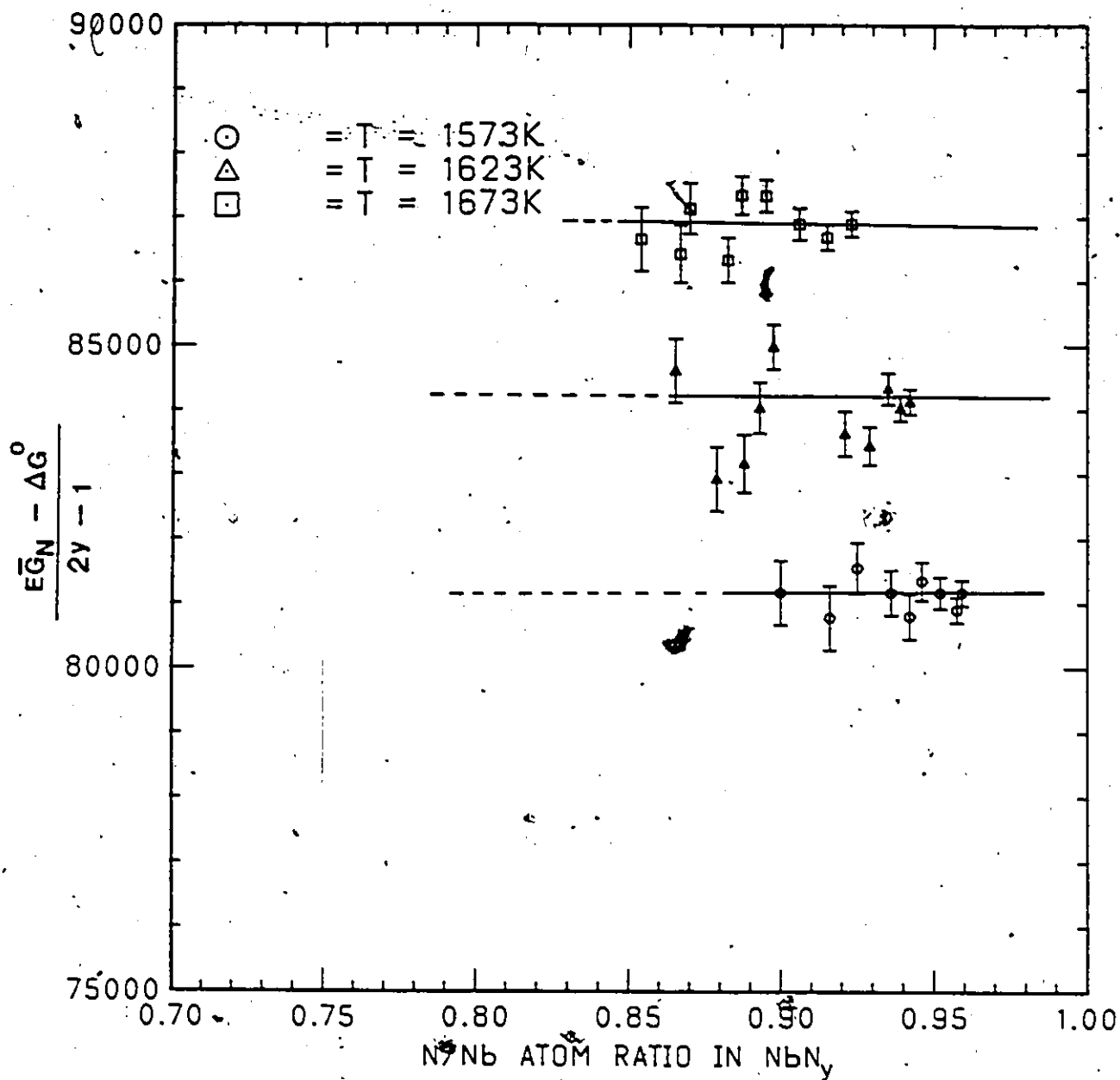


FIG. 6.16b DETERMINATION OF INTERACTION PARAMETER IN THE  
 NbN PHASE (RESULTS THIS STUDY)

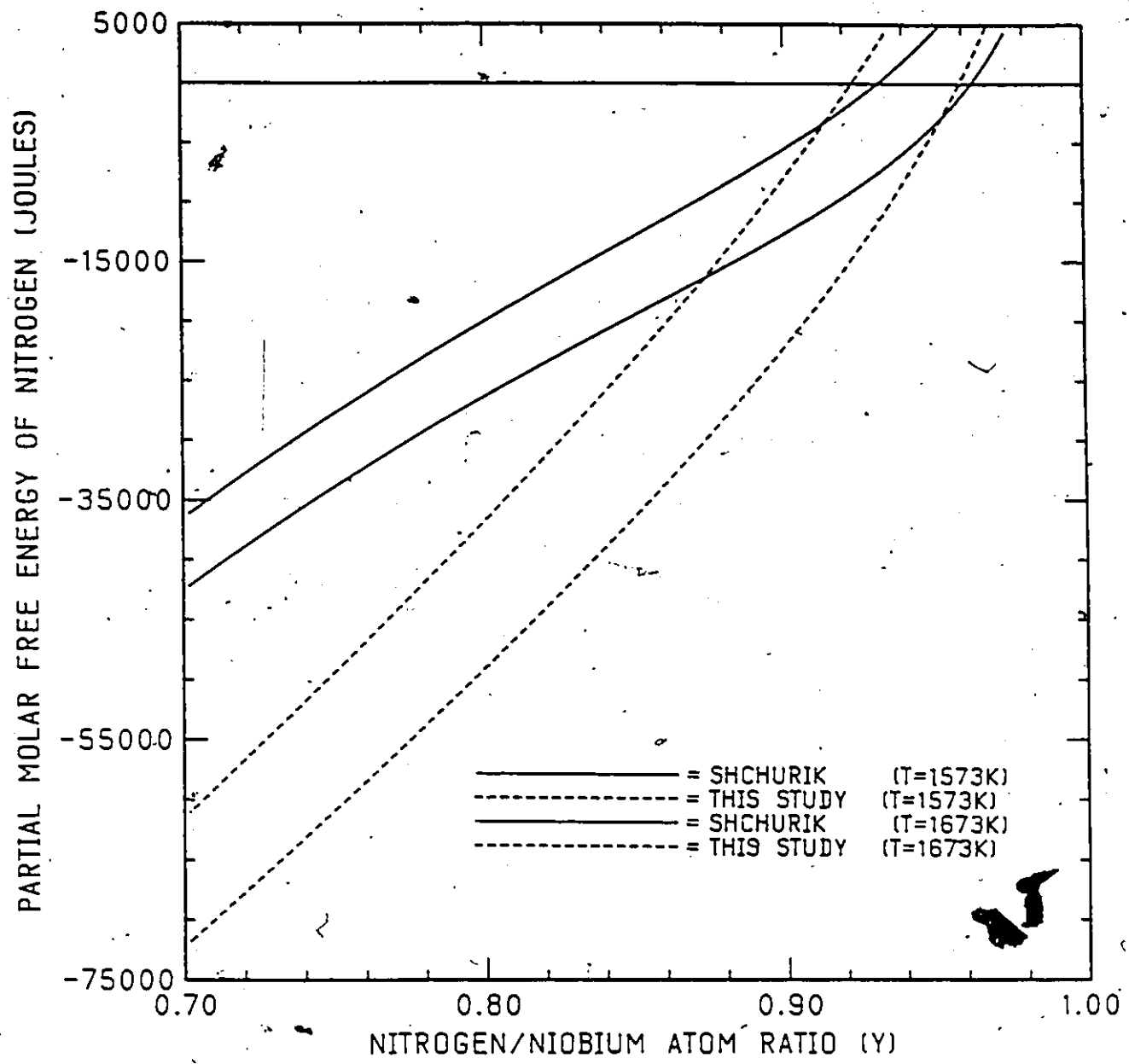


FIG. 6.17 VARIATION OF PARTIAL MOLAR FREE ENERGY OF N IN NbN PHASE. COMPARISON OF PREDICTIONS SHCHURIK AND THIS STUDY

composition variable  $(2y-1)$ . The slope of these curves gives the interaction parameter  $+L_0$ , while the intercept is the free energy of formation of stoichiometric nitride from fcc Nb. The results were expressed in this form to illustrate the following two features, viz., the results can be adequately described using one parameter, and secondly the intercept is far outside the investigated composition range. The solution range of  $NbN_y$  is very limited ( $0.80 < y < 0.95$ ) and therefore extrapolation over a large experimentally inaccessible range is required to obtain the intercept. A small change in slope would give a large change in the intercept and hence the error associated in the determination of the free energy of formation of  $NbN$  is large. In order to overcome this problem the free energy of formation of the stoichiometric nitride given in the literature can be subtracted from the partial molar excess free energy of nitrogen and the following function can be plotted against composition  $y$  (Figure 6.16b) to obtain the parameter  $L_0$  as well as to check the constancy of this parameter. The partial molar free energy on nitrogen in  $NbN_y$  at 1573K and 1673K as predicted by Shchurik's results and those obtained in this study is illustrated in Figure 6.17

$$\left[ \frac{(EG_N - \Delta G^U)}{(2y-1)} \right] = -L_0 = -9070 + 57.36T \text{ Joules} \quad (6.52)$$

### 6.7 Effects Due to Nonstoichiometry and Solute Interactions

In the last few sections we analyzed the variation of partial molar free energies of components in  $NbC_y$ ,  $TiC_y$ , and  $NbN_y$  phases using the sublattice - subregular model. It was demonstrated that these

partial molar quantities vary very strongly with composition. Therefore the composition of these interstitial phases can be expected to vary when precipitated in steels. The effects due to nonstoichiometry of the precipitate and the solute interactions in austenite on the solubility limit of the carbide will be investigated in this section. In order to delineate the effects due to the aforementioned factors, the following three cases in austenite - carbide equilibria will be considered, viz., case (i) the precipitate is stoichiometric and there are no solute interactions in austenite, case (ii) the precipitate is stoichiometric and there are solute interactions in austenite, and case (iii) the precipitate is nonstoichiometric and there are solute interactions in austenite.

In cases (i) and (ii), since the precipitate is assumed to be stoichiometric the mass action law can be applied to describe the austenite - carbide equilibrium. In the former, the behaviour of the solutes will be henrian while in the latter the solute interactions have been taken into account using the modified Wagner expansion for the activity coefficients. The interaction parameters in the Fe-Nb-C, Fe-Ti-C and Fe-Nb-N austenites have been summarized in Table 6.5. Mass action law is not applicable for case (iii) and hence equality of partial molar free energies of the solutes (Ti or Nb) and C will be used to solve for the solubility limit. The austenite - nonstoichiometric carbide is represented by

$$\bar{G}_M (\text{Austenite}) = \bar{G}_M (\text{Carbide}) \quad (6.53)$$

$$\bar{G}_C (\text{Austenite}) = \bar{G}_C (\text{Carbide}) \quad (6.54)$$

The partial molar expressions for the solutes in austenite are given in equations (5.1-5.3) while those for the carbides are given in equations (5.39) and (5.40). In general, equations (6.53) and (6.54) can be used to solve any two unknowns in compositions and interactions parameters. Since all the interaction parameters are known, these two equations can be solved for the composition of austenite ( $X_C$ ,  $X_M$  i.e., solubility limit) in equilibrium with various compositions ( $y$ ) of the carbide. Figures (6.18) and (6.19) show the solubility limit of the carbides in Fe-Nb-C and Fe-Ti-C systems respectively at 1273K and 1473K for the aforementioned three cases.

The solubility curves can be analyzed by considering three subregions, viz., high carbon and low metal contents (region A), low carbon and low metal contents (region B) and low carbon and high metal contents (region C). These three sub regions correspond roughly to the three areas marked by the two minima in the carbide solubility curve. In region A the carbon rich austenite is in equilibrium with the carbon rich carbide which is not far from stoichiometry. Regarding solute interactions the effect of substitutional solute on the carbon is significant enough to increase the amount of dissolved carbon in single phase austenite but the most pronounced effect is the reduction of the Ti or Nb activity due to carbon. Therefore Ti or Nb content has to increase to offset the reduction in its activity due to carbon and this is manifested as the increased solubility of the carbide. Thus the curves corresponding to cases (ii) and (iii) which consider solute interactions should lie above case (i) as depicted in Figures 6.18 and 6.19. The isoactivity experiments done in this study fall in this

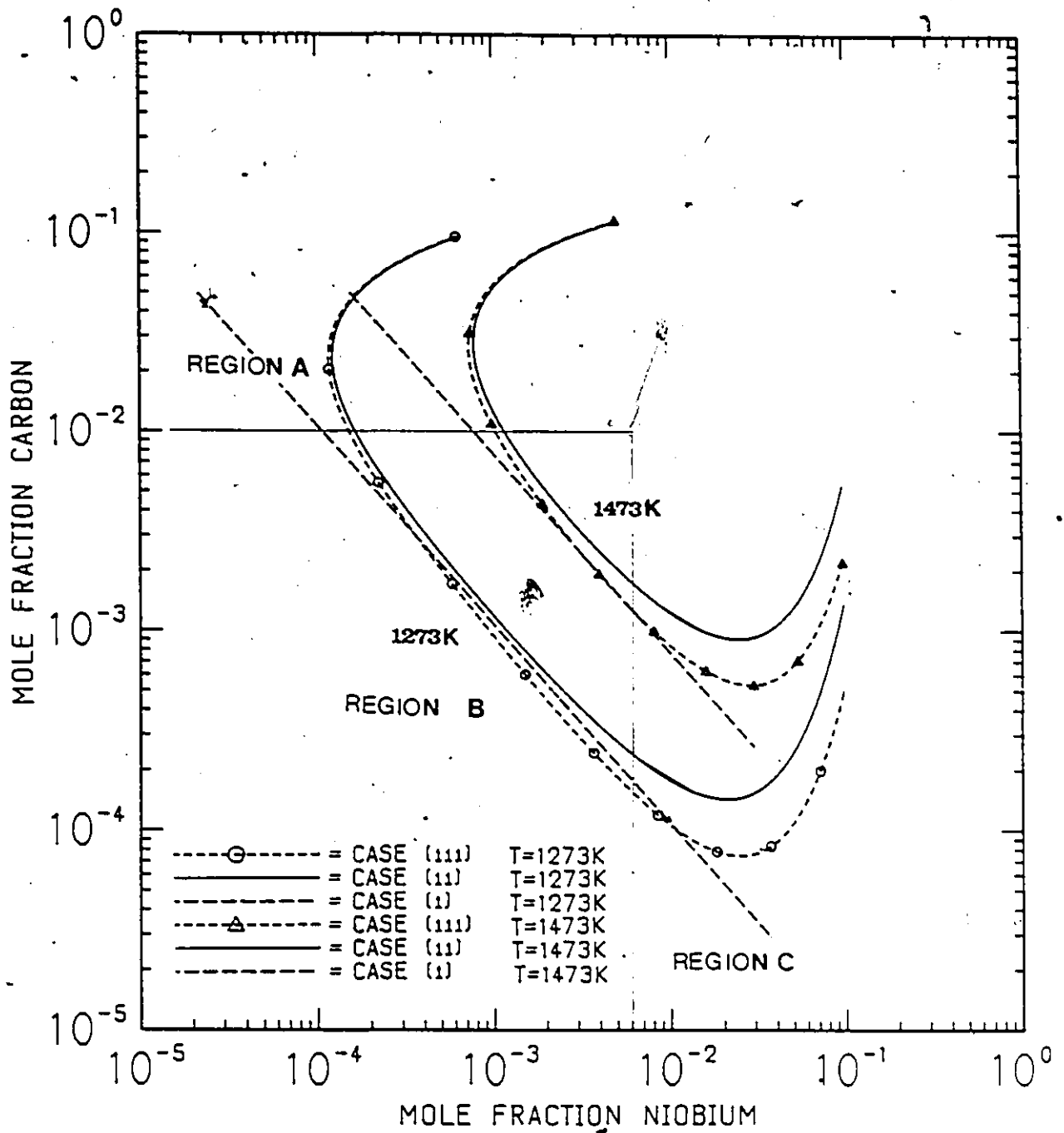


FIG. 6.18

EFFECT OF  
 NONSTOICHIOMETRY AND SOLUTE INTERACTIONS  
 AUSTENITE-CARBIDE EQUILIBRIUM  
 IN Fe-Nb-C SYSTEM (T=1273K AND T=1473K)

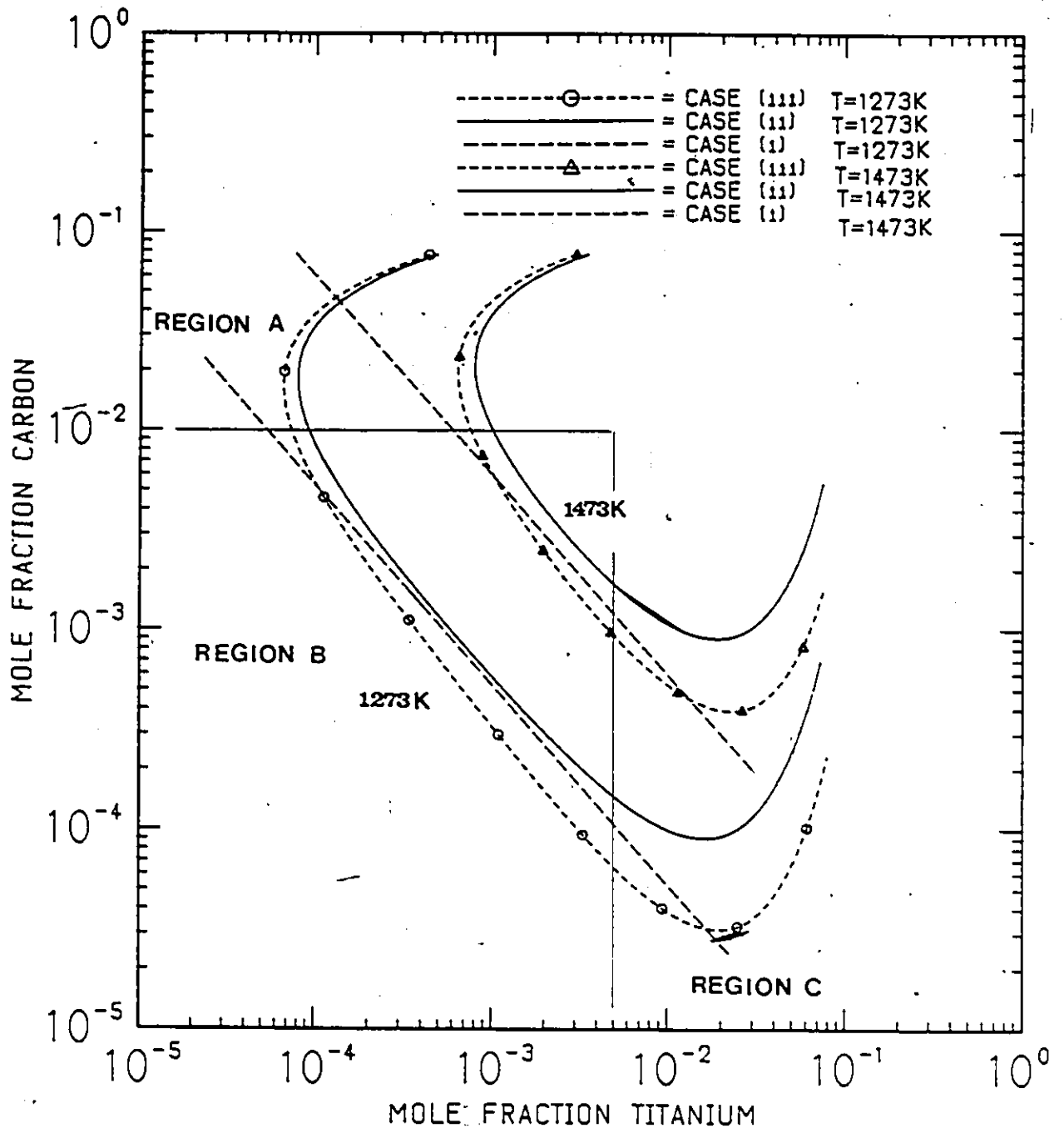


FIG. 6.19 EFFECT OF NONSTOICHIOMETRY AND SOLUTE INTERACTIONS AUSTENITE-CARBIDE EQUILIBRIUM IN Fe-Ti-C SYSTEM (T=1273K AND T=1473K)

region where the effects due to cross interactions of the solutes are pronounced. It is also to be noted that the microalloyed cast irons fall in this region. As can be seen from Figures 6.18 and 6.19 the content of microalloying element in austenite in equilibrium with carbon and the carbide as predicted by cases (ii) and (iii) differs from that predicted by case (i) by an order of magnitude. Hence solute interaction effects result in increased amounts of Ti or Nb required to precipitate the carbide in cast irons. The lower the temperature the higher is this solute interaction effect.

In the low carbon and low metal region (B) the carbide in equilibrium with austenite deviates from stoichiometry. The effects due to solute interactions are negligible due to low concentration of the solutes. The solubility product at these concentrations is to be expressed as  $(X_M X_C^y)$  and since  $X_C^y$  is always greater than  $X_C$  the carbon and/or metal content has to reduce to satisfy the reduced solubility product compared to case (i) and (ii). Hence the predominant effect on the solubility is the nonstoichiometry of the carbide which results in lower solute contents in austenite in equilibrium with carbide.

In the low carbon and high metal region (C) both nonstoichiometry and the solute interaction effects are very significant. As mentioned above, since the effective solubility product expression contains exponent  $y$  to the carbon activity, the carbon and/or metal has to reduce in comparison with the cases that ignored nonstoichiometry (cases (i) and (ii)). Regarding solute interaction effects the high Nb or Ti content has a pronounced effect in reducing the activity of carbon in austenite. This results in increased amounts

of carbon in austenite (in other words increased solubility of the carbide). Thus we have the optimum in the solubility curve, beyond which the effect of Ti or Nb becomes very significant. This region is not accessible for experimentation as the austenite phase is not stable at these high Ti or Nb concentrations. The equilibrium (metastable) in this region was calculated to illustrate the simultaneous effects of nonstoichiometry and the solute interactions. It is worth noting that the the minima exhibited in the ternary liquid - metal oxide equilibrium (140) in Fe-M-O systems falls in this region. Hence in general it can be concluded that the consideration of nonstoichiometry results in a reduction in solubility of the carbide, while consideration of solute interactions (primarily the cross interaction terms) results in increased solubility. The former is significant in regions B and C while the latter is important in regions A and C.

In the preceding paragraphs we considered the effects due to nonstoichiometry and solute interactions on the austenite - carbide equilibrium. These considerations can be extended in principle to the austenite - nitride equilibrium as well. However the amount of nitrogen dissolved in Fe-Nb-N and Fe-Ti-N systems is very small and the nitrides are very close to stoichiometry in the region of interest to steels. Effects due to Ti or Nb become significant only at low nitrogen and high Ti and Nb (greater than 1 wt%) levels. Therefore the solubility limit of the nitrides in austenite can for all practical purposes be adequately described using the mass action law and its attendant classical solubility product relationships.

### 6.8 Solubility of TiN in Fe-Ti-N Austenite

The thermodynamics of Fe-Ti-N austenite and the solubility of TiN in austenite have not been experimentally investigated in this study, the reason being the very low solubility of TiN even at 1473K. The solubility of TiN can be calculated to a high degree of accuracy if (i) the free energy of formation of TiN from pure Ti (bcc) and nitrogen gas at one atmosphere, (ii) the dissolution free energy of Ti in fcc Fe and (iii) the dissolution free energy of nitrogen gas in fcc Fe are known. The free energy of formation of TiN is accurately known from calorimetric studies and is listed in Table 2.1 along with the values for NbC, NbN and TiC. The dissolution free energy of Ti in fcc Fe has been analyzed and a reliable and consistent value (equation 6.37) has been recommended in section 6.2.7. The dissolution free energy of nitrogen is fairly well established and the value suggested by Hillert and Jarl(40) (equation 5.6 and Table 6.5) can be considered for the determination of solubility of TiN in Fe-Ti-N austenite.

The solubility of TiN calculated from the free energies mentioned in the previous paragraph is given below.

$$\log[\text{Wt}\% \text{Ti}][\text{Wt}\% \text{N}] = 4.01 - (13850/T) \quad (6.55)$$

This expression is to be compared with the solubility product values determined by various investigators given in Table 2.5. Figure 6.20 illustrates the solubility products obtained in these investigations. Two features can be noted from this figure, namely, the slope (enthalpic component) is more or less same in most of the investigations, except that of Matsuda et al.(115). The values range from -14400 to -16200 the average (barring that of Matsuda et al.) is around -15100. The

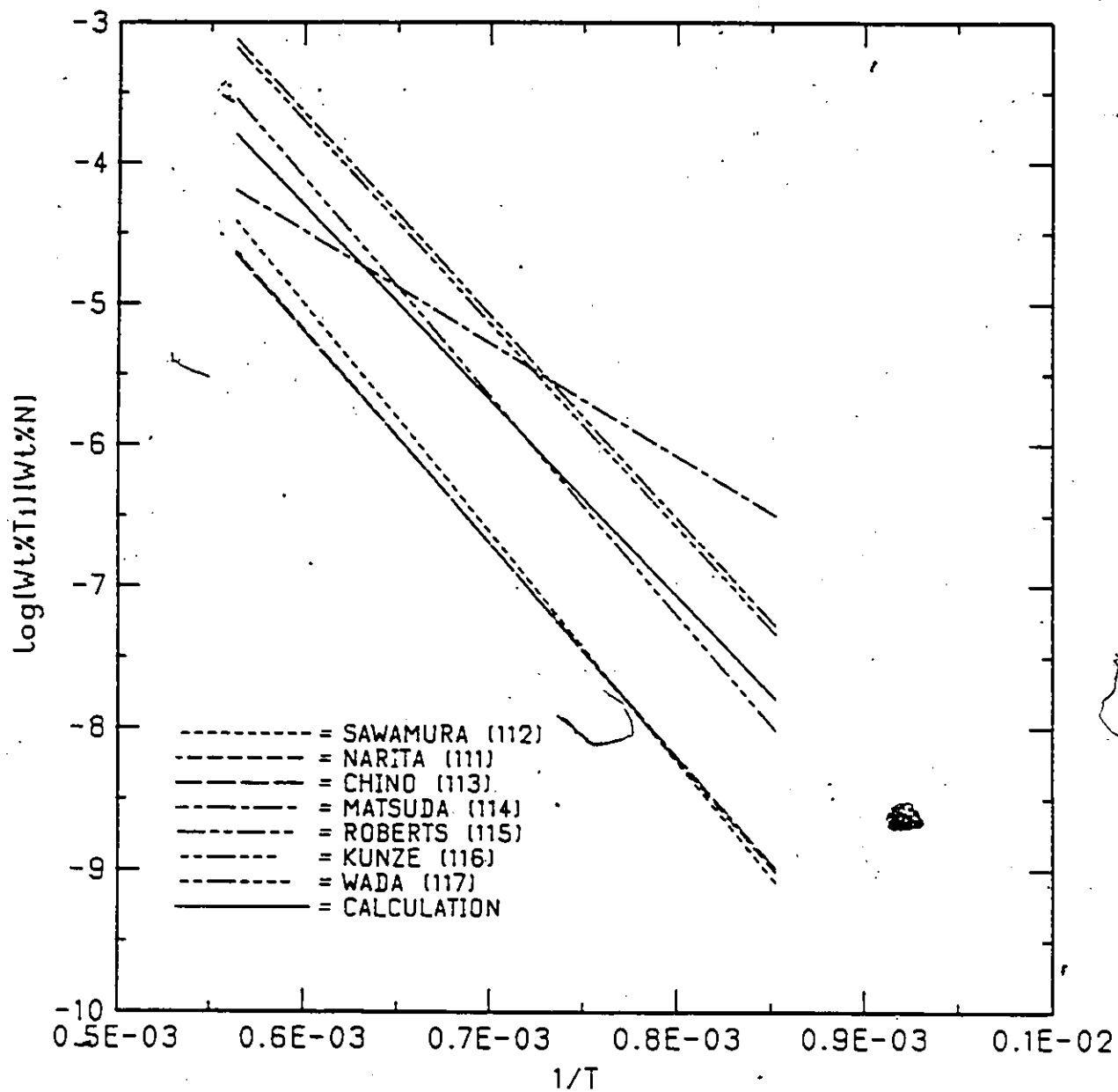


FIG. 6.20

VARIATION OF SOLUBILITY OF TiN IN  
Fe-Ti-N AUSTENITE WITH TEMPERATURE

calculated value of -13850 (equation (6.55)) is slightly lower but still is within ten percent of the other values. The intercept unfortunately varies from 3.82 (Chino(113)) to 5.19 (Kunze(116)) and this range gives an order of magnitude variation in the value of  $K' = [\text{Wt}\% \text{T}_1][\text{Wt}\% \text{N}]$ . The investigations illustrated in Figure (6.19) fall into three levels of solubility in the temperature range 1173K-1673K. The high solubility values are given by Roberts(115) and Wada et al.(117). In the middle level are the values determined by calculation (equation (6.55)) and those obtained by Kunze(116). The values obtained by Narita et al.(111), Sawamura et al.(112) and Chino et al.(113) lie in the lower level. It is difficult to assess the accuracy of the various investigations as the titanium content of austenite is very small upto 1473K and hence the error in its determination can give rise to the spread of solubility product values observed in Figure 6.20. Since the experiments can be conducted only in a limited temperature range, large extrapolations are required to obtain the intercept and hence a small change in the slope can give a large change in the intercept. As the free energy values used in the calculation of the solubility product are consistent and reliable, the calculated value is recommended.

The ternary nitrogen-titanium interaction parameter though large in magnitude is difficult to determine from experiments. Since the effects of interaction are not significant enough to be determinable, it can be ignored in most cases. An approximate value for this interaction can be obtained via suitable correlations as will be shown in the next section. The thermodynamics of nonstoichiometric  $\text{TiN}_y$  phase was not investigated in this study. Very low potentials of nitrogen (below

1E-05) required to obtain significant changes in the composition in the temperature range 1573K-1773K are not attainable in the gas equilibration technique used in this investigation. Other experimental techniques like high temperature vapour pressure measurements have to be used to obtain more information on the thermodynamics of this phase. The most recent assessment of the Ti-N system by Wreidt and Murray (142) points to the inconsistencies in the phase diagram and the lack of information on the thermodynamics of many phases in this system including the cubic  $TiN_y$  phase. Limited information available in the form of the vapour pressure measurements over the  $TiN_y$  phase by McClaine and Coppel (48) has been used in the analysis by Teyssandier et al. (77) and Kaufman and Agren (82) for the evaluation of parameters in the solution models. The values of the parameters in the sublattice - subregular model given by Kaufman and Agren are included in Table 6.6.

#### 6.9 Correlational Relationships and the Ternary Interaction Parameters

It is fairly well established (133) that there exists a regular pattern in the crystal structures of carbides and nitrides as one traverses along a period. The tendency to form close packed structures as interstitial solutes are added increases as one moves away from iron to the left of the periodic table. The group IV, V elements which exist in bcc and hcp lattices on addition of interstitial solutes stabilize the fcc phase in the form of a carbide or nitride. To the right of iron we see Ni, Co, Cu, etc., which already exist in fcc form and the carbides and nitrides of these elements are mostly unstable. Near iron we see the transition from bcc metals forming fcc carbides to fcc metals

forming unstable carbides and nitrides. Thus Cr, Mn and to some extent iron itself form complex carbides which exist in orthorhombic, cubic and hexagonal structures. The periodic pattern in structure is accompanied by the anticipated variation of the free energies of formation of carbides and nitrides, large negative values for group IV and V compounds to positive values for the unstable carbides in group VII and VIII. Since iron lies near the transition, the solutes to the far-left form very stable carbides and nitrides (TiC, NbC etc.) and the solutes near iron forms complex carbides with iron dissolved ( $(\text{Fe,Cr})_3\text{C}$  etc) in them.

In Chapter V we noted the periodic table pattern in the variation of the dissolution free energy of the solutes belonging to the first long period in fcc iron. In this section we explore the correlational relationships between the ternary interaction parameters and the free energies of formation of carbides and nitrides. The free energy of formation of a binary compound is one of the indicators of the degree of attraction/repulsion between the two components that make up the compound. The more negative the free energy of formation the higher is the degree of attraction. When the two elements that form the compound are dissolved in a solvent like Fe, depending on the nature and the magnitude of interaction of the individual solutes with the solvent the one to one correspondence between the free energy of formation and the degree of solute interaction will be affected. In the following paragraph the nature and the degree of correlation will be investigated.

Figures (6.21) and (6.22) illustrate the correlation between the ternary interaction parameters and the free energies of formation from

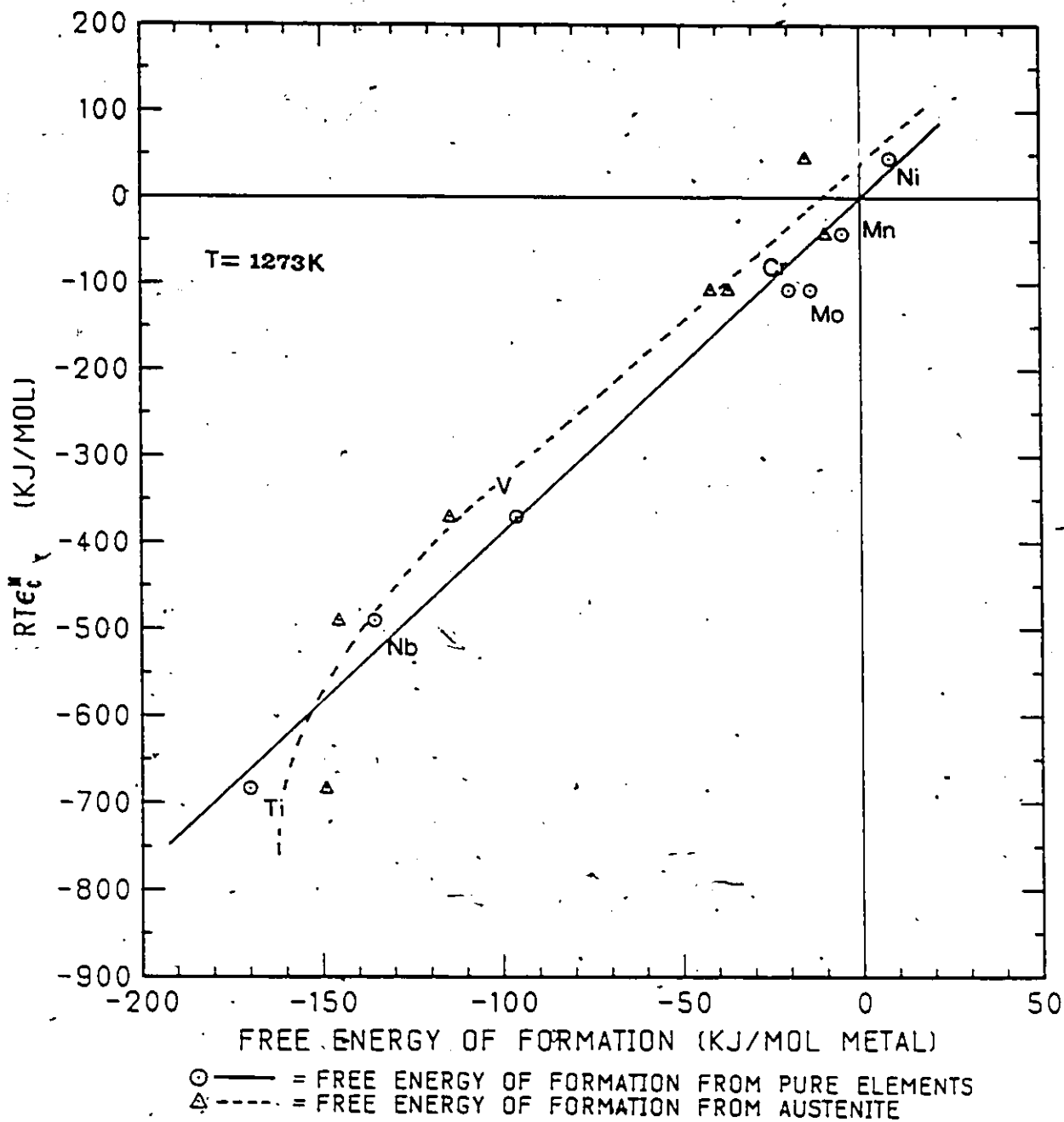


FIG. 6.21

CORRELATIONAL RELATIONSHIP  
 CARBON-METAL INTERACTION PARAMETER  
 $V_s$   
 FREE ENERGY OF FORMATION OF CARBIDES

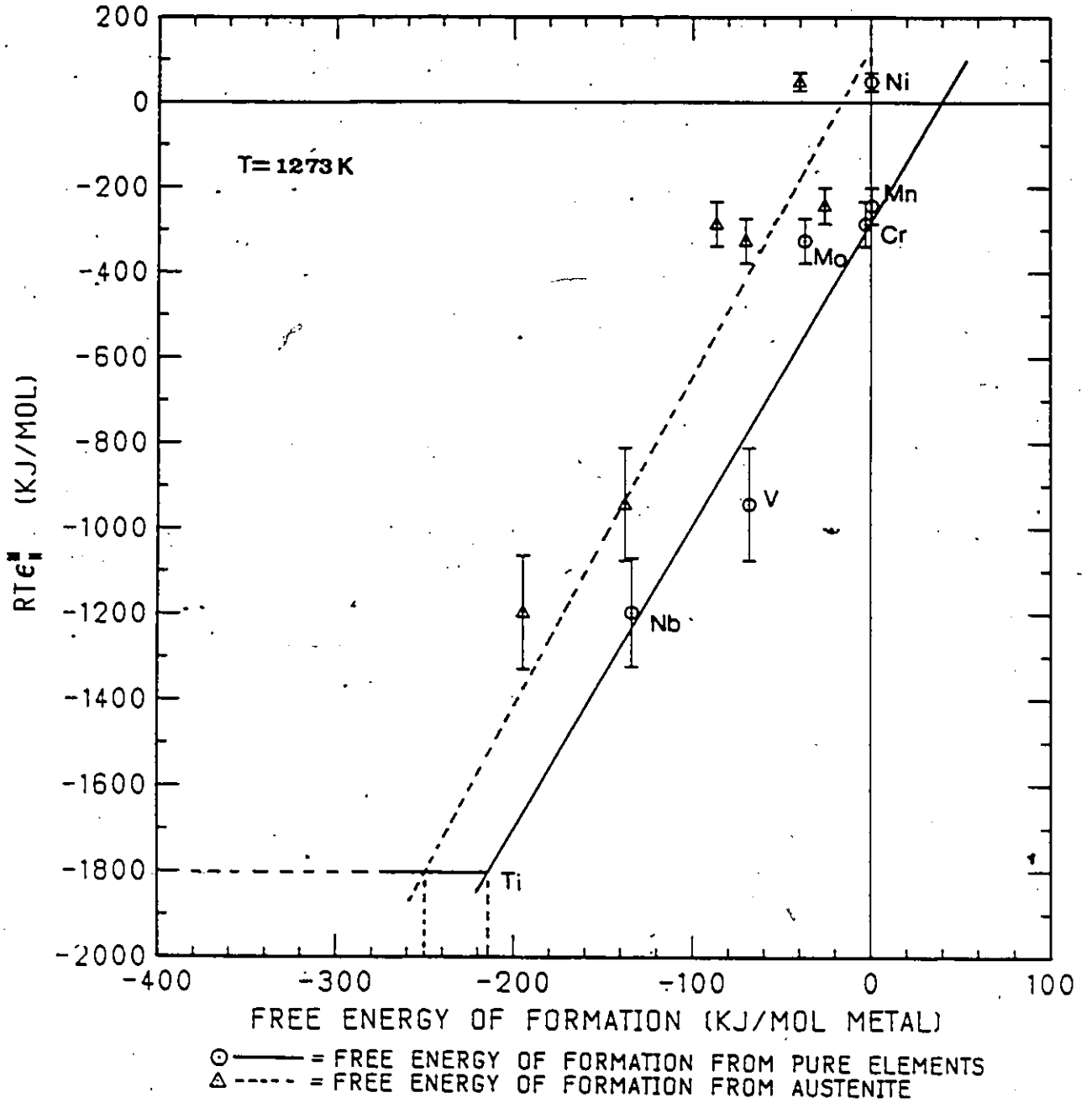


FIG. 6.22

CORRELATIONAL RELATIONSHIP  
 NITROGEN-METAL INTERACTION PARAMETER  
 $v_s$   
 FREE ENERGY OF FORMATION OF NITRIDES

pure elements as well as from austenite. The free energy values have been taken from compilations of Hultgren et al.(9) and Kubaschewski (143). The carbon interaction parameters for Ti, Nb and V have been taken from the results of Ohtani et al.(41,42) and that obtained in this study. The carbon and nitrogen interactions with Ni, Mn, Cr and Mo have been taken from the compilation by Sharma et al.(105). The recent determination of the V-N interaction parameter by Wada (144) and the Nb-N interaction parameter obtained in this study has been considered in the correlation. The free energies of formation from austenite have been determined using the dissolution free energy values listed in Table 5.2.

From Figure (6.21), it can be seen that there is a linear variation of the carbon-metal interaction with the free energy of formation from pure elements. This implies that the interaction of the solutes in fcc iron is very similar to the interaction between these elements in the carbide. This striking linear correlation is somewhat lost if we instead consider the free energy of formation from austenite. The dissolution free energies of transition metal solutes in the fcc form in fcc Fe (Figures 5.1 and 5.2) vary fairly linearly, but the lattice stabilities of solutes (free energy difference between the fcc and bcc forms) varies in a nonlinear way with group number. Therefore the combination of these energies which is used in the calculation of free energy of formation from austenite varies non linearly. However, two groups of solutes can be identified, those that form cubic carbides (group IV and V) and others that form hexagonal, orthorhombic carbides (Cr, Mn, W, Mo etc.) and a fairly good correlation exists within each

group.

The nitrogen-metal interaction shows a similar pattern as the carbon counterpart. However, the errors involved in the determination of the nitrogen interaction parameters are higher. The correlation of the interaction parameter with the free energy of formation of nitrides (from pure elements as well as from austenite) is fair. The correlation can be extrapolated to obtain an approximate value for the titanium-nitrogen interaction parameter. The value determined from the extrapolation is included in the summary of interaction parameters given in Table 6.5.

TABLE 6.1

Solubility Limit and Ternary Interactions  
in Fe-Ti-C and Fe-Nb-C Systems

Fe-Nb-C		
Solubility limit	- (8030/T) + 3.89 + [(1150/T)-0.05] Wt%C	(This study)
	- (4880/T) + 1.18 + [(1590/T)-0.10] Wt%C	(Ohtani)
$RT \ln \gamma_{Nb}^0$	- 27950 + 13.0 T Joules	(This study)
	- 88235 + 64.85T Joules	(Ohtani)
$\epsilon_c^{Nb}$	- (65840/T) + 2.5	(This study)
	- (87620/T) + 5.0	(Ohtani)
Fe-Ti-C		
Solubility limit	- (9420/T) + 4.47 + [(1545/T) - 0.1] Wt%C	(This study)
	- (8970/T) + 4.2 + [(940/T) - 0.2] Wt%C	(Ohtani)
	- (8970/T) + 4.2 + [(1600/T) - 0.2] Wt%C	(Ohtani; refitted)
$RT \ln \gamma_{Ti}^0$	- 51990 + 8.98T Joules	(This study)
	- 60595 + 14.08T Joules	(Ohtani)
$\epsilon_c^{Ti}$	- (85390/T) + 5.0	(This study)
	- (55435/T) + 10.0	(Ohtani)
	- (88115/T) + 10.0	(Ohtani; refitted)

TABLE 6.2

Dissolution Free Energy of bcc Niobium from Solubility Studies

Solubility Product $\log[\text{Nb}][\text{X}] = \text{A} + \text{B}/\text{T}$		$\text{RT} \ln \gamma_{\text{Nb}}^0$ (Joules)			Reference
A	B	1273K	1373K	1473K	
Fe-Nb-C					
2.90	- 7500	2557	5749	8940	de Kazinczy(96)
3.18	- 7700	- 438	2218	4873	Mori (97)
3.42	- 7900	- 2458	- 262	1933	Narita (98)
3.04	- 7290	- 4875	- 1952	971	Meyer (99)
3.70	- 9100	13693	15352	17013	Smith (100)
4.37	- 9290	1000	1337	1754	Johansen (101)
3.31	- 7970	1563	3970	6376	Koyama (103)
1.18	- 4880	- 5684	800	7285	Ohtani (41)
3.89	- 8030	-11425	-10130	- 8832	This study
Fe-Nb-N					
4.04	- 10230	-12166	-11807	-11226	Smith (109)
2.80	- 8500	-15067	-12333	- 9378	Narita (95)
3.79	- 10150	- 7604	- 6766	- 5707	Mori (110)
4.2	- 10000	-11840	-10960	-10070	This study

TABLE 6.3

Dissolution Free Energy of bcc Titanium from Solubility Studies

Solubility Product $\log[\text{Ti}][\text{C}] = A+B/T$		$-RT\ln\gamma_{\text{Ti}}$ (Joules)			
A	B	1273K	1373K	1473K	Ref.
5.33	-10475	-41423	-42180	-42936	Narita (106)
2.75	-7000	-45073	-40890	-36707	Irvine (107)
4.03	-8720	-43340	-41607	-39874	Sharaiwa (108)
4.47	-9420	-42696	-41289	-39883	Ohtani (41)
4.20	-8970	-40661	-39874	-38881	This study

TABLE 6.4

Niobium Activity Data From Vapour Pressure and EMF Studies

$\log a(\text{Nb}) = A + B/T$					
Vapour Pressure Measurements (2300-2500K)			EMF Measurements (1100-1350K)		
$y$ in $\text{NbC}_y$	A	B	$y$ in $\text{NbC}_y$	A	B
0.667	- 0.6913	+ 1059	0.720	+ 1.927	- 4358
0.696	- 1.1440	+ 1884	0.760	+ 1.537	- 4246
0.700	- 1.0426	+ 1554	0.810	+ 2.441	- 5915
0.752	- 0.3915	- 701	0.860	+ 2.610	- 6770
0.753	- 0.3370	- 720	0.910	+ 1.608	- 6772
0.837	- 0.7136	- 1203	0.956	+ 1.199	- 7494
0.842	- 0.1584	- 2547	0.980	+ 0.674	- 7872
0.950	- 0.3119	- 4200			
0.965	- 0.5915	- 3956			
$\text{NbC} + \text{C}$	- 0.4298	- 8147			

$\Delta G_{\text{NbC}}^{\circ}$	- 137653 + 1.79T J/Mol Nb	(Calorimetry, Schick(141))
$RT \ln[a(\text{Nb})]$ at $\text{NbC} + \text{C}$	- 155985 - 8.23T Joules	(Vapour Pressure, Storms(90))
$RT \ln[a(\text{Nb})]$ at $y = 0.98$	- 150720 + 12.9T Joules	(EMF, Hong (91))

TABLE 6.5

Summary of Interaction Parameters in Fe-Ti-C, Fe-Nb-C, Fe-Ti-N and Fe-Nb-N Austenites

(All values in Joules/Mole)

$$RT\ln^0 \gamma_C = 44184 - 17.7 T$$

$$RT\ln^0 \gamma_N = -55520 - 69.87 T \log T + 317.47 T$$

$$RT\ln^0 \gamma_{Nb} = -25500 + 10.9 T$$

$$RT\ln^0 \gamma_{Ti} = -60590 + 14.08 T$$

$$RT\epsilon_C^C = 73925$$

$$RT\epsilon_N^N = 52300$$

$$RT\epsilon_{Nb}^{Nb} = -2RT\ln^0 \gamma_{Nb}^*$$

$$RT\epsilon_{Ti}^{Ti} = 131035$$

$$RT\epsilon_C^{Nb} = -543300 + 20.75 T$$

$$RT\epsilon_C^{Ti} = -709980 + 41.50 T$$

$$RT\epsilon_N^{Nb} = -3379500 + 1970 T$$

$$RT\epsilon_N^{Ti} = -5861000 + 3190 T^{**}$$

\* Approximation

\*\* Obtained via correlations

TABLE 6.6

## Interaction Parameters for Ti and Nb Carbides and Nitrides

Phase	A	A	A'	B
	0	2	3	0
NbC	8995 + 3.56T	300950 - 96.32T	- 458100 + 134.31T	- 74750 - 30.93T
TiC	- 1004 + 3.77T	419655 - 136.94T	- 649360 + 184.60T	- 92350 - 34.06T
NbN	8995 + 3.56T	9070 - 57.36T	0	-227955 + 19.7T
TiN	- 1004 + 3.77T	-104600 + 18.41T	0	-441270 + 108.03T
	fcc o <sub>G</sub>	bcc o <sub>G</sub>	L	fcc o <sub>G</sub>
	M	M	L	MX
			1	M
				X
NbC	8995 + 3.56T	- 42625 + 4.42T	- 114525 + 33.58T	- 146650 - 1.762T
TiC	- 1004 + 3.77T	- 67365 + 1.51T	- 162340 + 46.15T	- 187326 + 10.577T
NbN	8995 + 3.56T	9070 - 57.36T	0	- 237025 + 77.069T
TiN	- 1004 + 3.77T	-104600 + 18.41T	0	- 336670 + 89.621T

(All values in Joules/mole of Metal)

## CHAPTER VII

### CONCLUSIONS

In the following, the salient features of this study are summarized.

1. The thermodynamics of Fe-Nb-C, Fe-Ti-C, and Fe-Nb-N austenites have been investigated via a dynamic gas equilibration method. A very sensitive Cahn microbalance has been used to determine the concentration of carbon or nitrogen from weight change measurements.
2. The effects of niobium-carbon and titanium-carbon interactions in austenite have been observed (i) as a minimum in the solubility curve, (ii) as increases in carbon contents due to Ti or Nb additions at constant carbon potentials and (iii) as the variation of solubility limit of the carbides with carbon content at high carbon levels.
3. The results on the isoactivity measurements in the ternary Fe-Ti-C and Fe-Nb-C and Fe-Nb-N austenites have been analyzed using the modified Wagner formalism. The ternary interaction parameter  $\epsilon_c^M$  ( $M = \text{Ti, Nb}$ ) has been quantitatively related to the solubility minimum and the relative increase in carbon content. The parameters  $\epsilon_c^{\text{Ti}}$  and  $\epsilon_c^{\text{Nb}}$  have been determined using the latter relationship.

4. The solubility limits of the carbides ( $TiC$  and  $NbC$ ) have been determined from the discontinuity in the variation of carbon content with Nb or Ti at constant carbon activity. A correction term depending on the ternary interaction parameter has been added to the classical solubility product relationship in order to describe the variation of the solubility limit of the carbides at high carbon levels. The solubility limits were used to cross-check the ternary interaction parameter obtained from relative increase in carbon content as well as to determine the dissolution free energy of Nb and Ti.
5. The dissolution free energies of Nb and Ti determined from the various solubility investigations have been analyzed. Periodic Table variation of the dissolution free energies and the consistency in the values obtained from various investigations on solubility have been used as the criteria in the assessment of the values for the Ti and Nb.
6. The Nb-N interaction parameter has been determined to a reasonable degree of accuracy from the relative increase in nitrogen contents due to Nb additions. The solubility of  $NbN$  has also been determined. The  $NbN$  solubility can be adequately described using the classical solubility relationship.
7. The thermodynamics of the nonstoichiometric monocarbides and mononitrides of Ti and Nb have been analyzed using the sublattice -

subregular model suggested by Hillert and Staffansson. Expressions describing the variation of the partial molar free energies of the components have also been obtained via statistical mechanical considerations of interstitial solutions. The variation of pair interaction free energies and the vibrational entropy with composition have been incorporated in the description. The parameters in the Hillert-Staffansson model have been related to the pair interaction energies.

8. The limitations in applying the classical Wagner-Schottky model to highly nonstoichiometric carbides and nitrides have been discussed. The necessary modifications to the Wagner-Schottky model have been made by referring to the expressions obtained via the statistical mechanical approach.
9. The thermodynamics of  $TiC_y$  and  $NbC_y$  phases have been investigated using the gas equilibration techniques at 1273K and 1473K. The  $NbN_y$  phase has also been investigated at 1573K, 1623K and 1673K. The results determined in this study together with those available in the literature have been analyzed for the evaluation of the interaction parameters in the sublattice model.
10. The effects due to solute interactions and the nonstoichiometry of the carbides on the solubility of  $NbC_y$  and  $TiC_y$  in their respective ternary austenites have been investigated. The nonstoichiometry is found to be significant in reducing the solubility at low carbon

levels, while the solute interactions (the cross interaction terms), increase the solubility at high carbon and high metal contents.

11. The solubility of TiN in Fe-Ti-N austenite was calculated using the free energy of dissolution of Ti evaluated in this study. The calculated value has been compared with the existing data in the literature.
12. Finally, a correlational relation between the ternary interaction parameters and the free energies of formation of carbides and nitrides was established. An approximate value for the nitrogen-titanium interaction parameter has been evaluated by extrapolating the correlational relationship.

REFERENCES

1. O. Kubaschewski, IRON - Binary Phase Diagrams, Springer-Verlag, Berlin, Heidelberg, New York (1982).
2. J.L. Murray, Bulletin of Alloy Phase Diagrams, 2, (1981) p 320.
3. E. Paul and L.J. Swartzendruber, Bulletin of Alloy Phase Diagrams, 7, (1986) p 248.
4. W.A. Fischer, K. Lorez, H. Fabritius, A. Hoffman, and G. Kalwa, Archiv.Eisenhüttenw., 37 (1966) p 79.
5. A. Hellawell and W. Hume-Rothery, Philosophical Transactions of Royal Society, London A 249 (1957) pp 426-459.
6. S.H. Moll and R.E. Ogilvie, TMS-AIME, 215 (1959) p 613.
7. T. Wada, Nippon Kinzoku Gaikkaishi, 27(3) (1963) p 119., English Version: Trans. Nat. Res. Inst. Met., 6(2) (1964) pp 44-46.
8. F.A. Shunk, Constitution of Binary Alloys McGraw-Hill, New York (1968), Second Supplement (1969).
9. R. Hultgren, P. Desai, D.T. Hawkins, M. Gleiser, K.K. Kelly, Selected Values of the Thermodynamic Properties of Binary Alloys, American Society of Metals (1973).
10. L. Kaufman and H. Nesor, CALPHAD, 2, (1978) pp 56-63, and p 117.
11. H. Eggers and W. Peter, Mitt. Kaiser-Wilhelm Inst. Eisenforsch., 20 (1938) pp 199-211.
12. W. Peter, Stahl Eisen, 58 (1938), p 1165.
13. R. Vogel and R. Ergang, Arch. Eisenhüttenwes., 12(3) (1938) p 155.
14. R. Genders and R. Harrison, J. Iron and Steel Inst., 140 (1939) p 29.
15. W.S. Gibson and W. Hume-Rothery, J. Iron and Steel Inst., 189 (1958) pp 243-250.
16. W.S. Gibson, J.R. Lee, and W. Hume-Rothery, J. Iron and Steel Inst., 198 (1961) pp 64-66.
17. A. Ferrier, E. Ubelacker, and E. Wachtel, C.R. Academy Sciences (Paris), 258 (1964) pp 5424-5427.
18. C. Wagner, Thermodynamics of Alloys, Addison-Wesley, Reading, MA (1962) p 51.

19. L.S. Darken, TMS-AIME, 239 (1967) pp 90-96.
20. A.D. Pelton and C.W. Bale, Met. Trans. 17A (1986) pp 1211-1215.
21. M. Hillert, Met. Trans., 17A (1986) pp 1878-1879.
22. L.S. Darken and R.W. Gurry, The Physical Chemistry of Metals, McGraw-Hill, New York (1953).
23. M. Benz and J.F. Elliott, Trans. TMS-AIME 221 (1961) pp 323-331.
24. H. Harvig, Jernkont. Ann., 155 (1971) pp 157-161.
25. J. Chipman, Met. Trans., 3 (1972) pp 55-64.
26. J. Agren, Met. Trans., 10A (1979) pp 1847-1852.
27. M. Hillert and M. Jarl, CALPHAD, 2 (1978) pp 227-238.
28. P. Gustafson, Scan. J. Metallurgy, 14 (1985) pp 259-267.
29. M. Hillert and L.I. Staffansson, Acta Chemica Scandinavica 24 (1970) pp 3618-3626.
30. L.S. Darken and R.P. Smith, J. Amer. Chem. Soc., 68 (1946) p 1172.
31. M. Tempkin and L. Swarczman, Zhur. Fiz. Khim., 23 (1949) p 755.
32. H. Schenck and H. Kaiser, Archiv. Eisenhüttenwes., 31 (1960) 227.
33. J.S. Kirkaldy and G.R. Purdy, Can. J. Phy., 40 (1962) p 202.
34. L. Kaufman, S.V. Radcliffe, and M. Cohen, AIME Symposium on Decomposition of Austenite, Ed. V. Zackay, (1962) p 312.
35. K.A. Moon, Trans. TMS-AIME 227 (1963) p 1116.
36. L.S. Darken, Trans. TMS-AIME, 239 (1967) p 80.
37. R. B. McLellan, T.L. Garrard, S.J. Horowitz, and J.A. Sprague, Trans TMS-AIME, 239 (1967) p 528.
38. J. Chipman and E.F. Brush, Trans. TMS-AIME, 242 (1968) p 35.
39. D.R. Poirier, Trans. TMS-AIME, 242 (1968) p 685.
40. M. Hillert and M. Jarl, Met. Trans., 6A (1975) pp 553-559.
41. H. Ohtani, T. Nishizawa, T. Tanaka, and M. Hasebe, Proc. Japan-Canada Seminar on Secondary Steelmaking, Tokyo, Japan., Publ. The Canadian Steel Industry Research Association (CSIRA) and The Iron and Steel Institute of Japan (ISIJ), (1985) p J-7-1.

42. T. Nishizawa, H. Ohtani, and M. Hasebe, Presentation, CALPHAD XIV, Boston, Mass., (1985).
43. E. Rudy, Compendium of Phase Diagram Data, AFML-TR-65-2 Part V (1969) p 159 and p 171.
44. G. Brauer, Z. Anorg. Chem., 277 (1954) p 249.
45. C.P. Kempter, J. Chem. Phys., 33 (1960) p 1873.
46. E.K. Storms and N.H. Krikorian, J. Chem. Phys., 33 (1960) p 1878.
47. E.K. Storms, Refractory carbides, Academic Press, New York and London (1967).
48. L.A. McClaine and C.P. Coppel, Technical Report, AFML-TR-65-299, Part I and II, Wright-Patterson Air Force Base, Ohio (1965).
49. R.W. Guard, J.W. Savage, and D.G. Swathout, Trans. TMS-AIME, 239 (1967) p 643.
50. L.E. Toth, m. Ishikawa, and Y.A. Chang, Acta Met., 16 (1968) p 1183.
51. L.E. Toth, Transition Metal Carbides and Nitrides, Academic Press, New York (1971) Chapter IV.
52. T.H. Geballe, B.T. Matthias, J.P. Remeika, A.M. Clogston, V.B. Compton, J.P. Maita, and H.J. Williams, Physics 2 (1966) p 293., (quoted in Toth(51)).
53. N. Pessall, J.K. Hulm, and M.S. Walker, Final Report, AF 33(615)-2729 (1967).., (quoted in Toth(51)).
54. R. Caudron, P. Costa, and B. Saulgeot, Second International Conference on Semi-Metallic Compounds of Transition Elements, Enschede (1967).., (quoted in Toth(51)).
55. L.B. Pankratz, W.W. Weller, and K.K. Kelley, U.S. Bur. Mines, Report No. 6446 (1964) p 9.
56. T.A. Sandenaw and E.K. Storms, Los Alamos Sci. Lab., Report No. LA 3331 (1965) and J. Phy. Chem. of Solids 27 (1966) p 217.
57. A.A. Rempel, S.J. Nazarova, and A.I. Gusev, Phys. Stat. Sol. A 86 (1984) p 11.
58. P.V. Gel'd and F.G. Kusenko, Izv. Akad. Nauk. SSSR, Otd. Tech. Nauk. Met. i. Toplivo, 2 (1960) p 79.
59. A.G. Turchanin and S.S. Ordan'ian and V.V. Fesenko, Poroshkovia

- Met., 9 (1967) p 23.
60. E.J. Huber Jr., E.L. Head, C.e. Holley Jr., E.K. Storms, N.H. Krikorian, J. Phys. Chem., 65 (1961) p 1846.
  61. F.G. Kusenko and P.V. Gel'd, Izv. Sibirsk. Otd. Akad. Nauk. SSSR, 2 (1960) p 46.
  62. A.N. Kornilov, I.D. Zaikin, S.M. Skwiatov, and G.P. Shveikin, Zh. Fiz. Khim., 40 (1966) p 1070.
  63. A.D. Mah and B.J. Boyle, J. Amer. Chem. Soc., 68 (1964) p 6512.
  64. A.N. Kornilov, V.Ya. Leonidov, and S.N. Skwiatov, Moscow Univ., Vestnik Serii Khim., 6 (1962) p 48.
  65. J.F. Smith, O.N. Carlson and R.R. de Avillez, J. Nucl. Mater., 48 (1987) pp 1-16.
  66. R.R. de Avillez, Dept. de Ciencia dos Materiais e Metalurgia, Pontificia Universidade catolica do Rio de Janeiro, Brasil, Private Communication.
  67. K.K Kelley, Ind. Eng. Chem., 36 (1944) p 565.
  68. B.F. Naylor, J. Amer. Chem. Soc., 68 (1946) p 370.
  69. C.D. Pears, S. Oglesby Jr., and D. Osment, Southern Research Institute Tech. Rep. No. ASD-TDR-62-765, (1963).
  70. N. Pessall, J.K. Hulm, and M.S. Walker, Tech. Rep. No. AFML-TR-67-168, Westinghouse Research Labs., Pittsburg, pa. (1967).. (quoted in Hultgren et al.(9) p 1175).
  71. C.H. Shomate, J. Amer. Chem. Soc., 68 (1946) p 310.
  72. R.A. McDonald, F.L. Oetting and H. Prophet, Report No. N64-18824, Dow Chemical Co., Midlands, Michigan, (1963).
  73. D.S. Neel, C.D. Pears, and S. Oglesby, Tech. Rep. No. ASD-TDR-62-765, Southern Research Inst., Birmingham, Atlanta, (1963).. (quoted in Hultgren et al (9) p 1176).
  74. G.L. Humphrey, J. Amer. Chem. Soc., 73 (1951) p 2261.
  75. B. Neumann, C. Kroger, and H. Kunz, Z. Anorg. Allgem. Chem. 176 (1934) p 289., (quoted in Hultgren et al.(9) p 1176).
  76. M.P. Morozova and M.M. Khernberg, Russ. J. Phy. Chem., 40 (1966) p 604.
  77. F. Tessandier, M. Ducarrior and C. Bernard, CALPHAD, 8

(1984) p 233.

78. L. Kaufman and H. Bernstein, Tech. Rep. No. AFML-TR-66-193, Wright-Patterson Air Force Base, Ohio (1966).
79. Y.A. Chang, Tech. Rep. No. AFML-TR-65-2, Part IV, Wright-Patterson Air Force Base, Ohio (1965).
80. W. Schottky and C. Wagner, Z. Phys. Chem., 11 (1930) p 163.
81. M. Hillert, Bo Jansson and Bo Sundman, TRITA-MAC-0346, Royal Institute of Technology, Stockholm, Sweden.
82. L. Kaufman and J. Agren, Tech. Rep. F 49620-80-C-0020, Air Force Office of Scientific Research (AFSC), Bolling Air Force Base, D.C. 20332 (1982).
83. B. Uhrenius, CALPHAD, 8 (1984) p 101.
84. G.L. DePoorter, J. Amer. Cer. Soc., 52 (1969) p 311.
85. M. Hoch, Anisotropy in Single Crystal Refractory Compounds, Vol. I, Plenum Press, New York (1968) p 163.
86. V.I. Alekseev, A.S. Panov, Ye.V. Fiveiskii, and L.A. Shvartsman, Proc. Thermodynamics of Nuclear Materials 1967, IAEA, Vienna (1968) pp 435-447.
87. P. Grieveson, Proc. British Ceramic Society, 8 (1967) pp 137-153.
88. V.I. Malkin and V.V. Pokidshev, Russ. J. Phys. Chem., 45 (1971) pp 1159-1161.
89. K. Koyama and Y. Hashimoto, Nippon Kinzoku Gakkai-si, 37 (1973) pp 406-411.
90. E.K. Storms, B. Calkin, and A. Yencha, High Temp. Sci., 1 (1969) p 430.
91. Y.R. Hong, R.V. Kumar, K. Balasubramanian, and D.A.R. Kay, Submitted to Met. Trans.
92. M.J. Linevsky, Tech. Rep., AFML-TR-64-420, (1964).
93. M. Hoch, D.P. Dingley, and H.L. Johnston, J. Amer. Chem. Soc., 77 (1955) p 304.
94. A.G. Shchurik, and I.A. Tomlin, Russ. J. Phy. Chem., 45 (1971) p 1162.
95. K. Narita, J. Chem. Soc. Japan, 77 (1956) P 1536.

96. F. de Kazínsky, A. Axnas, and P. Pachleiter, *Jernkont. Ann.*, 147 (1963) P 408.
97. T. Mori, *Tetsu-to-Hagane*, 50 (1964) p 911.
98. K. Narita and S. Koyama, *Jap. Inst. Metals, Journal*, 52 (1966) p. 292.
99. L. Meyer, Dissertation, Clausthal Berg., Hulten (1966) and *Z. Metallkunde*, 58 (1967) pp 334-339.
100. R.P. Smith, *Trans. TMS-AIME*, 236 (1966) p 220.
101. T.H. Johansen, N. Christensen and B. Augland, *Trans. TMS-AIME*, 239 (1967) p 1651.
102. H. Nordberg and B. Aronsson, *J. Iron and Steel Inst.*, 206 (1968) p 1263.
103. S. Koyama, *Japan Inst. Metals, Journal*, 52 (1972) p 1090.
104. V.K. Lakshmanan and J.S. Kirkaldy, *Met. Trans.*, 15A (1984) p 541.
105. R.C. Sharma, V.K. Lakshmanan, and J.S. Kirkaldy, *Met. Trans.*, 15A (1984) p 545.
106. K. Narita, *J. Chem. Soc. Japan*, 80 (1959) p 266.
107. K.J. Irvine, F.B. Pickering, and T. Gladman, *J. Iron and Steel Inst.*, 205 (1967) p 171.
108. T. Shiraiwa, N. Fujino, and J. Murayama, *Trans. Iron and Steel Inst. Japan*, 10 (1970) p 406.
109. R.P. Smith, *Trans. TMS-AIME*, 224 (1962) p 190.
110. T. Mori, M. Tokizane, and K. Yamaguchi, *Tetsu-to-Hagane*, 54 (1968) p 763.
111. K. Narita, *J. Chem. Soc. Japan*, 77 (1956) pp 1536-1539.
112. H. Sawamura and T. Mori, *Tetsu-to-Hagane*, 43 (1957) pp 31-38.
113. H. Chino, K. Wada, *Yawata Tech. Rep.*, 251 (1965) p 5817.
114. S. Matsuda and N. Okamura, *Trans. Iron and Steel Inst. Japan*, 18 (1978) p 198.
115. W. Roberts, *Tech. Rep. IM 1085*, Swedish Institute for Metals Research, (1975).
116. J. Kunze, *Metal Science*, 16 (1982) pp 217-218.

117. H. Wada and R.D. Pehlke, *Met. Trans.* 16B (1985) p 815.
118. H. Dunwald and C. Wagner, *Anorg. Allgem. Chem.*, 199 (1931) p 321.
119. L. Kaufman and H. Bernstein, Computer Calculation of Phase Diagrams, Academic Press (1970).
120. R.P. Smith, *TMS-AIME*, 68 (1946) pp 1163-1175.
121. R.J. Hawkins, British Steel Corporation (BSC) Corporate Laboratories - University of Sheffield, Symposium on Chemical Metallurgy of Iron and Steel, Iron and Steel Inst/Metal Soc., London (1973) p 310.
122. W. Hume-Rothery, Structures of Alloys of Iron, Pergamon Press, Chapter 5 (1966).
123. G. Kirchner, H. Harvig, K. R. Moquist and M. Hillert, *Arch. Eisenhüttenwes.*, 44 (1973) p 227.
124. Z. Moser, W. Zakulski, P. Spencer and H. Hack, *CALPHAD*, 10 (1985) p 259.
125. A. Jansson, Internal Report No. TRITA-MAC-0340, Royal Institute of Technology, Stockholm, Sweden, (1985)
126. S. Hertzman and Bo Sundman, Internal Report No. TRITA-MAC-0243, Royal Institute of Technology, Stockholm, Sweden, (1984).
127. J.O. Andersson and Bo Sundman, TRITA-MAC-0270, Royal Institute of Technology, Stockholm, Sweden, (1986).
128. J.O. Andersson and N. Lange, TRITA-MAC-0322, Royal Institute of Technology, Stockholm, Sweden, (1986).
129. H. Weiming, TRITA-MAC-0309, Royal Institute of Technology, Stockholm, Sweden, (1986).
130. J.O. Andersson, *CALPHAD*, 7 (1983) pp 295-305.
131. P. Gustafson, TRITA-MAC-0257, Royal Institute of Technology, Stockholm, Sweden, (1985).
132. E.A. Guggenheim, Chapters II and IV, Mixtures, Clarendon Press, Oxford (1952).
133. H.J. Goldschmidt, Section 2.5 and Section 4.1, Interstitial Alloys, Plenum Press, Butterwoths, London (1967).
134. W. Hume-Rothery, *Phil. Mag.*, 44 (1953) pp 1154-60.
135. R. Kiessling, Bonding in Metals, *Metall. Rev.* 2 (1957) p 77-107.

136. E. Dempsey, *Phil. Mag.* 8 (1963) p 285.
137. W. Philipp, *Acta Met.*, 10 (1962) p 583.
138. J.S. Umanski, *Dokl. Akad. Nauk SSSR* 26 (1943) p 127.
139. P.N. Smith and J.S. Kirkaldy, A Samarin Memorial Symposium, Academy of Sciences, Moscow (1972)
140. S.E. Feldman and J.S. Kirkaldy, *Can. Met. Quat.* 13 (1974) p 625.
141. H.L. Schick, Table 165, Thermodynamics of Certain Refractory Compounds, Vol. II, Academic Press (1966) p 2-177.
142. H.A. Wriedt and J.L. Murray, *Bulletin of Alloy Phase Diagrams*, 8 (1987) pp 378-388.
143. O. Kubaschewski, E. LL. Evans and C.B. Alcock, Metallurgical Thermochemistry, Fourth Edition, Pergamon Press (1967) pp 421-429.
144. H. Wada, *Trans. Iron and Steel Inst. of Japan*, 27 (1987) pp 649-657.
145. S.D. Conte, and C. de Boor, Chapter 6, Sections 6.1 - 6.4, Elementary Numerical Analysis - An Algorithmic Approach, Third Edition, McGraw-Hill (1980).